NASA Contractor Report 4765

An Analysis of the Pressures, Forces and Moments Induced by the Ground Vortex Generated by a Single Impinging Jet

Richard E. Kuhn

Defense Group, Inc.
901 North Stuart St., Suite 801
Arlington, VA 22203

Prepared for
Ames Research Center
CONTRACT NAS2-14384
February 1997

National Aeronautics and
Space Administration

Ames Research Center
Moffett Field, California 94035-1000

TABLE OF CONTENTS

AN ANALYSIS OF THE PRESSURES, FORCES AND MOMENTS INDUCED BY THE GROUND VORTEX GENERATED BY A SINGLE IMPINGING JET

By

Richard E Kuhn

INTRODUCTION

When a jet or fan powered STOVL aircraft is hovering, or in transition between hover and conventional flight, the lifting jet streams induce suction pressures on the lower surface that cause a lift loss and, generally, a nose up pitching moment. Sketches of the flow fields involved are presented in figure 1. These flow fields and the forces and moments they induce have been studied in many investigations, such as those summarized in references 1-6.

In hover out of ground effect (upper left in figure 1), the entrainment action of the downward directed jets induced suction pressures on the lower surface causing a small lift loss. Close to the ground, (upper right in figure 1) the wall jets flowing radially outward from the point at which the jets impinge greatly increase the entrainment area and the resulting lift loss or suckdown. A fountain flow is generated where the wall jets from multiple jet configurations meet. This fountain flow partially offsets the suckdown induced by the wall jets. Early methods for estimating the net suckdown are presented in references 7 and 8. These methods were extended to include estimation of the pitching moments in reference 9.

In transition out of ground effect (lower left in figure 1) the jet streams are swept rearward by the interaction with the free stream and roll up into vortex pairs. These vortices, and to a lesser extent the blockage and viscous entrainment action of the jet(s) induce suction pressures on the lower surface of the aircraft, generally causing a loss in lift and a nose up pitching moment. The path that the jets take and the pressures and forces induced are summarized in references 2 - 4 and the development of empirical methods for estimating the aerodynamic effects induced are presented in references 6, 7, 10 and 11.

In ground effect at transition speeds (STOL operation) all the above flow phenomena are present, but modified by the proximity of the ground. In addition a ground vortex is formed by the action of the free stream in opposing the wall jet flowing forward from the impingement point of the front jet (lower right in figure 1). Studies of the ground vortex and methods for estimating its effects are presented in references 5, 6, 10, 12 and 13.

Previous methods for estimating the effects of the Ground vortex have relied on force data. Detailed data on the pressures induced on the lower surface by the ground vortex on a delta wing model with several jet arrangements are presented in reference 14. The present study attempts to correlate the integration of these pressures into a method for estimating the jet induced lift and pitching moments experienced in ground effect.

SYMBOLS

A	Aspect ratio of planform or element of configuration under consideration	
A_n	Aspect ratio of jet nozzle	
A_j	Jet exit area, total area unless otherwise noted	sq. ft.
$A_{GV,aft}$	Planform area aft of the jet	sq. ft.
$A_{GV,fore}$	Planform area between zero pressure line and jet	sq. ft.
$A_{GV,p}$	Planform area forward of zero pressure line	sq. ft.
a	Exponent used in estimating wing-body upwash (eq. 20)	
C_{L_α}	Power off lift curve slope	
C_p	Pressure coefficient $C_p=\Delta P/q_j$	
d or D	Diameter of individual jet(s)	ft.
d_e	Equivalent diameter of total jet area	ft.
D_p	Equivalent diameter of planform area	ft.
e	Exponent used in estimating 'hover suck-down' pressures (eq. 28)	
f_p	Planform fineness ratio	
h	Height of flat plate or body lower surface above ground	ft.

h_w	Height of wing above ground	ft.
K_{gb}	Factor accounting for ground condition or type of ground simulation (eq. 3)	
K_{sj}	Factor used in estimating 'hover suckdown' increment (eq. 27)	
K_{tv}	Adjustment factor for effect of 'trapped vortex' in hover (eq. 29 and 30)	
K_{tgv}	Adjustment factor for effect of trapping of the ground vortex at low heights (eq. 14 and 15)	
$\Delta L, dL$	Lift loss increment	lb.
mac	Mean Aerodynamic Chord	ft.
$\Delta M, dM$	Pitching moment increment	ft. lb.
NPR	Nozzle Pressure Ratio	
ΔP	Increment of pressure induced by ground proximity	$lb./ft^2$
q	Free stream dynamic pressure	$lb./ft^2$
q_j	Jet dynamic pressure at nozzle exit	$lb./ft^2$
S	Total planform area of configuration, or part of configuration under consideration	sq. ft.
S_{ref}	Reference area used in calculation of coefficients	sq. ft.
T	Total jet thrust	lb.
V_e	Effective velocity ratio. $V_e=\sqrt{q/q_j}$	
x	Longitudinal distance ahead of jet station	ft.
X	Effective arm at which jet induced lift increment acts.	ft.
X'	Longitudinal distance of zero pressure point on model centerline ahead of jet (see fig. 3) (eq. 3)	ft.
X'_{mac}	Zero pressure line longitudinal distance ahead of jet at lateral station of MAC (eq. 16)	ft.
$X_{C.G.}$	Station at which moment reference point is located	ft.
X_{pos}	Station at which center of area of positive pressure region forward of the zero pressure line is located	ft.

X_{jet}	Station at which jet is located	ft.
$X_{L.E.}$	Station at which leading edge of MAC is located. (see fig. 16 & 17)	ft.
Y_{ave}	Average width of planform ahead of jet station	ft.
y	Lateral distance from centerline	ft.
y_{mac}	Lateral distance of MAC from centerline	ft.
α	Angle of attack	deg.
$\Delta\alpha$	Upwash angle induced by ground vortex. (eq. 11, 12, 18, 19 and 21)	deg.
δ	Jet deflection angle	deg.

SUBSCRIPTS

body	Body of wing-body conf. or flap plate conf.
C.G.	Center of gravity or moment reference point
data	Experimental data
fore	Region between zero pressure line and jet station
f	Front, or forward of jet center
GV	Ground vortex contribution
hov	'Hover suckdown' contribution
j	Jet
neg	Negative pressure region
p or pos	Positive pressure region
sj	Single jet
tv	Trapped vortex condition
us	Upper surface contribution
wake	Jet wake contribution
wb	Wing-body
wing	Wing

PRESENTATION OF METHOD

ESTIMATION OF INDUCED LIFT

The method developed in this study is re-presented here for the convenience of the user. The lift loss induced at forward speed in ground effect can be expressed as;

$$\frac{\Delta L}{T} = \left(\frac{\Delta L}{T}\right)_{GV} + \left(\frac{\Delta L}{T}\right)_{hov} + \left(\frac{\Delta L}{T}\right)_{wake} \quad (1)$$

where the first term accounts for the ground vortex effect (developed in this study), the second term accounts for the 'hover suckdown' effect (from ref. 9 or experimental data, if available; modified here for the effects of cross flow), and the third term accounts for the jet wake effect (from ref. 11 or experimental data, if available; modified here for the effects of ground proximity).

Ground Vortex Term

The ground vortex term is made up of 4 terms;

$$\left(\frac{\Delta L}{T}\right)_{GV} = \left(\frac{\Delta L}{T}\right)_{GV,pos} + \left(\frac{\Delta L}{T}\right)_{GV,neg} + \left(\frac{\Delta L}{T}\right)_{us} + \left(\frac{\Delta L}{T}\right)_{wb} \quad (2)$$

The first two terms represent the effects of pressures induced on the lower surface ahead of the jet. As depicted in figure 3 positive pressures are induced in the upwash region ahead of the vortex and negative pressures are induced over the vortex. These positive and negative pressure regions are divided by the zero pressure line.

The method requires calculating the location of the zero pressure line. The location of the zero pressure line on the model centerline is given by;

$$\frac{X'}{d} = K_{gb}\ .6\left(\frac{S}{A_j}\right)^{.2} V_e^{-.4}\left(\frac{h}{d}\right)^{.06V_e^{-.7}} + \frac{h}{d}\tan(\delta - 90) \quad (3)$$

where for an aircraft moving over the ground, or a model tested over a moving belt ground board;

$K_{gb} = .67$

and for a model over a fixed ground board, or an aircraft hovering in a crosswind;

$K_{gb} = 1.0$

At spanwise stations off the centerline, the zero pressure point moves aft as expected. The zero pressure line is parabolic in shape and is given by;

$$y = 2\sqrt{X'(X'-x)} \tag{4}$$

where x is the distance forward of the station of the jet.

The lift increment due to the pressures in the positive pressure region is given by;

$$\left(\frac{\Delta L}{T}\right)_{GV,p} = C_{p,GV,p}\,\frac{A_{GV,p}}{2A_j} \tag{5}$$

where $A_{GV,p}$ is the lower surface area forward of the zero pressure line and $C_{p,GV,p}$ is the average pressure coefficient in the positive pressure region and is given by;

$$C_{p,GV,p} = K_{gb}\,\frac{\left(\frac{\delta}{90}\right)^2}{A_n^{.25}}\,\frac{.46\ V_e\ f_p^{.5}}{\left(\frac{h}{d}\right)\left(\frac{S_{fwd}}{A_j}\right)^{.4}} \tag{6}$$

The lift increment due to the negative pressures in the area between the zero pressure line and the jet is given by;

$$\left(\frac{\Delta L}{T}\right)_{GV,neg.} = C_{p,GV,fore}\,\frac{A_{GV,fore}}{2A_j} \tag{7}$$

and the average pressure is the less negative of the pressures calculated by the two following expressions;

at the lower heights;

$$C_{p,GV,fore} = K_{gb}\,\frac{-10\ V_e}{A_n^{.25}}\left(\frac{\delta}{90}\right)^2\left(\frac{Y_{ave}}{d}\right)^{-2}\left(\frac{h}{d}\right)^{-8.4/\sqrt{S_{fwd}/A_j}} \tag{8}$$

at the higher heights;

$$C_{p,GV,fore} = K_{gb}\,\frac{-.1\ f_p^{.25}}{A_n^{.25}}\left(\frac{\delta}{90}\right)^2\left(\frac{h}{d}\right)^{-2} \tag{9}$$

In addition to the pressures induced on the lower surface the presence of the ground vortex forces the free stream to flow up and over itself putting the configuration in an upwash flow field (fig. 3b). This upwash induces lifting pressures on the upper surface. The method assumes that the upper surface increment is equivalent to the configuration operating at an increased angle of attack and that, for a body or a flat plate configuration, the lift increment is given by;

$$\left(\frac{\Delta L}{T}\right)_{us} = C_{L\alpha,body}\,\Delta\alpha_{us}\,\frac{S_{ref}}{2A_j}V_e^2 \tag{10}$$

and the induced upwash angle is given by;

for negative values of X"

$$\Delta\alpha_{us} = K_{gb}^{.2\left(\frac{X_{jet}-X_{L.E.}}{d}\right)}\left[.7 - .7\frac{X''}{d} - .35\left|\frac{X''}{d}\right|^{1.2}\right]\frac{K_{tgv}}{V_e\ h/d}\ \frac{(\delta/90)^2}{A_n^{.25}} \tag{11}$$

for positive values of X"

$$\Delta\alpha_{us} = K_{gb}^{.2\left(\frac{X_{jet}-X_{L.E.}}{d}\right)}\left[.7 - .7\frac{X''}{d} + .16\left(\frac{X''}{d}\right)^{1.5}\right]\frac{K_{tgv}}{V_e\ h/d}\ \frac{(\delta/90)^2}{A_n^{.25}} \tag{12}$$

where X" is the distance from the assumed center of the ground vortex to the wing leading edge, given by;

$$\frac{X''}{d} = \frac{\frac{X'_{mac}}{2} - (X_{jet} - X_{L.E.})}{d} \tag{13}$$

and K_{tgv} accounts for the effects of the ground vortex being 'trapped' under the configuration at low heights (fig. 3c) and below $h = .5\sqrt{S/A_j}\ V_e\ X'_{mac}$

$$K_{tgv} = \frac{h}{.5\sqrt{S/A_j}\ V_e\ X'_{mac}} \tag{14}$$

and above $h = .5\sqrt{S/A_j}\ V_e\ X'_{mac}$

$$K_{tgv} = 1.0 \tag{15}$$

The distance from the jet station to the vortex center is calculated at the spanwise location of the MAC (Y_{mac}) and (accounting for the parabolic shape of the zero pressure line) is given by;

$$X'_{mac} = X' - \frac{Y_{mac}^2}{4X'} \tag{16}$$

For a wing-body configuration the wing lift due to the induced upwash is given by;

$$\left(\frac{\Delta L}{T}\right)_{wb} = C_{L\alpha,wing}\,\Delta\alpha_{wb}\,\frac{S_{ref}}{2A_j}V_e^2 \tag{17}$$

the induced upwash angle is a function of the distance of the wing leading edge ahead of the jet and is given by;

for negative values of X"

$$\Delta\alpha_{wb} = K_{gb}^{.2\left(\frac{X_{jet}-X_{L.E.}}{d}\right)}\left[-.06\frac{X''}{d} + .016\left(\frac{X''}{d}\right)^2\right]\frac{K_{tgv}}{V_e^2\,(h_w/d)^4}\,\frac{(\delta/90)^2}{A_n^{.25}} \tag{18}$$

for positive values of X"

$$\Delta\alpha_{wb} = K_{gb}^{.2\left(\frac{X_{jet}-X_{L.E.}}{d}\right)}\left(-.06\frac{X''}{d}\right)\frac{K_{tgv}}{V_e^2\,(h_w/d)^a}\,\frac{(\delta/90)^2}{A_n^{.25}} \tag{19}$$

where the exponent, a, is given by;

$$a = 1 + .06V_e\left(\frac{X_{jet}-X_{L.E.}}{d}\right)^2 \tag{20}$$

If the wing lower surface is not co-planer with the body lower surface the height of the wing h_w above the ground is used for h in calculating the upwash (eq. 18 and 19).

At some combinations of low velocity ratio, V_e, and low height, h_w. equation 48 will calculate increments of induced upwash angle of attack that would carry the wing beyond stall. For these conditions it is suggested that;

$$\textit{if}\quad \Delta\alpha > (\alpha_{stall} - \alpha) \qquad \textit{then use} \qquad \Delta\alpha = (\alpha_{stall} - \alpha) \tag{21}$$

'Hover Suckdown' Term

The 'hover suckdown' term is made up of three terms;

$$\left(\frac{\Delta L}{T}\right)_{hov} = \left(\frac{\Delta L}{T}\right)_{\infty} + \left(\frac{\Delta L}{T}\right)_{hov,body} + \left(\frac{\Delta L}{T}\right)_{hov,wing} \tag{22}$$

where $\left(\frac{\Delta L}{T}\right)_{\infty}$ is the lift loss induced out-of-ground effect (ref. 9) and is given by;

$$\left(\frac{\Delta L}{T}\right)_{\infty} = -.0001\sqrt{S_{hov}/A_j}\,\frac{(per/d)^{1.58}}{\sqrt{NPR}}$$

The method assumes that the pressures induced in hover by the impingement of the jet, estimated by the method of ref. 9, are not altered by the cross flow but that their effects are constrained to the region on the lower surface aft of the zero pressure line. The 'hover suckdown' term therefore is the sum of the lift loss induced forward of the jet and that induced aft of the jet and for a body or flat plate configuration is given by;

$$\left(\frac{\Delta L}{T}\right)_{hov,body} = C_{p,hov}\left(\frac{A_{GV,fore} + A_{GV,aft}}{2A_j}\right)_{body} \tag{24}$$

Likewise the 'hover suckdown' experienced on the exposed wing of a wing body configuration is given by;

$$\left(\frac{\Delta L}{T}\right)_{hov,wing} = C_{p,hov}\left(\frac{A_{GV,fore} + A_{GV,aft}}{2A_j}\right)_{wing} \tag{25}$$

The pressures induced in hover are given by (from ref. 9);

$$C_{p,hov} = \frac{\sin^2\delta}{1+V_e(A_n-1)}\left(\frac{h}{D_p-d}\right)^{e} K_{sj}\,K_{tv} \tag{26}$$

where

$$K_{sj} = -.043\frac{(NPR)^{-.1}(f_p)^{.13}}{S_{hov}/A_j} \tag{27}$$

and

$$e = -2.3(NPR)^{-.1}(f_p)^{.13} \tag{28}$$

The term K_{tv} is introduced to correct for the effects of the trapped vortex region where, above $(h/d)_{tv}$

$$K_{tv} = 1.0 \tag{29}$$

and in the trapped vortex height range, below $(h/d)_{tv}$

$$K_{tv} = 1 - \left(1 - \frac{h/d}{(h/d)_{tv}}\right)^{1.66} \tag{30}$$

where the 'trapped vortex' condition occurs (ref. 9) at heights below;

$$\left(\frac{h}{d}\right)_{tv} = \frac{.2\,(D_p - d)}{d} \tag{31}$$

Jet Wake Term

The effect of the proximity of the ground in truncating the jet wake is to reduce the suction pressures induced by the jet wake in the region aft of the jet. For the present method the jet wake increment in ground proximity is assumed to be given by;

$$\left(\frac{\Delta L}{T}\right)_{wake} = \left(\frac{\Delta L}{T}\right)_{\infty,body} + \left(\frac{\Delta L}{T}\right)_{GV,aft} + \left(\frac{\Delta L}{T}\right)_{\infty,wing} \tag{32}$$

where $\left(\frac{\Delta L}{T}\right)_{\infty,body}$ and $\left(\frac{\Delta L}{T}\right)_{\infty,wing}$ are estimated by the method of reference 11. Only the body term is corrected for the effects of ground proximity by;

$$\left(\frac{\Delta L}{T}\right)_{GV,aft} = C_{p,GV,aft}\frac{S_{aft}}{2A_j} \tag{33}$$

where

$$C_{p,GV,aft} = K_{gb}\ .05\ V_e\ A_n^{.5}\left(\frac{\delta}{90}\right)^2\left(\frac{h}{d}\right)^{-1.5} \tag{34}$$

ESTIMATION OF MOMENTS

The pitching moment, like the lift, can be expressed as;

$$\frac{\Delta M}{Td} = \left(\frac{\Delta M}{Td}\right)_{GV} + \left(\frac{\Delta M}{Td}\right)_{hov} + \left(\frac{\Delta M}{Td}\right)_{wake} \tag{35}$$

where the first term accounts for the ground vortex effect (developed in this study), the second term accounts for the 'hover suckdown' effect (from ref. 9 modified here for the effects of cross flow), and the third term accounts for the jet wake effect (from ref. 11 modified here for the effects of ground proximity).

The moment contributions are estimated by assuming the lift to be acting at an effective arm. In most cases the distance from the moment reference point to the center of the area for which the lift was being estimated is used as the effective arm.

Ground Vortex Term

The ground vortex term is made up of 4 terms;

$$\left(\frac{\Delta M}{Td}\right)_{GV} = \left(\frac{\Delta M}{Td}\right)_{GV,pos} + \left(\frac{\Delta M}{Td}\right)_{GV,neg} + \left(\frac{\Delta M}{Td}\right)_{us} + \left(\frac{\Delta M}{Td}\right)_{wb} \tag{36}$$

For the first term; the positive lift generated forward of the zero pressure line, the moment increment is given by;

$$\left(\frac{\Delta M}{Td}\right)_{GV,p} = \left(\frac{\Delta L}{T}\right)_{GV,p} \frac{(X_{C.G.} - X_p)}{d} \tag{37}$$

For the negative lift generated between the jet and the zero pressure line the moment contribution is given by;

$$\left(\frac{\Delta M}{Td}\right)_{GV,fore} = \left(\frac{\Delta L}{T}\right)_{GV,fore} \frac{(X_{C.G.} - X_{GV,fore})}{d} \tag{38}$$

The upwash induced lift increments are generated in a curved flow field (fig. 16) which produces a camber type loading. It is therefore assumed that the lift is applied at the mid chord point of the Mean Aerodynamic Chord of the planform or wing. For the

present method the moment due to the upper surface lift increment is given by;

$$\left(\frac{\Delta M}{Td}\right)_{us} = \left(\frac{\Delta L}{T}\right)_{us} \frac{(X_{C.G.} - X_{.suac,body})}{d} \tag{39}$$

and the moment due to the upwash induced lift on the exposed wing is given by;

$$\left(\frac{\Delta M}{Td}\right)_{wb} = \left(\frac{\Delta L}{T}\right)_{wb} \frac{(X_{C.G.} - X_{.suac,wing})}{d} \tag{40}$$

'Hover Suckdown' Term

The pitching moment induced in hover is the difference between the nose down moment generated by the suckdown ahead of the jet and the nose up moment induced aft of the jet. At the higher heights, as shown in reference 9, these moments are given by the lift loss acting at the center of area. However below a height equal to the distance from the jet to the center of area the moment arm, X_e, reduces rapidly.

Forward of the jet (between the zero pressure line and the jet) and above $h = X_{C.G.} - X_{fore}$

$$X_{e,fore} = (X_{C.G.} - X_{fore}) \tag{41}$$

below $h = X_{C.G.} - X_{fore}$

$$X_{e,fore} = (X_{C.G.} - X_{fore})\left(1 - \left(1 - \frac{h}{(X_{C.G.} - X_{fore})}\right)^2\right) \tag{42}$$

Aft of the jet,
and above $h = |X_{C.G.} - X_{aft}|$

$$X_{e,aft} = (X_{C.G.} - X_{aft}) \tag{43}$$

below $h = |X_{C.G.} - X_{aft}|$

$$X_{e,aft} = (X_{C.G.} - X_{aft})\left(1 - \left(1 - \frac{h}{-(X_{C.G.} - X_{aft})}\right)^2\right) \tag{44}$$

And the moment due to the 'hover' suckdown effects is given by;

$$\left(\frac{\Delta M}{Td}\right)_{hov} = C_{p,hov}\left[\left(\frac{A_{GV,fore}}{2A_j}\right)\left(\frac{X_{e,fore}}{d}\right) + \left(\frac{A_{GV,aft}}{2A_j}\right)\left(\frac{X_{e,aft}}{d}\right)\right] \quad (45)$$

Jet Wake Term

The pitching moment due to the jet wake effects is given by;

$$\left(\frac{\Delta M}{Td}\right)_{wake} = \left(\frac{\Delta M}{Td}\right)_{-,body} + \left(\frac{\Delta M}{Td}\right)_{GV,aft} + \left(\frac{\Delta M}{Td}\right)_{-,wing} \quad (46)$$

where $\left(\frac{\Delta M}{Td}\right)_{-,body}$ and $\left(\frac{\Delta M}{Td}\right)_{-,wing}$ are estimated by the method of reference 11,

and $\left(\frac{\Delta M}{Td}\right)_{GV,aft}$ is given by;

$$\left(\frac{\Delta M}{Td}\right)_{GV,aft} = \left(\frac{\Delta L}{T}\right)_{GV,aft}\frac{(X_{C.G.} - X_{GV,aft})}{d} \quad (47)$$

ANALYSIS AND DEVELOPMENT OF METHOD

The method for estimating the lift loss induced at forward speed in ground effect can be expressed as;

$$\frac{\Delta L}{T} = \left(\frac{\Delta L}{T}\right)_{GV} + \left(\frac{\Delta L}{T}\right)_{hov} + \left(\frac{\Delta L}{T}\right)_{wake} \quad (48)$$

where the first term accounts for the ground vortex effect, the second term accounts for the 'hover suckdown' effect, and the third term accounts for the jet wake effect (the effect of the free stream in generating the vortex pair in the jet wake).

The method of reference 9 can be used to estimate the second term for hovering flight (if experimental data is not available) but either must be modified to account for the effects of forward

speed. Similarly the method of reference 11 can be used to estimate the third term for transition out-of-ground-effect (if experimental data are not available) but either must be modified to account for the effects of ground proximity.

Unfortunately when operating at forward speed close to the ground (as in STOL operation) the data contains the effects of all three terms and there is no way to clearly identify and separate them. Some assumptions must be made in developing expressions for each of the terms. The data used and the assumptions made in developing each of the three terms in equation 48 will be presented and discussed in the following sections.

Ground Vortex Effects - Flat Plate Configurations

As shown in figure 2 a horseshoe shaped ground vortex is formed when the free stream, opposing the wall jet flowing forward from the impingement point of the front jet, rolls the wall jet back on itself. This ground vortex induces suction pressures on the ground (as depicted in the lower part of figure 3a) and, if the configuration is close to the ground, on the lower surface of the configuration (upper part of figure 3a).

Smaller positive pressures are induced ahead of the ground vortex. These positive pressures are generated by the blockage effect of the ground vortex causing the free stream to flow up and over the ground vortex. This up-flow puts the configuration at a positive angle of attack inducing positive pressure on the lower surface and negative pressures (not measured) on the upper surface.

Pressure Distribution Data

Detailed pressure distributions on a delta wing configuration with a variety of jet locations were obtained in reference 14. Figure 4 shows the planform of the configuration; two of the jet locations and the distribution of the pressure taps. The estimating method developed here is based largely on the data from this investigation and on the data and method developed in references 12 and 13. Figures 5 and 6 show typical pressure distributions. The pressure coefficients presented in reference 14, and as used here, are based on the jet dynamic pressure as defined in;

$$C_p = \frac{\Delta P}{q_j} = \frac{\Delta P}{T/2A_j} \qquad (49)$$

Out of ground effect (upper left of figure 5a) only the pressures induced by the jet/free-stream interaction are experienced. High suction pressures are induced (particularly on the centerline aft of the jet) by the roll up of the jet into a vortex pair (lower left in fig. 1). With the exception of the positive pressure close

to the jet on the centerline (in the stagnation region ahead of the jet) the positive pressures forward of the jet are negligible and within the scatter of the data. As the height is lowered the pressure distribution does not change significantly (essentially out-of-ground-effect results persist) until the height is lowered below about 8 diameters.

The effects of the ground vortex become apparent at the lower heights (fig. 5b). Large negative pressures are induced on the lower surface immediately over the ground vortex and positive pressures are induced ahead of it (lower right in figure 5b). The point at which the pressures change from negative to positive is further aft for the more outboard stations (y=7 and y=9 for example) reflecting the 'horseshoe shape' of the ground vortex. The magnitude of the pressures due to the ground vortex reduce rapidly with height and at a height of about 8 diameters the pressure distribution regains the shape typical of out-of-ground-effect conditions (very similar to figure 5a).

Close to the ground the ground vortex and the entrainment action of the wall jet created in hover predominate in generating the induced pressures. As the crossflow velocity is reduced the ground vortex contribution reduces and goes to zero at zero crossflow (in the hover mode). These effects of velocity ratio on the pressure distributions in ground proximity are shown in figure 6.

At the lowest height (h/d=1.7, fig. 6a) the pressure distribution in hover (V_e=0, lower right in fig. 6a) indicates that the hover suckdown is being generated in a condition referred to in ref. 9 as the 'trapped vortex' mode. That is, the lower surface is so close to the ground that the thickness of the wall jet essentially fills the space between the model and the ground. In this condition the normal entrainment effects are altered and somewhat below this height the methods for estimating the hover suckdown begin to breakdown.

At a height of h/d=3.3 (fig. 6b) the model is essentially out of the 'trapped vortex' mode and the more conventional pressure distribution induced in hover (V_e=0, lower right in fig. 6b) is obtained.

With a crossflow velocity (V_e=.06, lower left in fig. 6 a and b) the effects of the ground vortex become apparent as an increase in the negative pressures ahead of the jet and slight positive pressures further forward. The magnitude of these increments increase as the crossflow velocity increases (V_e=.1 and .2). Also the point at which the pressures change from negative to positive (the zero pressure point) moves aft as the velocity ratio increases.

Positive and Negative Pressure Regions

The pressure distributions presented in figures 5 and 6 represent only part of the data available for analysis. Unfortunately the data contain simultaneously the hover suckdown, the jet wake effects and the ground vortex effects. There is no direct way of separating the increments due to each of these. The present method was developed by dividing the planform into three areas (shown at the top of fig. 3a) and integrating the pressure distribution in each area to determine the lift and moment contribution of that area. The three areas are, 1) the positive pressure region forward of the zero pressure line, 2) the area between the zero pressure line and the jet, and 3) the area aft of the jet.

The zero pressure line was determined by examining all the pressure distributions (like fig. 5 and 6) to determine the station at which the pressure changed from negative to positive on the model centerline and at each spanwise station. The distance that the zero pressure point is forward of the jet, on the centerline of the model's lower surface (for the heights where it can be determined) is presented in figure 7 and compared with the position of the ground vortex on the ground (ref. 13 and 15) in figure 8. This distance X', for the configuration of reference 14, is given by;

$$\frac{X'}{d} = \frac{2}{V_\infty^{.4}} \left(\frac{h}{d}\right)^{.06 V_\infty^{-.7}} \qquad (50)$$

Figure 8 shows that, at the lower heights and velocity ratios, the zero pressure line is much further aft than the ground vortex position predicted by references 13 and 15. The position of the ground vortex on the ground was determined, in reference 13 from pressures on the ground and in reference 15 from flow visualization studies. Also at the higher velocity ratios and heights the zero pressure line is further forward of the predicted ground vortex position. These differences are probably due to the fact that the data of references 13 and 15 were for isolated jet impingement. The presence of the model affects the flow field and introduces the 'trapped vortex' condition at low heights (fig. 3c) which limits the forward projection of the ground vortex at low heights and velocities.

Subsequent development of the method and application to smaller planforms and bodies suggested that the position of the zero pressure line is a function of the planform area and that in the more general case;

$$\frac{X'}{d} = \frac{.6}{V_\infty^{.4}} \left(\frac{S}{A_j}\right)^{.2} \left(\frac{h}{d}\right)^{.06 V_\infty^{-.7}} \qquad (51)$$

At spanwise positions off the centerline the zero pressure point moves aft as expected, (fig. 9). The line dividing the positive pressures forward, from the negative pressures aft, is parabolic in shape and is given by;

$$y = 2\sqrt{X'(X'-x)} \tag{52}$$

where x is the distance forward from the jet station.

Negative Lift Increment

The net lift increment induced by the ground vortex (as defined here) consists of the difference between the suckdown induced aft of the line of zero pressure and the positive lift induced ahead of that line plus the upper surface increment.

The highest negative pressures induced by the ground vortex are felt at the lower heights in the region between the zero pressure line and the jet. Figure 10 presents the average pressure measured in this region and figure 11 presents the corresponding pressure aft of the jet. (Note the difference in scale between fig. 10 and fig. 11.) Separating out the contribution the ground vortex makes to these pressures is not straightforward because both the hover suckdown and the jet wake effects also induce suckdown pressures. The jet wake effects predominate at the highest heights (fig. 11a) and are felt primarily aft of the jet. The hover suckdown effects are felt mostly at the lowest heights and are present both fore and aft of the jet (fig. 10 and 11).

The increments of pressure induced by the ground vortex were extracted from the data by subtracting the increments induced by the impingement of the jet on the ground (the hover suckdown pressures) and those induced by the jet wake. The method used, and the assumptions made, in order to subtract these increments are presented in the following section.

Removal of 'Hover' increment;

The hover suckdown pressures were estimated by the method of reference 9. The average pressures induced in hover are compared with the estimated hover suckdown pressures in figure 12.
The hover suckdown pressures (ref. 9) were corrected for the effects of the 'trapped vortex' condition, that occurs at the lowest heights, by the method developed here. The 'trapped vortex' condition (ref. 9) occurs at heights below;

$$\left(\frac{h}{d}\right)_{tv} = .2\,(D_p - d)/d \tag{53}$$

Above this height the pressures induced in hover are given by (from reference 9);

$$C_{p,hov} = K_{aj}\left(\frac{h}{D_p - d}\right)^{e} K_{tv} \tag{54}$$

where

$$K_{aj} = -.043\frac{(NPR)^{-.1}(f_p)^{.13}}{S/A_j} \tag{55}$$

and

$$e = -2.3(NPR)^{-.1}(f_p)^{.13} \tag{56}$$

and above $(h/d)_{tv}$

$$K_{tv} = 1.0 \tag{57}$$

below $(h/d)_{tv}$, in the trapped vortex height range.

$$K_{tv} = 1 - \left(1 - \frac{h/d}{(h/d)_{tv}}\right)^{1.66} \tag{58}$$

Equation 54 was used to estimate the 'hover' increments that were subtracted from the data.

Removal of Jet wake increment;

The jet wake effects induced out of ground effect are estimated by the method of reference 11. Reference 6 suggested that these jet wake effects are reduced by the effects of ground proximity in truncating the wake. However part of the reduction is probably due to the upper surface increment (discussed below) which could not be separately identified by the analysis of reference 6.

For the present analysis the averaged pressures induced at the higher heights, fore and aft of the jet, were used as the jet wake increment, $C_{p,wake}$, and subtracted from the data throughout the height range.

Resulting ground vortex increment;

The ground vortex effect was obtained by subtracting the pressure increments due to hover suckdown and jet wake effects from the data;

$$C_{p,GV} = C_{p,data} - C_{p,hov} - C_{p,wake} \tag{59}$$

Figure 13 presents the increment of pressure induced by the ground vortex in the region forward of the jet and aft of the zero pressure line. As expected this increment decreases rapidly with height and increases with velocity ratio. There is also a significant effect of jet position, probably because the pressure distribution tends to be peaked on the centerline and near the jet. Also the induced pressures are reduced as the area forward of the jet is reduced. Other force data suggest that, for bodies, the fineness ratio of the configuration becomes a factor.

At the higher heights there is considerable scatter but the data indicates that the average pressure is inversely proportional to the square of the height. At the lower heights, where the ground vortex tends to fill the space between the lower surface and the ground, the slope is greatly reduced. The ground vortex increment induced forward of the jet is given by:

at the lower heights;

$$C_{p,GV,fore} = \frac{-10\ V_e}{(Y_{ave}/d)^2} \left(\frac{h}{d}\right)^{-8.4/\sqrt{S_{fwd}/A_j}} \tag{60}$$

at the higher heights;

$$C_{p,GV,fore} = -.1\ (f_p)^{.25} \left(\frac{h}{d}\right)^{-2} \tag{61}$$

The net negative lift increment induced by the ground vortex is given by;

$$\left(\frac{\Delta L}{T}\right)_{GV,neg.} = C_{p,GV,fore} \frac{A_{GV,fore}}{2A_j} \tag{62}$$

Most of the effects of the ground vortex are felt forward of the jet. Figure 14 presents the effect of ground proximity on the pressures aft of the jet. Because the average pressure increments induced aft of the jet are small there is considerable scatter in the data. But they are also <u>positive</u>! These increments are positive because they are obtained by subtracting the out-of-ground effect jet wake increment from the data throughout the height range, and at the lower heights the jet wake increment decreases as the jet wake is truncated by the ground proximity.

The average pressure shown in figure 14 therefore represents the reduction in the jet wake induced pressures rather than positive pressures induced by the ground vortex. This increment is given by;

$$C_{p,GV,aft} = .05\ V_e \left(\frac{h}{d}\right)^{-1.5} \tag{63}$$

The corresponding lift increment is given by;

$$\left(\frac{\Delta L}{T}\right)_{GV,aft} = C_{p,GV,aft}\frac{S_{aft}}{2A_j} \tag{64}$$

Positive Lift Increment

Determination of the positive lift increment assumes that the positive pressures forward of the zero pressure line are produced by the ground vortex. The positive lift increment induced by the ground vortex is given by;

$$\left(\frac{\Delta L}{T}\right)_{GV,p} = \frac{C_{p,GV,p}\ q_j\ A_{GV,p}}{T} = C_{p,GV,p}\ \frac{A_{GV,p}}{2A_j} \tag{65}$$

where $A_{GV,p}$ is the lower surface area forward of the zero pressure line and $C_{p,GV,p}$ is the average pressure coefficient in the positive pressure region. This pressure coefficient was determined by summing all the positive pressure increments forward of the zero pressure line and dividing by the product of the jet dynamic pressure and the area forward of the zero pressure line. The correlation of the average pressure coefficients thus obtained is presented in figure 15. The pressure coefficient is inversely proportional to the height, and to the .4 power of the ratio of the area forward of the jet to the jet area. Subsequent application of the correlation shown in figure 15 to the bodies of wing/body configurations showed that these positive pressures are also a function of the fineness ratio of the planform. The pressure coefficient is given by;

$$C_{p,GV,p} = \frac{.46\ V_e\ f_p^{.5}}{\left(\frac{h}{d}\right)\left(\frac{S_{fwd}}{A_j}\right)^{.4}} \tag{66}$$

Induced Upwash Lift

In addition to the pressures induced on the lower surface by the ground vortex there are apparently related, but unmeasured, pressures induced on the upper surface. As depicted in figure 16 the free stream is forced to flow up and over the ground vortex putting the configuration in an upwash.

This upwash produces the positive lifting pressures induced forward of the zero pressure line on the lower surface as discussed above. In addition it apparently induces lifting pressures on the upper surface that were not measured. This upper surface lift shows up (in the data of reference 14) as a difference between the balance data and that obtained by integrating the lower surface pressures.

The increment of lift carried on the upper surface was obtained by subtracting the lift determined by integrating the lower surface pressures from the balance lift;

$$\left(\frac{\Delta L}{T}\right)_{us} = \left(\frac{\Delta L}{T}\right)_{balance} - \left(\frac{\Delta L}{T}\right)_{lower\ surf.} \tag{67}$$

For estimating purposes it is assumed that the upper surface increment is equivalent to the configuration operating at an increased angle of attack and that the lift increment is given by;

$$\left(\frac{\Delta L}{T}\right)_{us} = C_{L_{\alpha_{body}}} \Delta\alpha_{us} \frac{qS}{T} = C_{L_{\alpha_{body}}} \Delta\alpha_{us} \frac{S}{2A_j} V_e^2 \tag{68}$$

and the induced upwash angle was obtained from;

$$\Delta\alpha = \frac{\left(\frac{\Delta L}{T}\right)_{us}}{C_{L_{\alpha_{body}}} \frac{S}{2A_j} V_e^2} \tag{69}$$

An example of the calculated induced upwash angle (for the configuration of reference 14 with a lift curve slope of $C_{L_{,\alpha}}$=.034,) is shown in figure 17. These data, and the other data at lower velocity ratios, indicate that the induced angle of attack is inversely proportional to the height, except at the lowest heights where the induced up wash angle appears to level off. This leveling off occurs because at the lower heights the ground vortex becomes flattened (top of figure 17) when it is trapped under the configuration. The height at which the effects of 'trapping' the ground vortex becomes significant is a function of the velocity ratio V_e.

At the lower heights the effective upwash angle is adjusted for the effect of this flattening by dividing the upwash angle calculated by equation 69 by the factor K_{tgv}. It is assumed that;

Below $h = .5\sqrt{S/A_j}\, V_e\, X'_{mac}$

$$K_{tgv} = \frac{h}{.5\sqrt{S/A_j}\, V_e\, X'_{mac}} \tag{70}$$

and above $h = .5\sqrt{S/A_j}\, V_e\, X'_{mac}$

$$K_{tgv} = 1.0 \tag{71}$$

The adjusted induced upwash angles experienced by the configuration of reference 14 are presented in figure 18. With the jet at station 20 an upwash is shown for all heights. However with the jet moved forward to station 12 the upwash is reduced and some downwash (negative lift increments) is experienced at the lower velocity ratios.

Downwash angles are to be expected if the ground vortex moves sufficiently forward. As sketched in figure 16 upwash angles are induced forward, and downwash angles aft, of the center of the vortex. Examination of the pressure data shows that the maximum negative pressure (which should occur at the vortex center) falls approximately midway between the jet and the zero pressure line. The distance X" is introduced to account for the location of the vortex center with respect to the configuration and is given by;

$$X'' = X'_{mac}/2 - (X_{jet} - X_{L.E.}) \tag{72}$$

where the distance from the jet station to the vortex center is calculated at the spanwise location of the MAC (Y_{MAC}) and (accounting for the parabolic shape of the ground vortex) is given by;

$$X'_{mac} = X' - \frac{Y^2_{mac}}{4X'} \tag{73}$$

A reasonable collapse of the upwash data for the model of reference 14 (fig. 19) was obtained by assuming that the upwash angle is inversely proportional to both the height, h/d, and velocity ratio, V_e. This correlation shows that if the wing leading edge is ahead of the apparent center of the ground vortex (negative values of X") the upwash induced on this configuration can be calculated by;

$$\Delta\alpha_{us} = \left[.7 - .7\frac{X''}{d} - .35\left|\frac{X''}{d}\right|^{1.2}\right]\frac{K_{tgv}}{V_e\ h/d} \tag{74}$$

If the wing leading edge is aft of the apparent center of the ground vortex (positive values of X") the induced flow changes to downwash and;

$$\Delta\alpha_{us}=\left[.7\ -.7\frac{X''}{d}\ +.16\left(\frac{X''}{d}\right)^{1.5}\right]\frac{K_{bgv}}{V_\infty\ h/d} \tag{75}$$

Net Lift increment induced by the Ground Vortex

The net lift increment induced by the ground vortex on a flat plate configuration is the sum of the lift loss induced between the zero pressure line and the jet and the positive lift increments induced ahead of the zero pressure line and on the upper surface;

$$\left(\frac{\Delta L}{T}\right)_{GV}=\left(\frac{\Delta L}{T}\right)_{GV,jet}+\left(\frac{\Delta L}{T}\right)_{GV,fore}+\left(\frac{\Delta L}{T}\right)_{us} \tag{76}$$

Moment Contribution of Ground Vortex

The moment contributions are estimated by assuming the lift to be acting at an effective arm. In general it was found that the distance from the moment reference point to the center of the area for which the lift was being estimated could be used as the effective arm. Thus for the positive lift generated forward of the zero pressure line, the moment increment is given by;

$$\left(\frac{\Delta M}{Td}\right)_{GV,p}=\left(\frac{\Delta L}{T}\right)_{GV,p}\frac{(X_{c.g.}-X_p)}{d} \tag{77}$$

For the negative lift generated between the jet and the zero pressure line the moment contribution is given by;

$$\left(\frac{\Delta M}{Td}\right)_{GV,fore}=\left(\frac{\Delta L}{T}\right)_{GV,fore}\frac{(X_{c.g.}-X_{GV,fore})}{d} \tag{78}$$

The upper surface lift increment is generated in a curved flow field (fig. 16) with upwash ahead of the jet and a smaller downwash aft of the jet. This curved flow field produces a camber type loading with the lift applied at the mid chord point of the Mean Aerodynamic Chord of the planform. For the present method the moment due to the upper surface lift increment is given by;

$$\left(\frac{\Delta M}{Td}\right)_{us}=\left(\frac{\Delta L}{T}\right)_{us}\frac{(X_{c.g.}-X_{.sMAC})}{d} \tag{79}$$

The total moment increment due to the ground vortex is given by;

$$\left(\frac{\Delta M}{Td}\right)_{GV} = \left(\frac{\Delta M}{Td}\right)_{GV,pos} + \left(\frac{\Delta M}{Td}\right)_{GV,fore} + \left(\frac{\Delta M}{Td}\right)_{us} \quad (80)$$

Jet Wake Effects

As indicated above in the section on estimating the ground vortex effect of the suckdown fore and aft of the jet, the jet wake effect is reduced by the effect of the ground in reducing the suction pressures aft of the jet.

For the present analysis the jet wake increment in ground proximity is assumed to be given by;

$$\left(\frac{\Delta L}{T}\right)_{wake} = \left(\frac{\Delta L}{T}\right)_{\infty} + \left(\frac{\Delta L}{T}\right)_{GV,aft} \quad (81)$$

where $\left(\frac{\Delta L}{T}\right)_{\infty}$ is estimated by the method of reference 11 and $\left(\frac{\Delta L}{T}\right)_{GV,aft}$ is given by equation 63.

The pitching moment due to the jet wake effects, like the lift loss reduces with height, and is given by;

$$\left(\frac{\Delta M}{Td}\right)_{wake} = \left(\frac{\Delta M}{Td}\right)_{\infty} + \left(\frac{\Delta M}{Td}\right)_{GV,aft} \quad (82)$$

where $\left(\frac{\Delta M}{Td}\right)_{\infty}$ is estimated by the method of reference 11 and $\left(\frac{\Delta M}{Td}\right)_{GV,aft}$ is given by;

$$\left(\frac{\Delta M}{Td}\right)_{GV,aft} = \left(\frac{\Delta L}{T}\right)_{GV,aft} \frac{(X_{c.g.} - X_{GV,aft})}{d} \quad (83)$$

'Hover' Suckdown Effects

The method used above in estimating the ground vortex increments assumes that the pressures induced in hover by the impingement of the jet are not altered by the cross flow but that their effects are constrained to the region aft of the zero pressure line on the lower surface of the configuration. The average suckdown pressure

was subtracted from the measured average pressure to get the average pressure attributed to the ground vortex. The 'hover' suckdown effects are therefore estimated by applying the average suckdown pressure estimated from the method of reference 9 to the appropriate areas.

The hover suckdown term therefore is the sum of the lift loss induced forward of the jet and that induced aft of the jet and is given by;

$$\left(\frac{\Delta L}{T}\right)_{hov} = C_{p,hov}\left(\frac{A_{GV,fore} + A_{GV,aft}}{2A_j}\right) \tag{84}$$

The hover suckdown pressures, estimated by the method of reference 9, were corrected for the effects of the 'trapped vortex' condition that occurs at the lowest heights, by the method developed here. The 'trapped vortex' condition occurs (ref. 9) at heights below;

$$\left(\frac{h}{d}\right)_{tv} = \frac{.2(D_p - d)}{d} \tag{85}$$

Above this height the pressures induced in hover are given by (from ref. 9);

$$C_{p,hov} = K_{aj}\left(\frac{h}{D_p - d}\right)^{e} K_{tv} \tag{86}$$

where

$$K_{aj} = -.043\frac{(NPR)^{-.1}(f_p)^{.13}}{S/A_j} \tag{87}$$

and

$$e = -2.3(NPR)^{-.1}(f_p)^{.13} \tag{88}$$

and above $(h/d)_{tv}$

$$K_{tv} = 1.0 \tag{89}$$

In the trapped vortex height range, below $(h/d)_{tv}$

$$K_{tv} = 1 - \left(1 - \frac{h/d}{(h/d)_{tv}}\right)^{1.66} \tag{90}$$

The pitching moment induced in hover is the difference between the nose down moment generated by the suckdown ahead of the jet and the nose up moment induced aft of the jet. At the higher heights, as shown in reference 9, these moments are given by the lift loss acting at the center of area. However below a height equal to the distance from the jet to the center of area the moment arm, X_e, reduces rapidly.

Forward of the jet (between the zero pressure line and the jet) and above $h = X_{C.G.} - X_{fore}$

$$X_{e,fore} = (X_{C.G.} - X_{fore}) \tag{91}$$

below $h = X_{C.G.} - X_{fore}$

$$X_{e,fore} = (X_{C.G.} - X_{fore})\left(1 - \left(1 - \frac{h}{(X_{C.G.} - X_{fore})}\right)^2\right) \tag{92}$$

Aft of the jet,
and above $h = |X_{C.G.} - X_{aft}|$

$$X_{e,aft} = (X_{C.G.} - X_{aft}) \tag{93}$$

below $h = |X_{C.G.} - X_{aft}|$

$$X_{e,aft} = (X_{C.G.} - X_{aft})\left(1 - \left(1 - \frac{h}{-(X_{C.G.} - X_{aft})}\right)^2\right) \tag{94}$$

And the moment due to the 'hover' suckdown effects is given by;

$$\left(\frac{\Delta M}{Td}\right)_{hov} = C_{p,hov}\left[\left(\frac{A_{GV,fore}}{2A_j}\right)\left(\frac{X_{e,fore}}{d}\right) + \left(\frac{A_{GV,aft}}{2A_j}\right)\left(\frac{X_{e,aft}}{d}\right)\right] \tag{95}$$

Comparison with Experiment

The ability of the method to estimate the data from which it was developed is presented in figures 20 to 22. The data are for two flat plate models of reference 14.

Figure 20 shows the comparison for $V_e = 0$ (hover) where the ground vortex and wake effects are not present. This comparison is included for completeness and is the same comparison shown in reference 9 except that the effects of the trapped vortex condition, which occurs at the lowest heights, are included here.

Figures 21 and 22 show the effect of forward speed (for the jets located at stations 20 and 12 respectively) and also include the relative magnitude of the 'hover suckdown' term, the 'jet wake' term and the breakdown of the vortex term. The agreement is relatively good except for the moments estimates for the case of the jet at station 12. The problem appears to be with the jet wake effect at high heights. There is probably an error in the out-of-ground-effect force data. These force data were not even presented in reference 11 (the method for estimating the induced effects out-of-ground effect) because these force data were totally inconsistent with all the other data available.

Figure 23 presents comparisons of the estimates made by the present method and by the methods of reference 6 and 13 with the data for two flat plate models of reference 6.

Wing-Body Configurations

The above analysis applies to delta wing, flap plate and body configurations where the lower surface is of uniform planform and in one plane. Data on the effects of the ground vortex on wing-body configurations are available from references 6 and 13. The ground vortex induced upwash on three of the models of reference 13 and the one circular jet model from reference 6 are presented in figure 24. These data were obtained by subtracting the estimated contribution of the ground vortex to the body lift from the ground vortex induced wing-body lift data to calculate the induced upwash angles. Thus these data contain the effects of the pressures induced on both the upper and lower surface of the wing. The lift increments (and therefore the associated effective upwash angles) are therefore larger (at a given height) than those for the upper surface lift increment for the delta wing configuration of reference 14.

The induced upwash is seen to be a function of the position of the wing relative to the jet. More specifically the analysis shows that the effective induced upwash angle depends on the location of the

wing leading edge relative to the center of the ground vortex. The correlation presented in figure 25 indicates that the induced upwash is given by;

for negative values of X"

$$\Delta\alpha_{wb} = \left[-.06\frac{X''}{d} + .016\left(\frac{X''}{d}\right)^2 \right] \frac{K_{tgv}}{V_e^2\left(\frac{h_w}{d}\right)^a} \tag{96}$$

for positive values of X"

$$\Delta\alpha_{wb} = \left(-.06\frac{X''}{d} \right) \frac{K_{tgv}}{V_e^2\left(\frac{h_w}{d}\right)^a} \tag{97}$$

where the exponent, a, is given by;

$$a = 1 + .06V_e\left(\frac{X_{jet} - X_{L.E.}}{d}\right)^2 \tag{98}$$

and where X" is the distance from the assumed center of the ground vortex to the wing leading edge, given by;

$$\frac{X''}{d} = \frac{\frac{X'_{mac}}{2} - (X_{jet} - X_{L.E.})}{d} \tag{99}$$

There are little data available on the effect of wing height on mid- and high-wing configurations. Most of the data available for this study were for configurations with the wing and body lower surface in the same plane as the jet exit. It is suggested that in using this method, the ground vortex characteristics and their effect on the pressures induced on the body should be based on the height of the jet exit (assuming the jet is issuing from the lower surface of the body). If the wing lower surface is not co-planer with the body lower surface the height of the wing above the ground h_w is used in calculating the upwash (eq. 96 and 97).

At some combinations of low velocity ratio, V_e, and low height, h_w. equation 48 will calculate increments of induced upwash angle of attack that would carry the wing beyond stall. For these condi-

tions it is suggested that; if $\Delta\alpha > (\alpha_{stall} - \alpha)$ *then use* $\Delta\alpha = (\alpha_{stall} - \alpha)$

Comparisons of the estimates with the data for the body alone, for three wing-body configurations of reference 13 and one wing-body configuration from reference 6 are presented in figures 26 and 27.

The estimated increase in lift (decrease in lift loss) due to raising the wing from the low to the high position for the model of reference 6 is in good agreement with the data for the lowest velocity ratio (fig. 27 a) but the comparison is poor at the higher velocity ratios. Part of the problem is in the less than satisfactory agreement out of ground effect.

Jet Deflection and Jet Shape

The energy of the wall jet flowing outward from the impingement point of a vertically impinging circular jet is the same in all directions. However if the jet is deflected fore or aft, or is non-circuclar in shape, the radial distribution of the energy in the wall jet is no longer uniform and, in the presence of a crossflow, the position and strength of the ground vortex and therefore the pressures induced are changed.

In hover, deflection of the jet fore or aft significantly reduces the suckdown pressures and associated lift loss. Reference 6 showed that the lift loss in hover is a function of the square of the sine of the deflection angle. For the present method it is assumed that the suckdown pressures induced in hover are given by;

$$C_{p,hov} = \sin^2 \delta \left(\frac{h}{D_p - d}\right)^{*} K_{sj} K_{cv} \qquad (100)$$

At forward speeds deflection of the jet forward or aft of the vertical moves the ground vortex for or aft and will move the zero pressure line, and change the size of the negative and positive pressure regions as well. Unfortunately there are no data available on the effect of jet deflection on the location of the zero pressure line. The method developed here was arrived at by reviewing previous methods for estimating the effects of jet deflection (ref. 6 and 13) and by cut and try applications of various possible approaches to the limited data available (ref. 6).

Two effects determine the distance the ground vortex is moved by deflection of the jet. The projected impingement point of the jet is moved a distance of $\frac{h}{d}\tan(\delta - 90)$. In addition when the jet impinges on the ground at an angle more of the jet flow is directed

in the direction the jet is deflected and less is directed in the other direction. (That is, if the jet is deflected aft less than half of the jet flow is directed forward to oppose the free stream flow and the ground vortex is moved further aft than would be computed from the projected impingement point.) However this second effect appears to have little effect on the effective position of the zero pressure line and for the present method the expression for estimating the forward projection of the zero pressure line, including the effects of jet deflection, is;

$$\frac{X'}{d} = \frac{h}{d}\tan(\delta - 90) + .6\left(\frac{S}{A_j}\right)^{.2} V_e^{-.4}\left(\frac{h}{d}\right)^{.06V_e^{-.7}} \qquad (101)$$

Although the dividing of the impinging flow appears to have little effect of the location of the zero pressure line it apparently does affect the pressures induced on the lower surface. It was found that a good estimate of the effect of jet deflection on the net lift and moment could be obtained by multiplying these pressures, as well as the induced upwash angles, by $\left(\frac{\delta}{90}\right)^2$. In addition it was found that the effects of the jet shape, on most terms, could be accounted for by dividing by the 1/4 power of the nozzle aspect ratio.

Thus the pressure in the positive pressure region is given by;

$$C_{p,GV,p} = \frac{\left(\frac{\delta}{90}\right)^2}{A_n^{.25}} \frac{.46\ V_e\ f_p^{.25}}{\left(\frac{h}{d}\right)\left(\frac{S_{fwd}}{A_j}\right)^{.4}} \qquad (102)$$

The effect on the negative pressures between the zero pressure line and the jet is given by;

at the lower heights;

$$C_{p,GV,fore} = \frac{-10\ V_e}{A_n^{.25}}\left(\frac{\delta}{90}\right)^2\left(\frac{Y_{ave}}{d}\right)^{-2}\left(\frac{h}{d}\right)^{-0.4/\sqrt{S_{fwd}/A_j}} \qquad (103)$$

at the higher heights;

$$C_{p,GV,fore} = \frac{-.1\ f_p^{.25}}{A_n^{.25}}\left(\frac{\delta}{90}\right)^2\left(\frac{h}{d}\right)^{-2} \qquad (104)$$

The effect of nozzle aspect ratio on the wake term was found to be opposite that on most other terms, in that the incremental pressures induced by the ground vortex aft of the jet appeared to be increased by increasing the nozzle aspect ratio. The average pressure in the wake region is given by;

$$C_{p,gv,aft} = .05\ V_e\ A_n^{.5} \left(\frac{\delta}{90}\right)^2 \left(\frac{h}{d}\right)^{-1.5} \tag{105}$$

The upwash induced on a flat plate, with the leading edge forward of the apparent center of the ground vortex (negative values of X"), is given by;

$$\Delta\alpha_{us} = \left[.7 - .7\frac{X''}{d} - .35\left|\frac{X''}{d}\right|^{1.2}\right] \frac{K_{tgv}}{V_e\ h/d}\ \frac{(\delta/90)^2}{A_n^{.25}} \tag{106}$$

If the wing leading edge is aft of the apparent center of the ground vortex (positive values of X") the induced flow changes to downwash and;

$$\Delta\alpha_{us} = \left[.7 - .7\frac{X''}{d} + .16\left(\frac{X''}{d}\right)^{1.5}\right] \frac{K_{tgv}}{V_e\ h/d}\ \frac{(\delta/90)^2}{A_n^{.25}} \tag{107}$$

where X" is given by;

$$X'' = X'_{MAC}/2 - (X_{jet} - X_{L.E.}) \tag{108}$$

Similarly the induced upwash angle on the wing of a wing body configuration is given by;

for negative values of X"

$$\Delta\alpha_{wb} = \left[-.06\frac{X''}{d} + .016\left(\frac{X''}{d}\right)^2\right] \frac{K_{tgv}}{V_e^2\ (h_w/d)^a}\ \frac{(\delta/90)^2}{A_n^{.25}} \tag{109}$$

for positive values of X"

$$\Delta\alpha_{wb} = \left(-.06\frac{X''}{d}\right) \frac{K_{tgv}}{V_e^2\ (h_w/d)^a}\ \frac{(\delta/90)^2}{A_n^{.25}} \tag{110}$$

where the exponent, a, is given by;

$$a = 1 + .06 V_e \left(\frac{X_{jet} - X_{L.E.}}{d}\right)^2 \tag{111}$$

and where X" is the distance from the assumed center of the ground vortex to the wing leading edge, given by;

$$\frac{X''}{d} = \frac{\frac{X'_{mac}}{2} - (X_{jet} - X_{L.E.})}{d} \qquad (112)$$

In addition the 'hover suckdown' term is modified by the nozzle aspect ratio and jet deflection and is given by;

$$C_{p,hov} = \frac{\sin^2 \delta}{1+V_e(A_R-1)}\left(\frac{h}{D_p-d}\right)^* K_{aj}\, K_{tv} \qquad (113)$$

Estimates for the configurations of reference 6 with the jets deflected fore and aft of the vertical are compared with the data in figure 28.

Similarly estimates for the configurations of reference 6 with rectangular jets are compared with the data in figure 29.

Fixed vs. Moving Ground

Most of the data on the effects of the ground vortex (including that from ref. 14, the primary reference used in developing the present method) were obtained in a wind tunnel over a fixed ground board. A fixed ground board simulates the configuration hovering in a cross wind (with an arbitrary boundary layer) but, as shown in figure 30, does not adequately simulate the flow field generated when the configuration is moving over the ground.

Two factors are involved. First, the boundary layer between the free stream flow and the fixed ground board is absent when the model is moving over the ground. Second when the configuration is moving over the ground (or tested over a moving belt), as shown in figure 30, the ground (or belt) tends to erode the forward flowing wall jet. (The layer of air on the ground (or belt) is pulled aft with the ground or belt.) Both effects, the boundary layer and the absence of scrubbing action allow the wall jet (and therefore the ground vortex) to project further forward over the fixed ground than would be the case with the moving model.

The results of several investigations of the effect of moving model and moving ground (belt) on the ground vortex position (ref. 13, 15, 16 and 17) are compared in figure 31. (The results from ref. 16 and 17 are presented in the 'fairing of moving model data (fig. D4 of ref. 13).) First it should be noted, as pointed out in

references 15 and 18, that the ground vortex is very unsteady making it difficult to accurately determine the average penetration of the vortex. This results in considerable scatter in the data.

The two methods for estimating the forward penetration of the ground vortex are in reasonable agreement with the data for the fixed model over the fixed ground. The most scatter is for the belt/moving-model data, particularly at the lower velocity ratios, (higher values of $1/V_e$). Never the less the data suggest that with the belt, or with a moving model, the forward projection is only about 2/3 that observed with a fixed model over a fixed ground. Reference 19 also shows less forward projection of the ground vortex over the 'rolling road' (as they refer to a belt ground board) but the ratio is closer to 3/4 than to 2/3 as shown in figure 31.

For the present method it is assumed that the position of the zero pressure line will also be further aft for the moving model case and that the expression (eq. 50) for calculating the position of the zero pressure line will be changed to;

$$\frac{X'}{d} = K_{gb}\left(\frac{.6}{V_e^{.4}}\left(\frac{S}{A_j}\right)^{.2}\left(\frac{h}{d}\right)^{.06/V_e^{.7}}\right) \qquad (114)$$

where for a model tested over a moving belt ground board or an aircraft moving over the ground; $K_{gb} = .67$
and for a model over a fixed ground board or an aircraft hovering in a crosswind; $K_{gb} = 1.0$

Figure 32 shows the effect of the change in the position of the zero pressure line due to the moving ground (applying only eq. 68). Moving the zero pressure line aft increases the positive pressure area forward of the zero pressure line and also increases the upwash angle, resulting in an increase in induced lift. However the experimental increment due to the belt shows a lift loss at the higher velocity ratios.

This lift loss induced by the belt (moving ground) is probably associated with a reduction in the ground vortex strength. As sketched in figure 30 (and discussed above) the effect of the ground surface moving aft under the wall jet is to erode the forward projected wall jet and reduce its energy.

There have been no direct measurements of the ground vortex strength, therefore the method presented here was arrived at by cut and try applications of logical approaches. Reducing the pressures induced by the ground vortex in direct proportion to the forward projection of the zero pressure line worked well for the flat plate configurations. Thus the average pressure in the positive

pressure region is given by;

$$C_{p,GV,p} = K_{gb} \frac{\left(\frac{\delta}{90}\right)^2}{A_n^{.25}} \frac{.46\ V_e\ f_p^{.5}}{\left(\frac{h}{d}\right)\left(\frac{S_{fwd}}{A_j}\right)^{.4}} \tag{115}$$

The effect on the negative pressures between the zero pressure line and the jet is given by;

at the lower heights;

$$C_{p,GV,fore} = K_{gb} \frac{-10\ V_e}{A_n^{.25}} \left(\frac{\delta}{90}\right)^2 \left(\frac{Y_{ave}}{d}\right)^{-2} \left(\frac{h}{d}\right)^{-8.4/\sqrt{S_{fwd}/A_j}} \tag{116}$$

at the higher heights;

$$C_{p,GV,fore} = K_{gb} \frac{-.1\ f_p^{.25}}{A_n^{.25}} \left(\frac{\delta}{90}\right)^2 \left(\frac{h}{d}\right)^{-2} \tag{117}$$

The average pressure in the wake region is given by;

$$C_{p,GV,aft} = K_{gb}\ .05\ V_e\ A_n^{.5} \left(\frac{\delta}{90}\right)^2 \left(\frac{h}{d}\right)^{-1.5} \tag{118}$$

The data from the wing/body models of reference 13 showed that the effect of the moving ground on the induced upwash depends on the location of the wing leading edge with respect to the jet. It was found that reasonable agreement could be obtained by multiplying the induced upwash angle by $K_{gb}^{.12\left(\frac{X_{jet}-X_{L.E.}}{d}\right)}$

for negative values of X"

$$\Delta\alpha_{wb} = K_{gb}^{.2\left(\frac{X_{jet}-X_{L.E.}}{d}\right)} \left[-.06\frac{X''}{d} + .016\left(\frac{X''}{d}\right)^2 \right] \frac{K_{tgv}}{V_e^2\ (h_w/d)^2} \frac{(\delta/90)^2}{A_n^{.25}} \tag{119}$$

for positive values of X"

$$\Delta\alpha_{wb} = K_{gb}^{.2\left(\frac{X_{jet}-X_{L.E.}}{d}\right)} \left(-.06\frac{X''}{d}\right) \frac{K_{tgv}}{V_e^2\ (h_w/d)^2} \frac{(\delta/90)^2}{A_n^{.25}} \tag{120}$$

where the exponent, a, is given by;

$$a = 1 + .06 V_e \left(\frac{X_{jet} - X_{L.E.}}{d} \right)^2 \qquad (121)$$

Similarly the upwash angle induced on a flat plate, or body, configuration is given by;

for negative values of X"

$$\Delta\alpha_{us} = K_{gb}^{.2\left(\frac{X_{jet}-X_{L.E.}}{d}\right)} \left[.7 - .7\frac{X''}{d} - .35\left|\frac{X''}{d}\right|^{1.2} \right] \frac{K_{tgv}}{V_e \; h/d} \; \frac{(\delta/90)^2}{A_n^{.25}} \qquad (122)$$

for positive values of X"

$$\Delta\alpha_{us} = K_{gb}^{.2\left(\frac{X_{jet}-X_{L.E.}}{d}\right)} \left[.7 - .7\frac{X''}{d} + .16\left(\frac{X''}{d}\right)^{1.5} \right] \frac{K_{tgv}}{V_e \; h/d} \; \frac{(\delta/90)^2}{A_n^{.25}} \qquad (123)$$

Comparisons of estimates of the effects of testing over fixed and moving ground with the corresponding experimental increments for several configurations of ref. 13 are presented in figures 33.

Problems had been encountered during the development of the method, at low heights and velocity ratios where equation 122 and 123 predicted excessively large induced upwash angles; upwash angles that would carry the wing beyond stall. For these conditions it was suggested above that; if $\Delta\alpha > (\alpha_{stall} - \alpha)$ *then use* $\Delta\alpha = (\alpha_{stall} - \alpha)$

A limiting upwash angle of $\Delta\alpha = 10$ deg. was assumed in making the estimates presented in figure 33. The effect of this limiting angle of attack is shown in figure 34 in the leveling off of the wing contribution at the lower velocity ratios and heights. However, for some configurations at low heights and velocity ratios (see fig. 33 c and 33 f) the method tends to over predict the reduction in lift loss. Never the less, as shown in figure 35, the general trends of the difference between lift increment induced over fixed and moving ground tends to be generally well predicted.

Vogler, in one of the first investigations of the effect of the ground on jet induced lift (ref. 20) had shown little or no difference between fixed and moving ground. The model was a high wing configuration with a relatively small total planform area to jet area ratio, and as shown in figure 36 the present method is in general agreement with his conclusions in that the predicted increments due to moving ground are of the same order of magnitude as the experimental scatter.

CONCLUDING REMARKS

The method developed here is based on detailed pressure distribution data and thereby gives some insight into the origin of the lift and moments induced by the ground vortex.

The method includes the effects of configuration variables, height and operating conditions as well as the effects of the location, deflection and shape of the jet. However it is limited to single jet configurations at subcritical nozzle pressure ratios.

An analysis of the effects of moving over the ground vs. tests at forward speeds over a fixed ground board is included.

REFERENCES

1. Kotansky D.R.; "Jet Flowfields" in "Special Course on V/STOL Aerodynamics," AGARD-R-710, pp 7-1 to 7-48, April 1984.
2. Margason, R.J.; "Fifty Years of Jet in Cross Flow Research." Presented at 72nd AGARD Fluid Dynamics Panel Meeting and Symposium on Computational and Experimental Assessment of Jet in Cross Flow. April, 1993.
3. Margason, R.J.; "Propulsion-Induced Effects Caused by Out-of-Ground Effects," SAE 872307, in "Proceedings of the International Powered Lift Conference," SAE P-203, Dec. 1987, pp 31-58.
4. Anon.; "Analysis of a jet in a Subsonic Crosswind," NASA SP-218, Sept. 1969.
5. Margason, R.J.; "1987 Ground Vortex Workshop" NASA CP-10008, April 1987.
6. Stewart, V.R. and Kuhn, R.E.; "A Method for Estimating the Propulsion Induced Aerodynamic Characteristics of STOL Aircraft in Ground Effect," NADC 80226-60, Aug. 1983.
7. Henderson, C., Clark, J, and Walters, M,; "V/STOL Aerodynamics and Stability and Control Manual," NADC-80017-60, Jan. 1980.
8. Kuhn, R.E.; "An Engineering Method for Estimating the Induced Lift on V/STOL Aircraft Hovering in and out of Ground Effect" NADC Rept. No. NADC-80246-60, Jan. 1981.

9. Kuhn, R.E., Stewart, V.R. and Wardwell, D.A.; "Estimation of Lift and Pitching Moment Induced on Jet STOVL Aircraft Hovering in Ground Effect" WL-TR-93-3046. Aug. 1993.

10. Stewart, V.R. and Kuhn, R.E.; "A Method for Prediction of the Aerodynamic Stability and Control Parameters of STOL Aircraft Configurations - Volume II: STOL Aerodynamic Stability and Control Parameter Estimation Methods" AFWAL-TR-87-3019, June 1987.

11. Kuhn, R.E.; "An Empirical Method for Estimating the Jet Induced Lift and Pitching Moment on STOVL Aircraft out of Ground Effect" WL-TR-96-3042.

12. Stewart, V.R. and Kuhn. R.E.; "Lift and Pitching moment induced on Jet STOVL Aircraft by the Ground Vortex - Data Report" WL-TR-93-3045, June 1993.

13. Stewart, V.R. and Kuhn, R.E.; "Estimation of Lift and Pitching Moment Induced on Jet STOVL Aircraft by the Ground Vortex" WL-TR-93-3061, Aug. 1993.

14. Kuhn, R.E. and Stewart, V.R.; "Lift and Pitching Moment Induced on Jet STOVL Aircraft Hovering in Ground Effect - Data Report" WL-TR-93-3044. June 1993.

15. Kuhn, R.E., Del Frate, J.H. and Eshleman, J.E.; "Ground Vortex Flow Field Investigation" in "1987 Ground Vortex Workshop" NASA CP-10008, pp 61 - 90, April 1987.

16. Abbott, W.A.; "Studies of Flow Fields created by Vertical and Inclined Jets Moving over a Horizontal Surface", ACR Cp No. 911, 1967.

17. Stewart, V.R. and Kemmerly, G.; "Characteristics of the Ground Vortex Formed by a Jet Moving over a Fixed Ground Plane", AIAA 89-0650, Jan. 1989.

18. Cimbala, J.M., Billet, M.L. and Gaublomme, D.P.; "Experiments on the Unsteady Ground Vortex" NASA CR 177566, Aug. 1990.

19. Knowles, K., Bray, D. Bailey, P.J. and Curtis, P.; "Impinging Jets in Cross Flow" RAS Aeronautical Journal, paper # 1848, Feb. 1992.

20. Vogler, R.D.; "Ground Effects on Single- and Multiple-jet VTOL Models at Transition Speeds over Stationary and Moving Ground Planes" NASA TN D-3213, Jan. 1966.

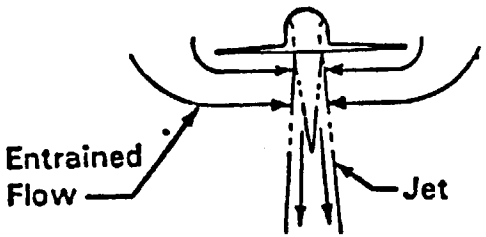

Out-of-Ground-Effect

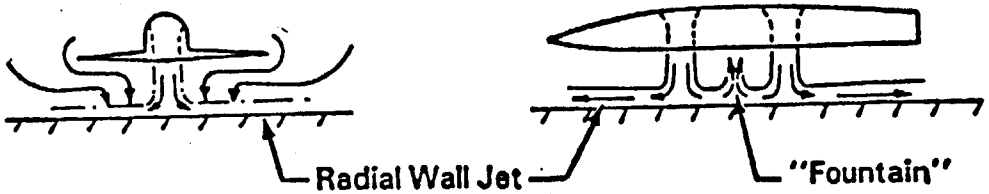

Hover In-Ground-Effect

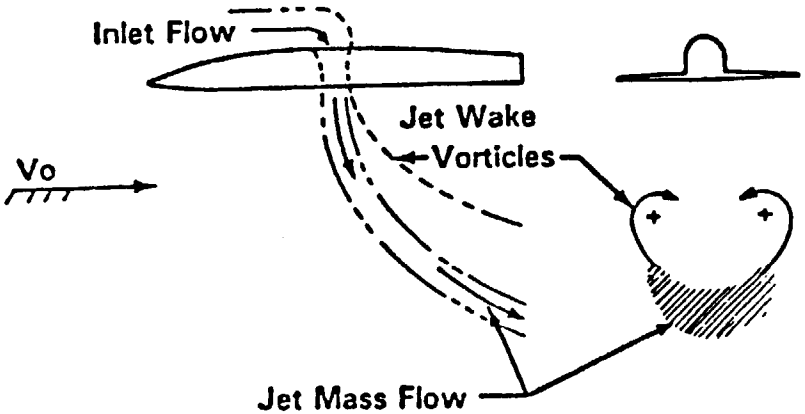

Transition Out-of-Ground-Effect

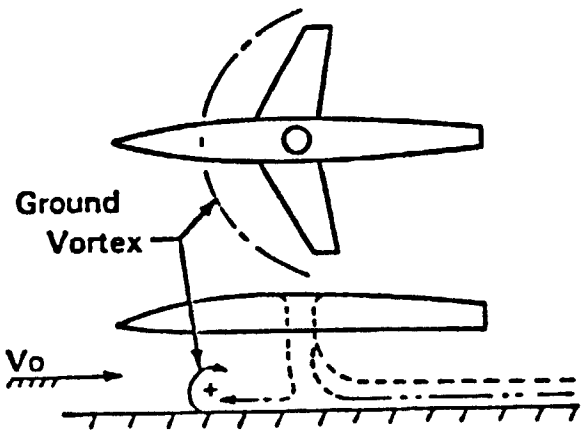

Transition In-Ground-Effect
(STOL Operation)

Figure 1.- Flow fields in and out of ground effect.

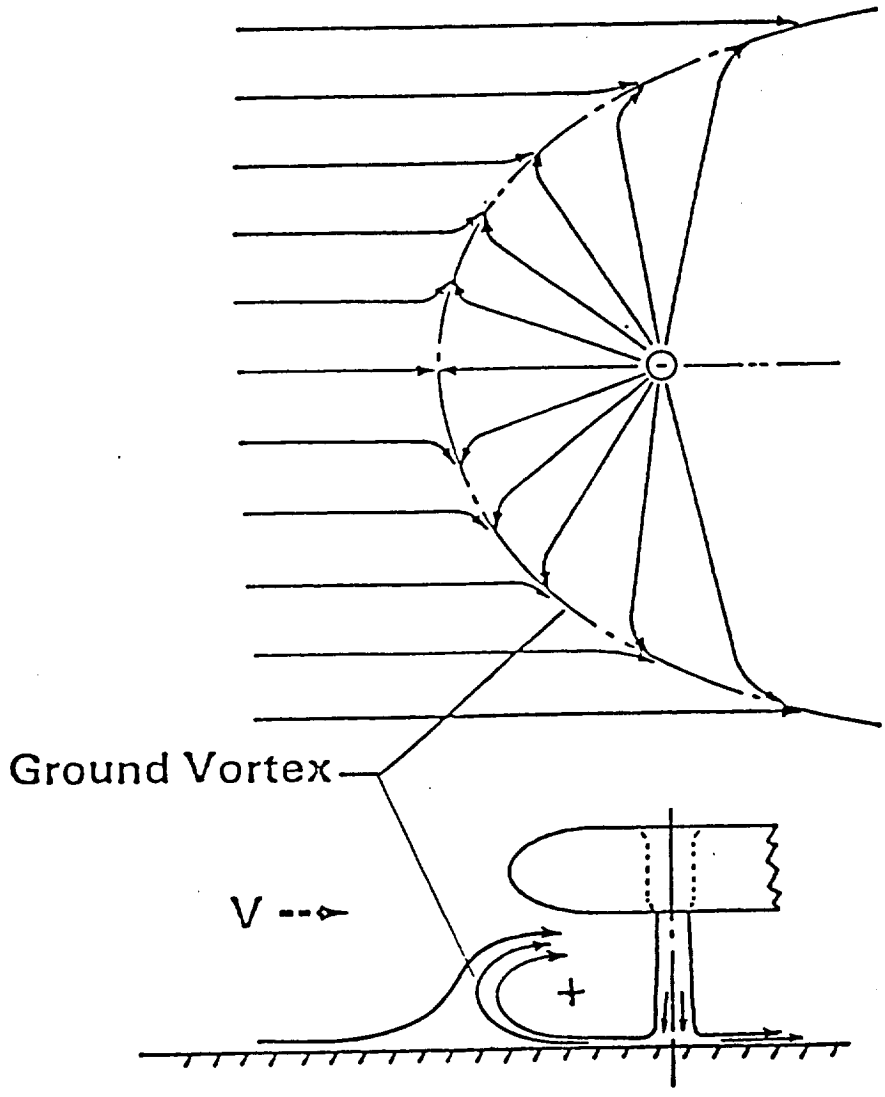

Figure 2.- Formation of the ground vortex

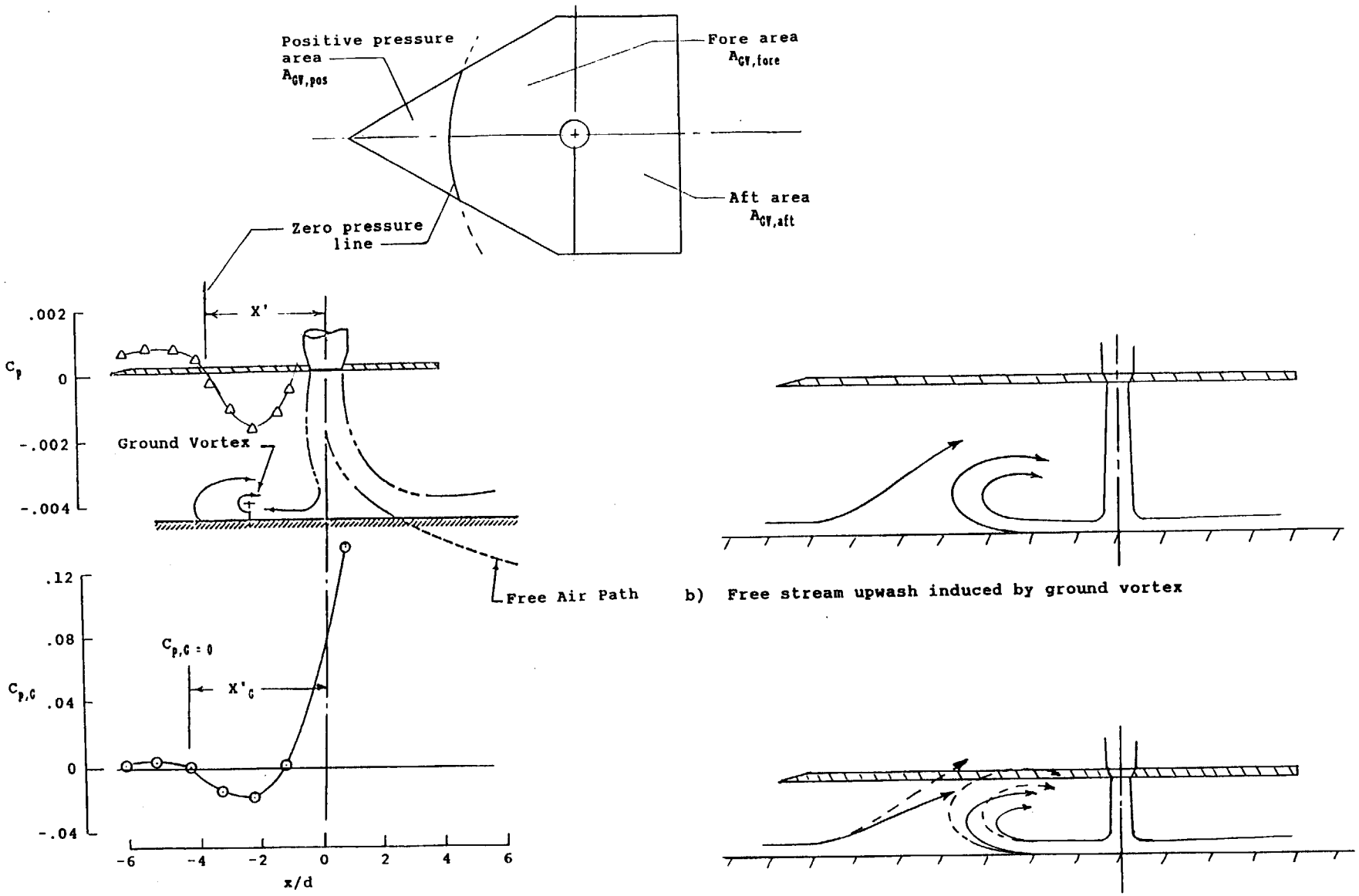

Figure 3.- Schematic sketches of ground vortex induced flow fields and pressures.

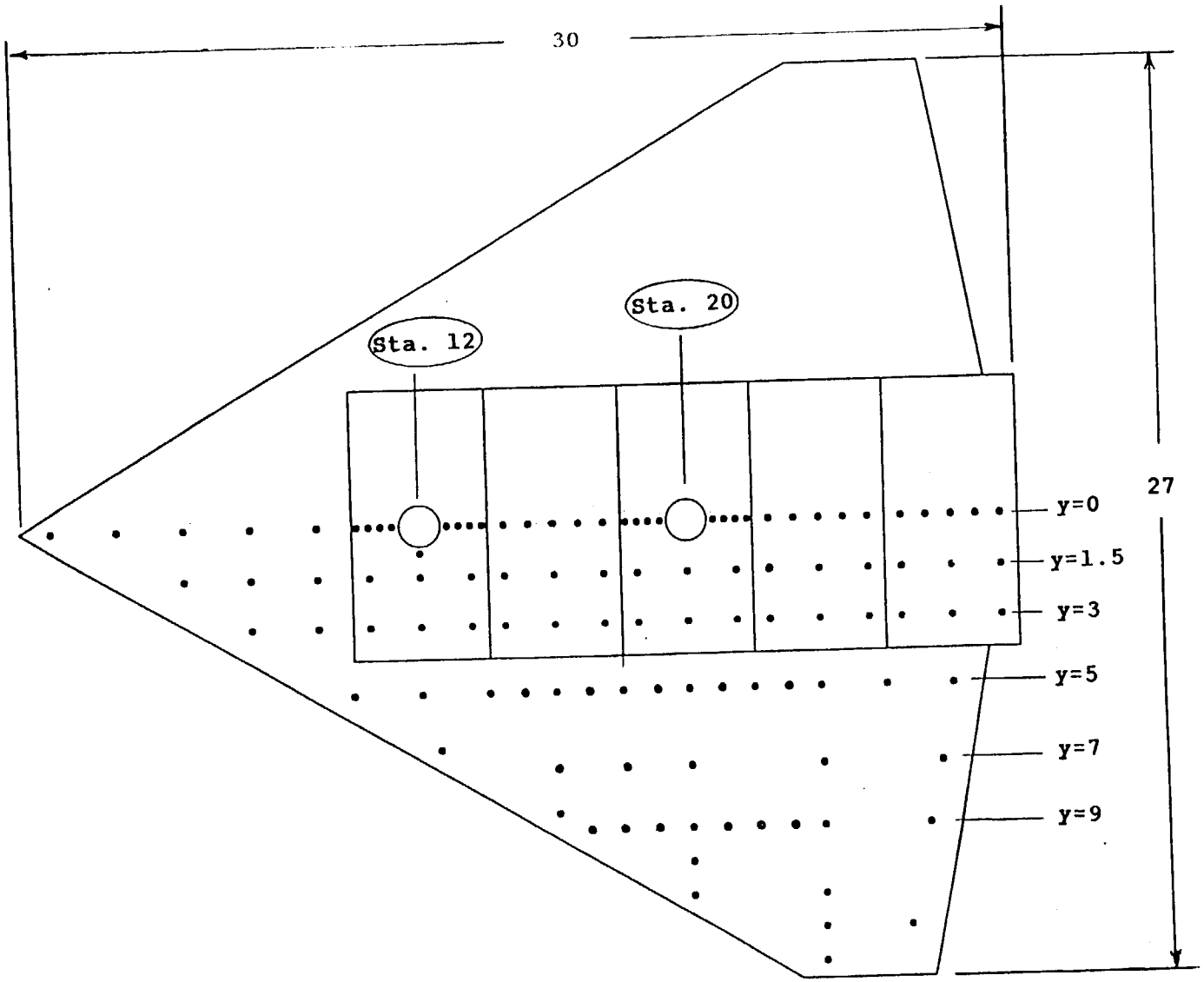

Figure 4.- Configuration of model of reference 14, showing locations of pressure taps and two jets positions.

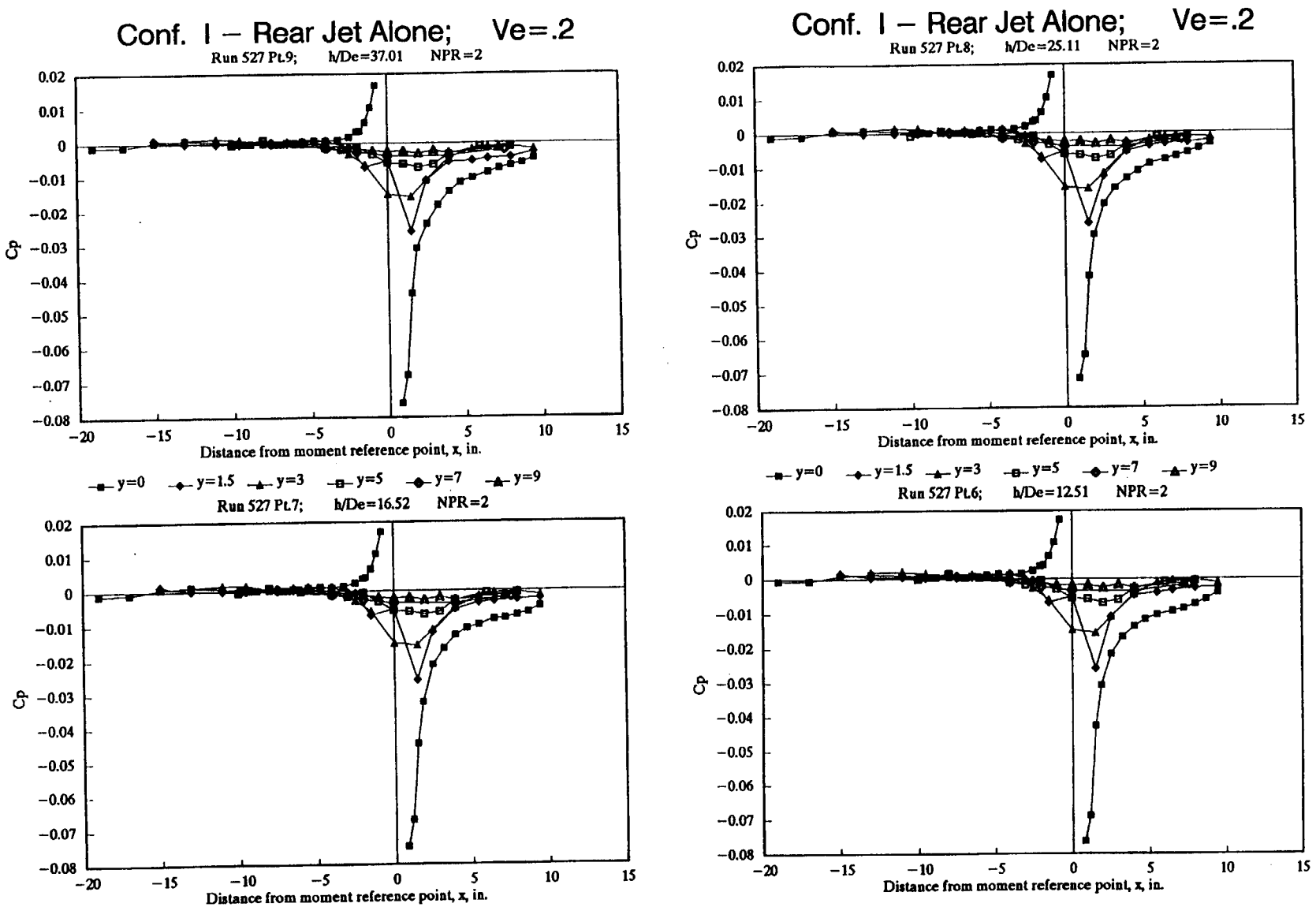

a) Higher heights,

Figure 5.- Effect of height on the pressure distributions at several spanwise stations; Ve=.2, Jet at station 20.

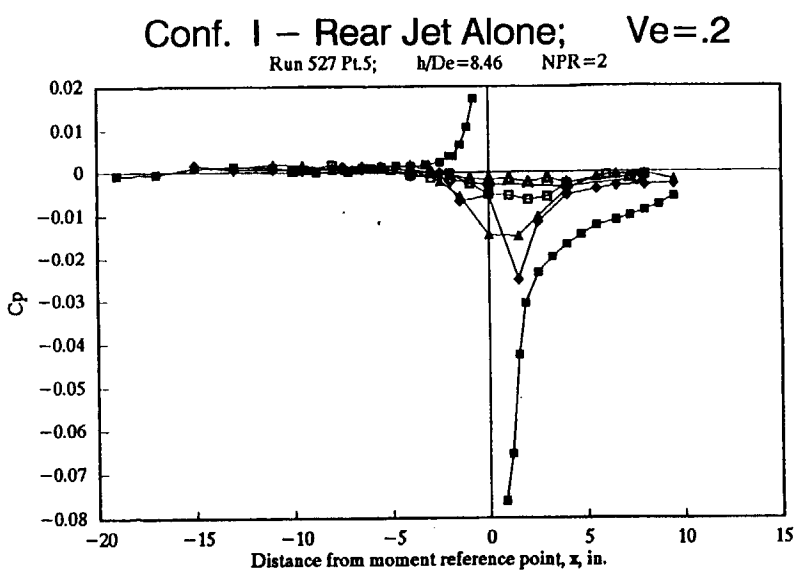

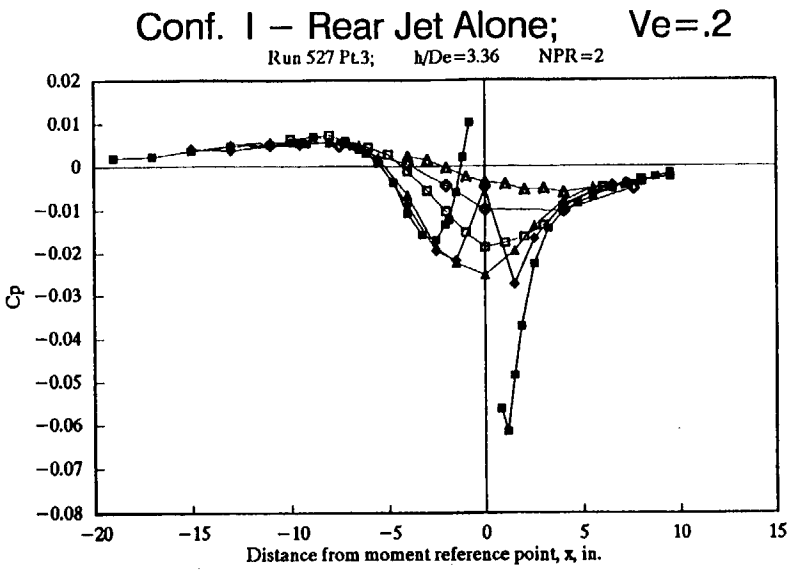

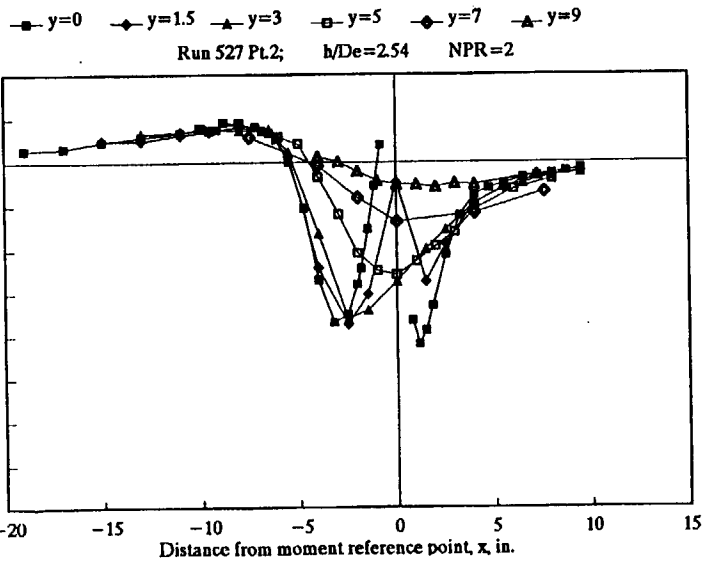

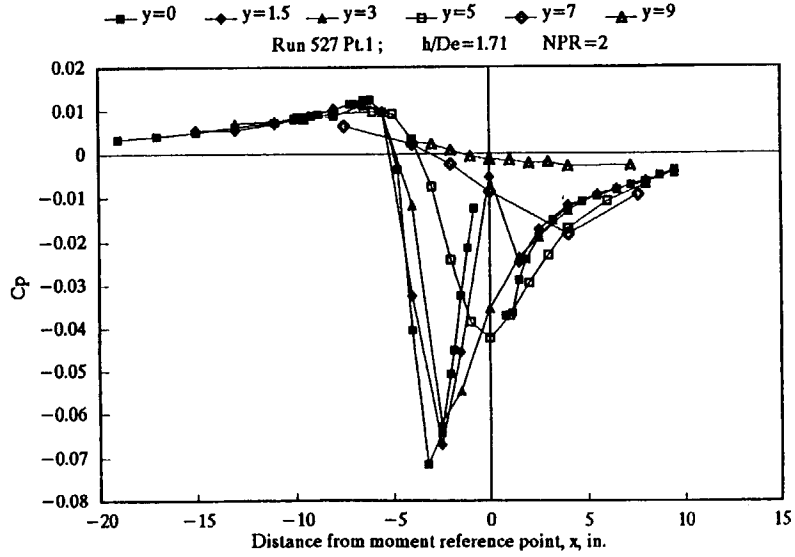

b) Lower heights,

Figure 5.- Concluded.

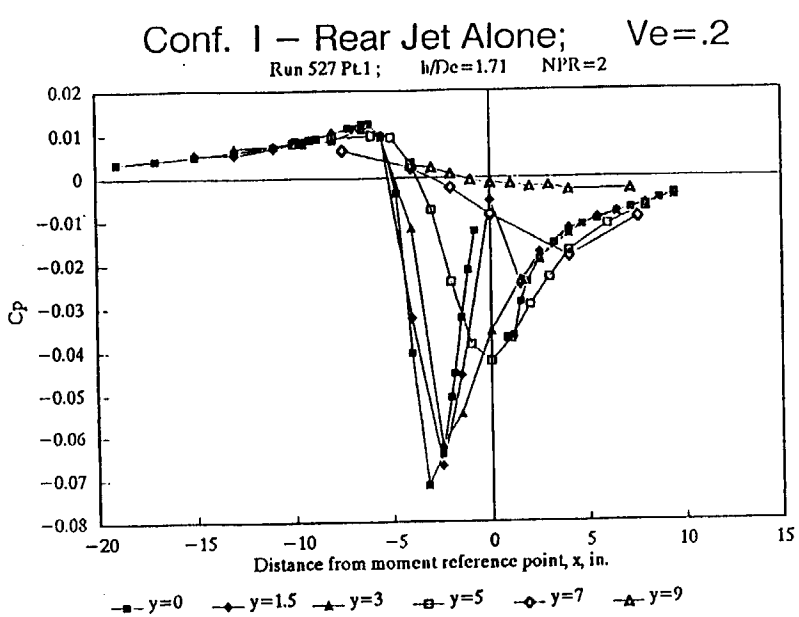

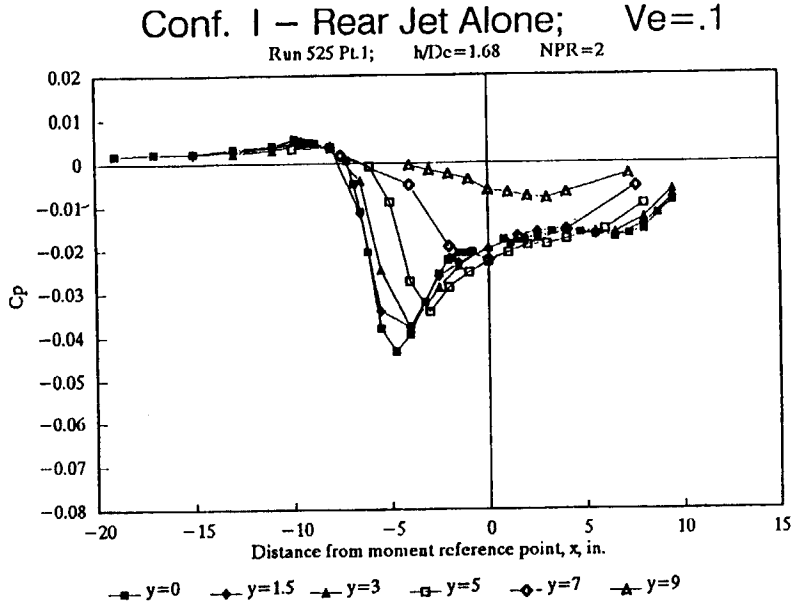

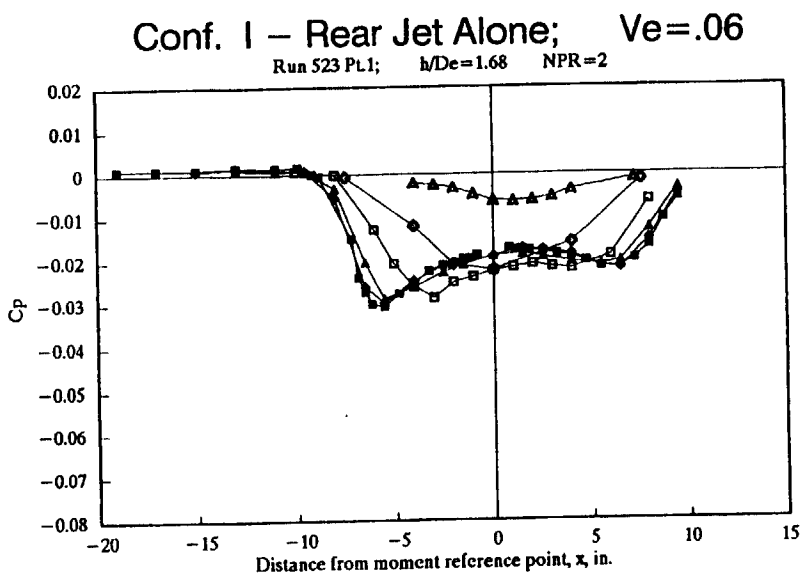

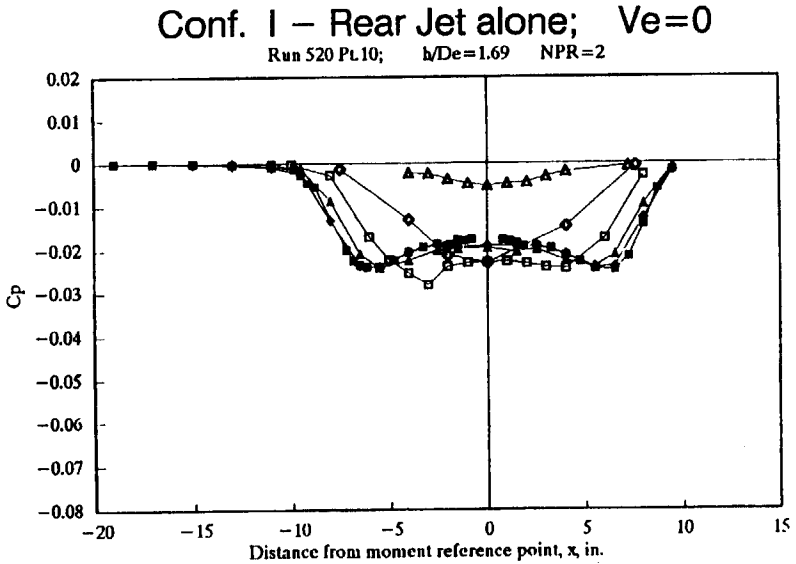

a) h/d = 1.7

Figure 6.- Effect of Velocity ratio, Ve, on the pressure distributions at several spanwise stations; Jet at station 20.

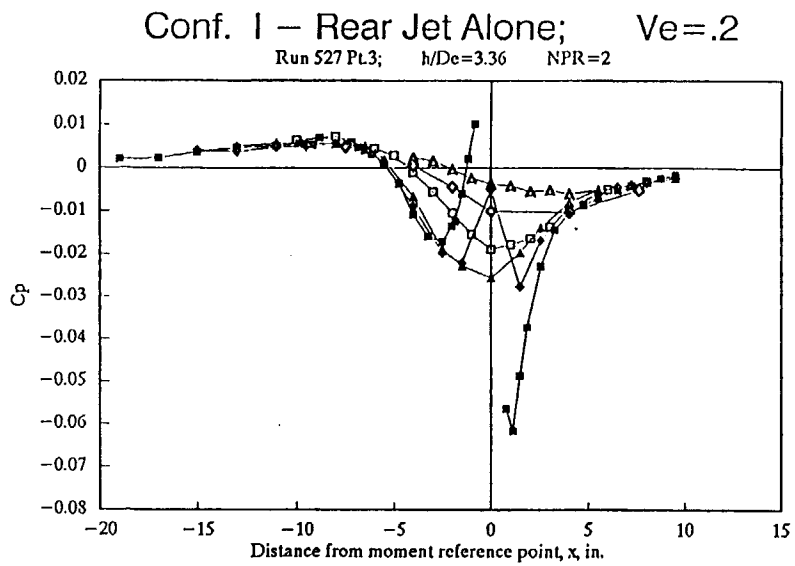

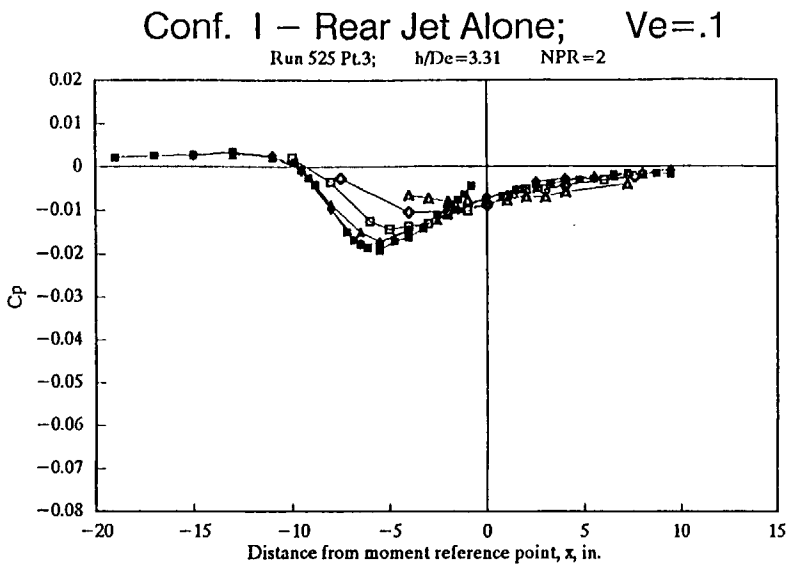

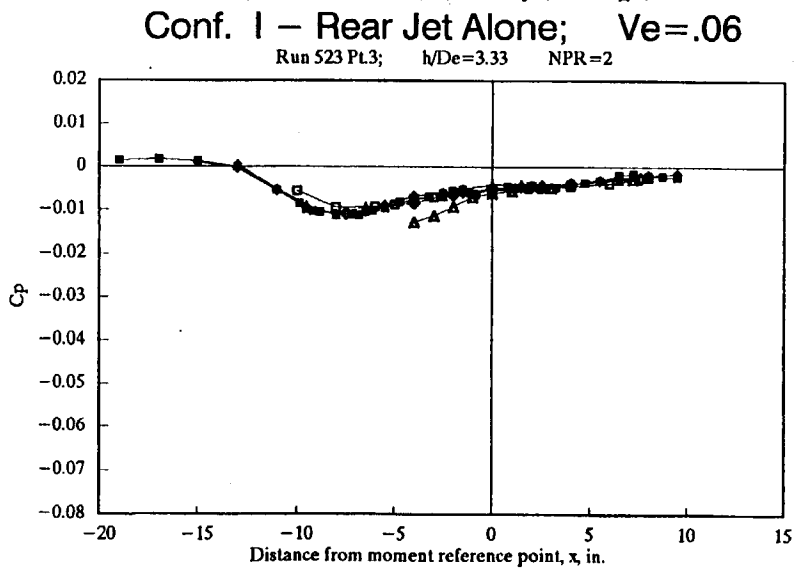

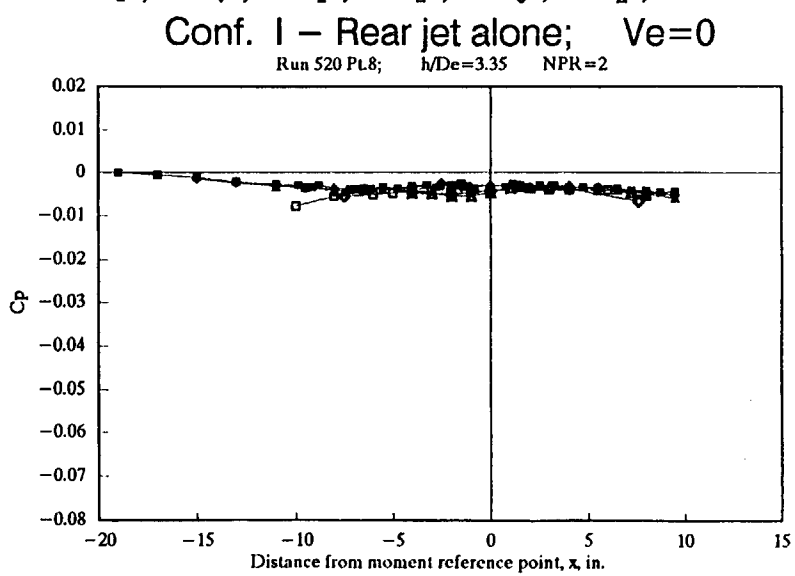

b) h/d = 3.3

Figure 6.- Concluded.

$$\frac{X'}{d} = 2\ V_e^{-.4} \left(\frac{h}{d}\right)^{.06 V_e^{-.7}}$$

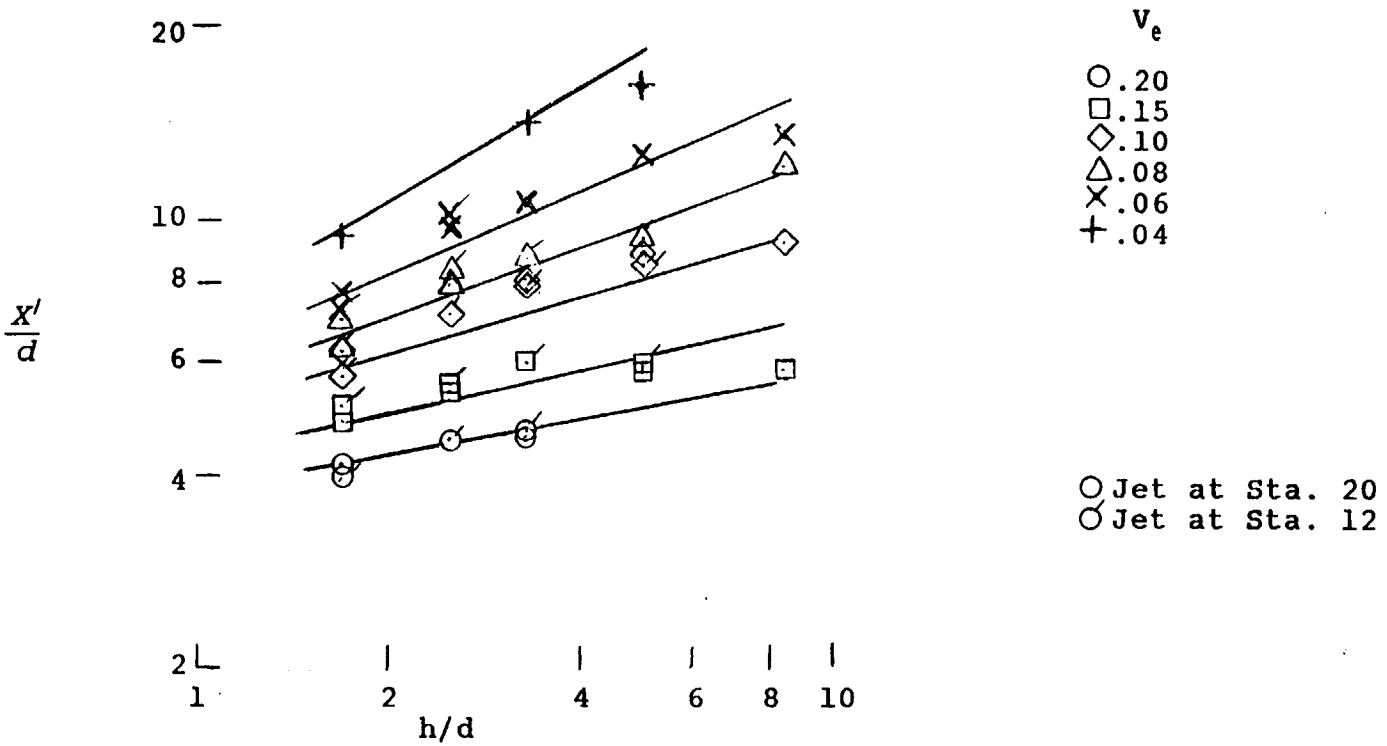

Figure 7.- Location of zero pressure point on model centerline.

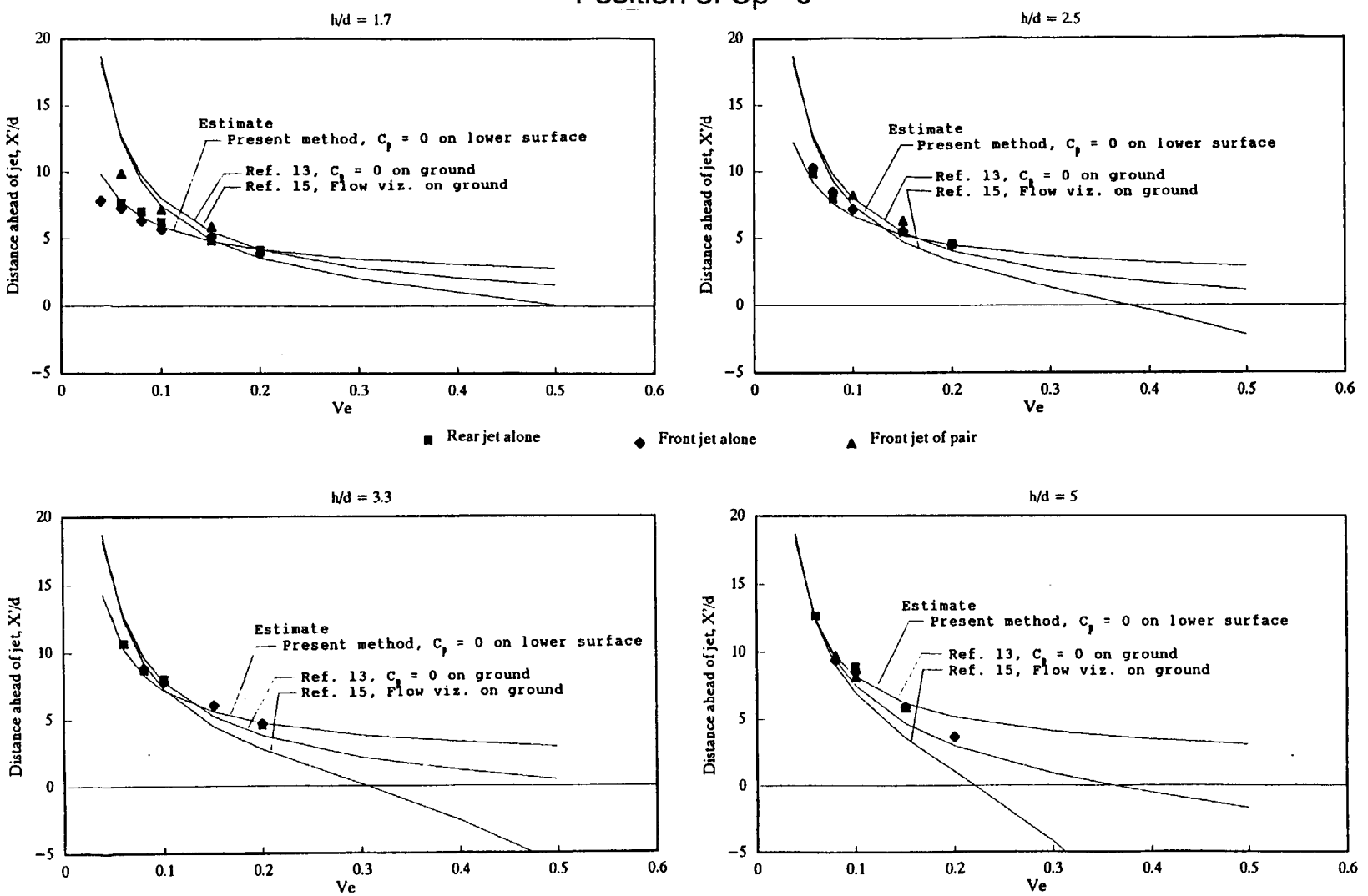

Figure 8.- Comparison of data and estimates of the location of the zero pressure point on the model center line to the estimates of the location on the ground.

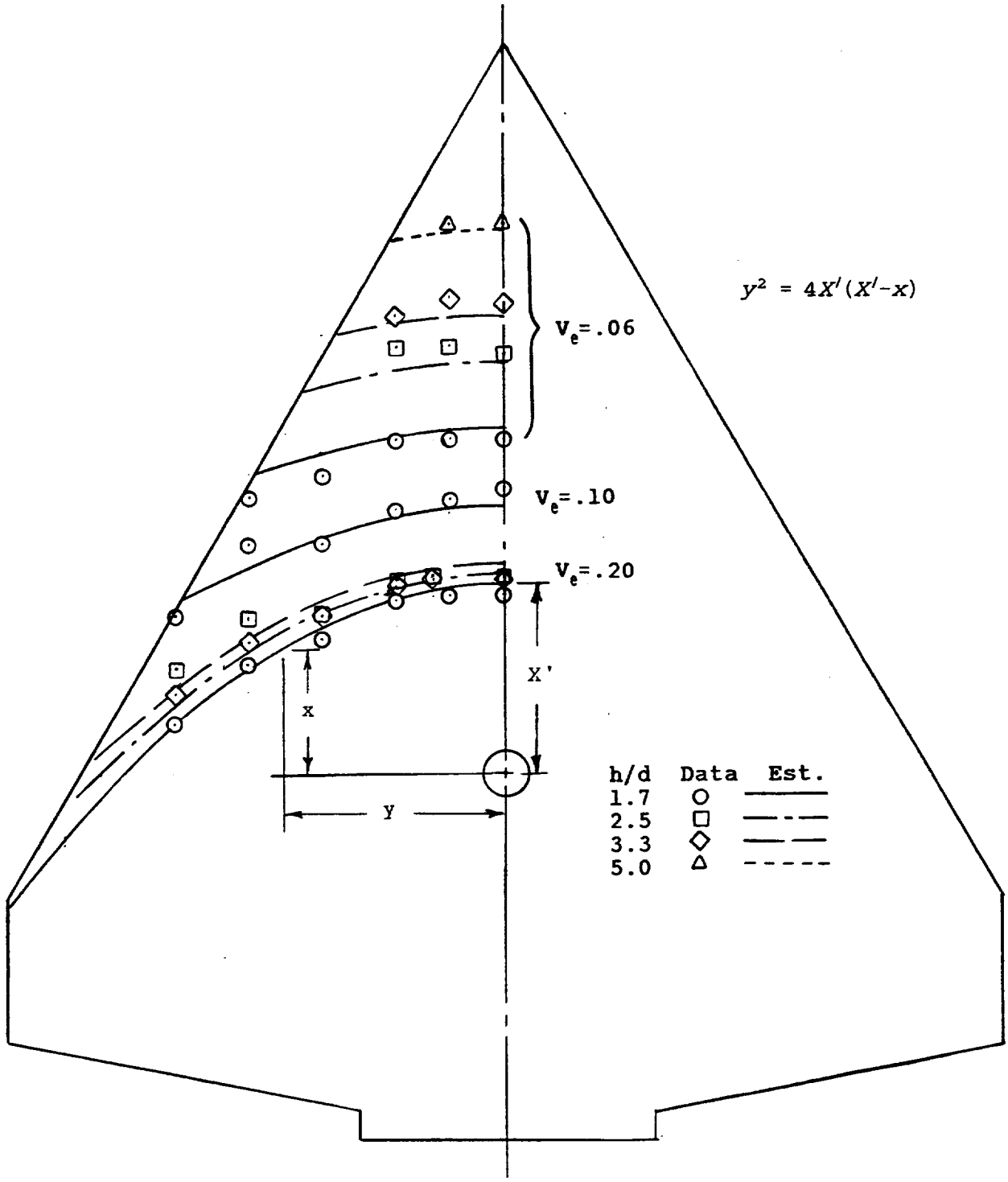

Figure 9.- Location of the zero pressure line on the model lower surface.

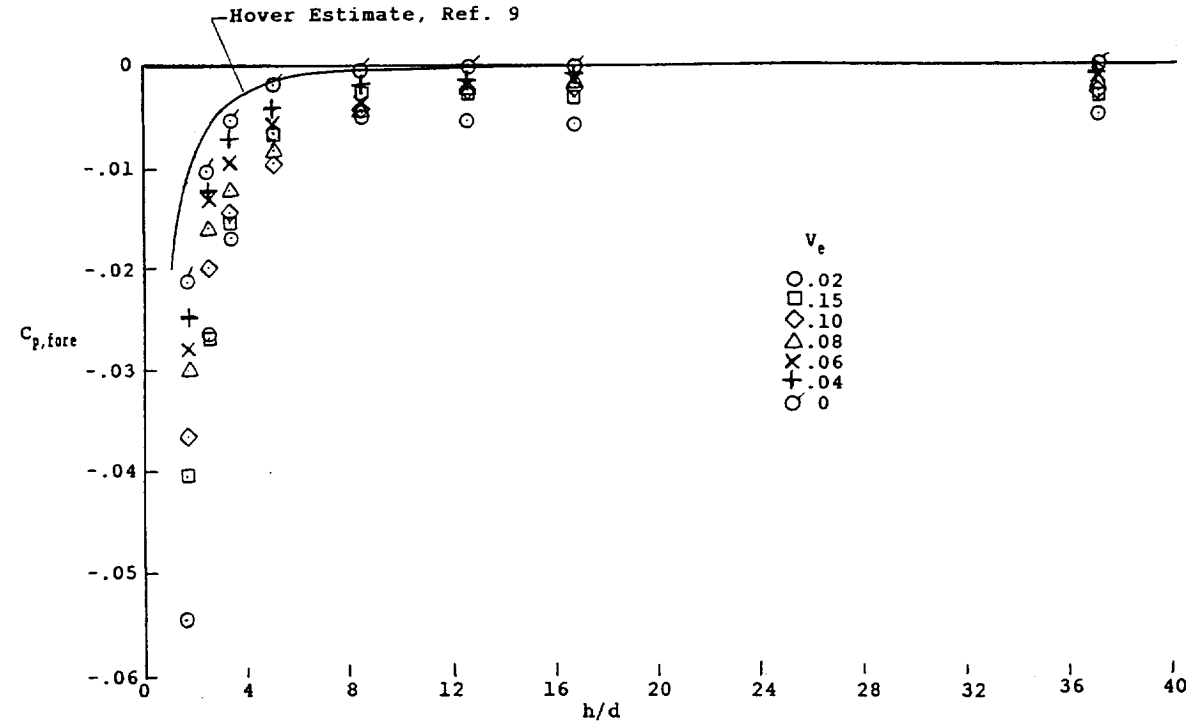

a) Jet at Sta. 12

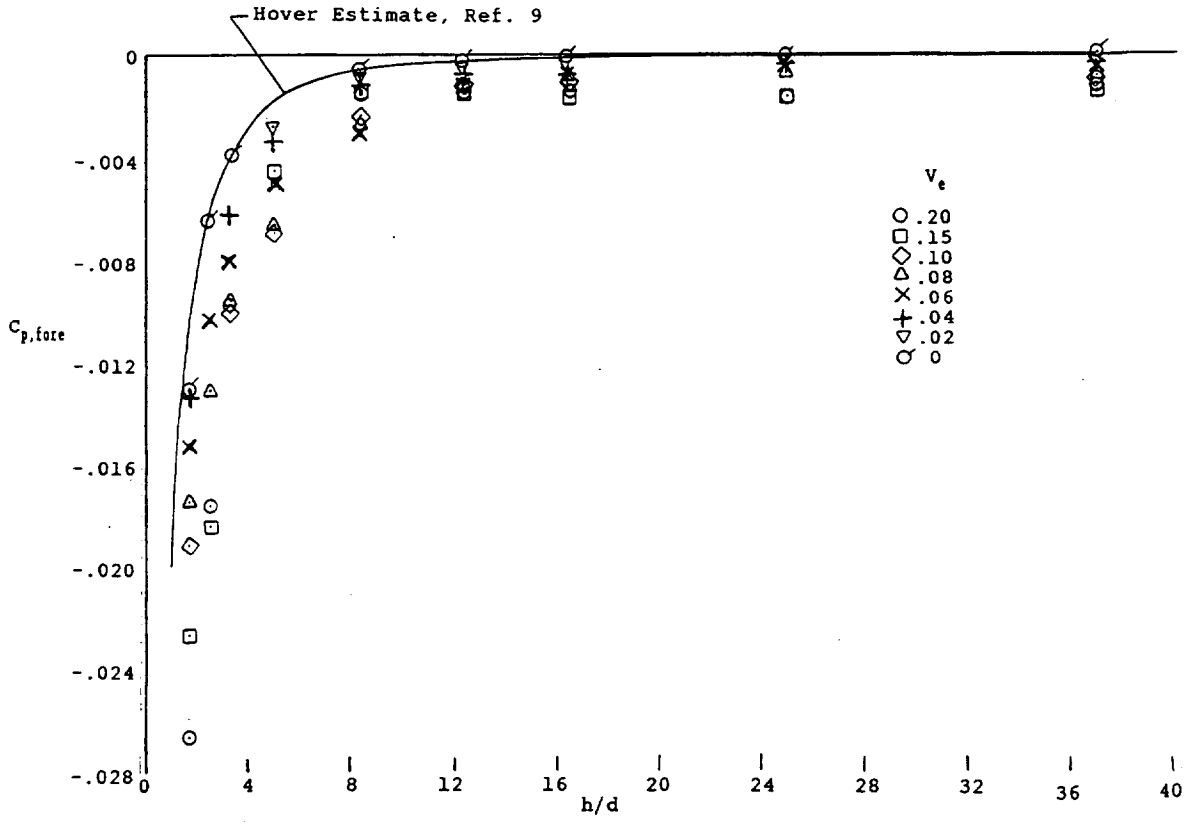

b) Jet at Sta. 20

Figure 10.- Average of negative pressures induced forward; between the zero pressure line and the jet.

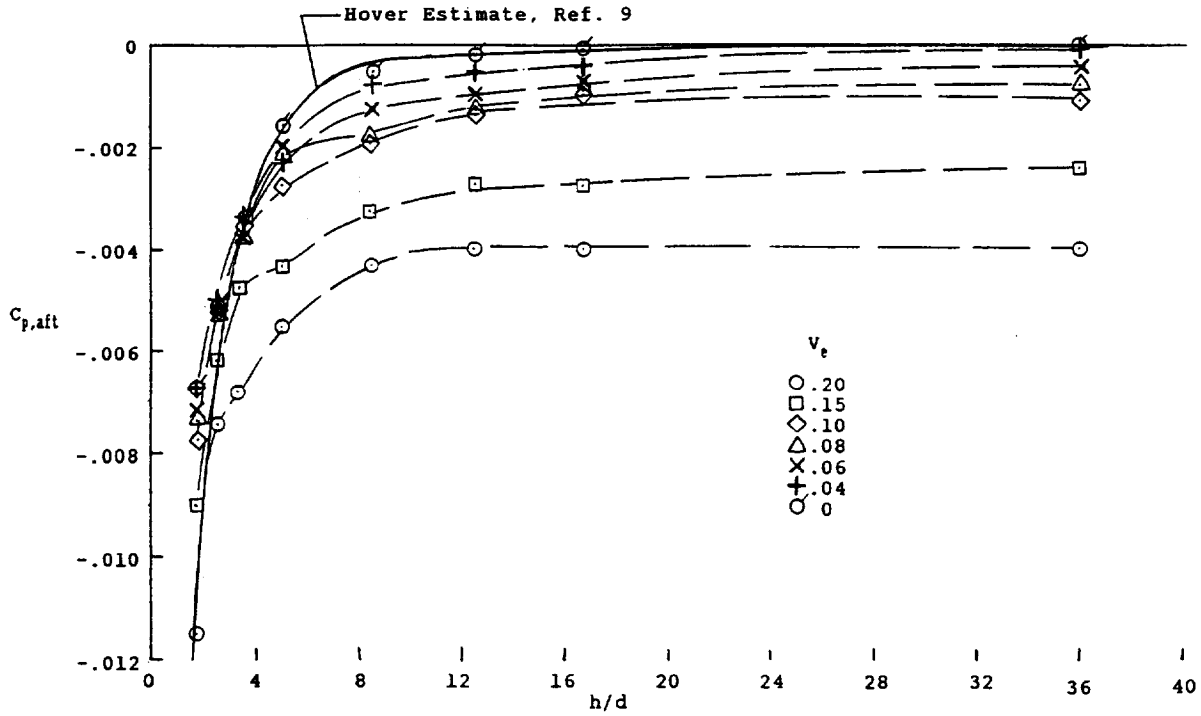

a) Jet at Sta. 12

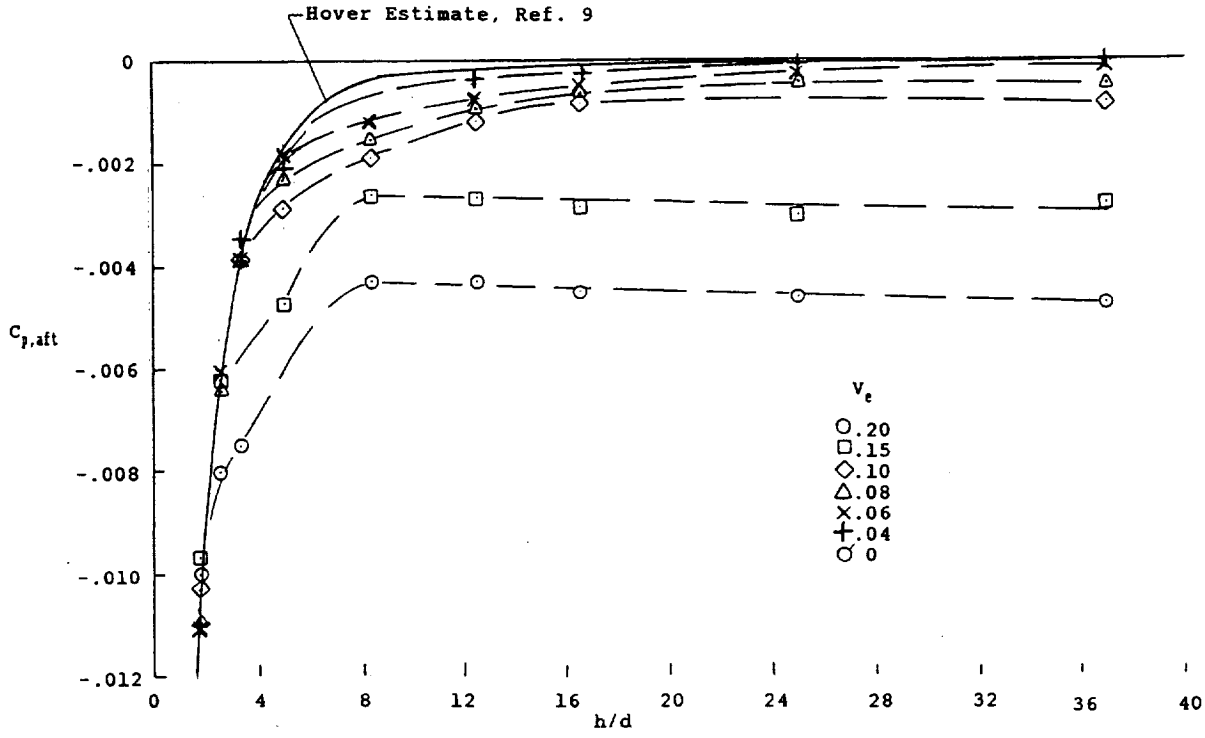

b) Jet at Sta. 20

Figure 11.- Average of negative pressures induced aft of the jet.

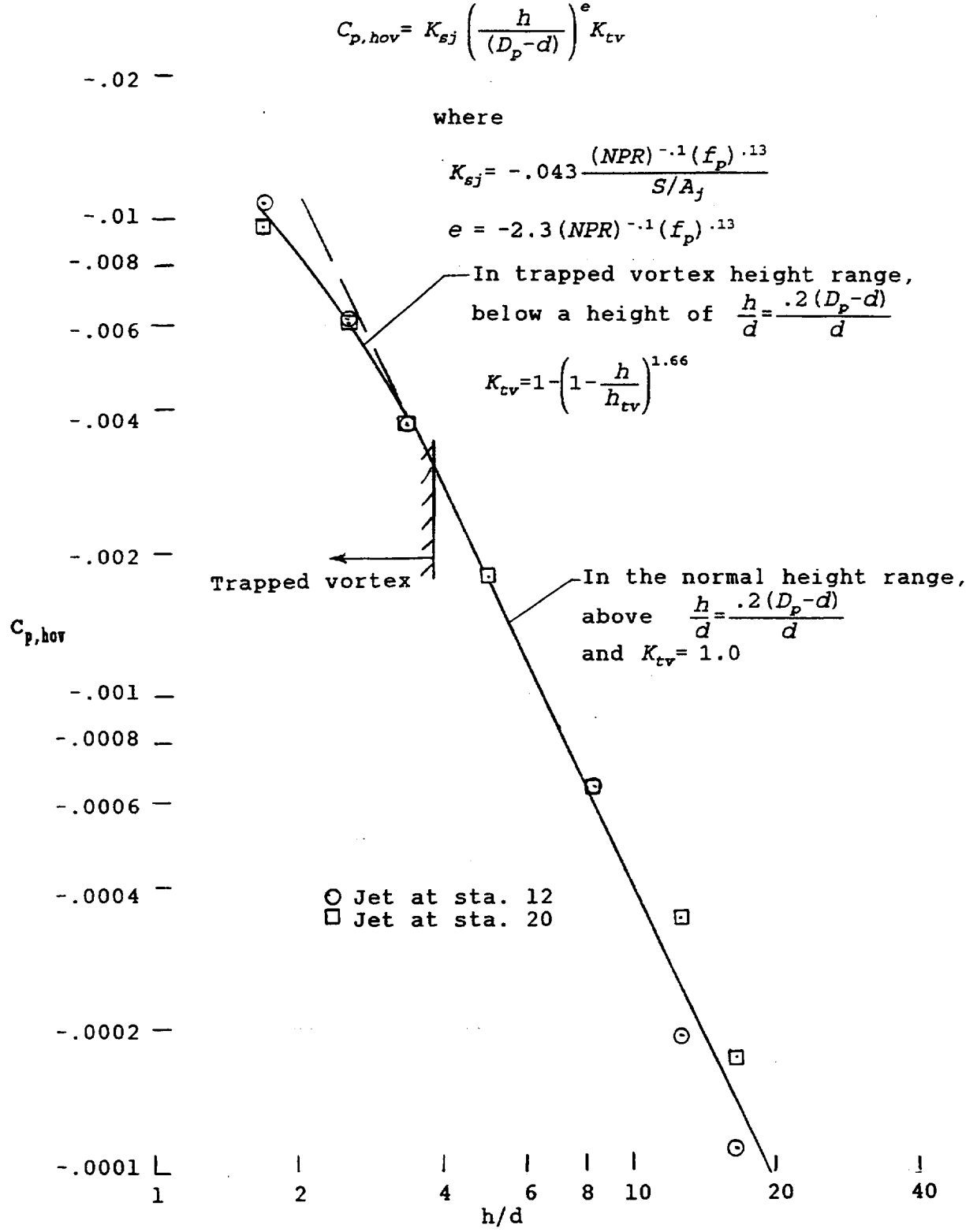

Figure 12.- Effect of jet location on average pressure induced in hover and comparison with estimate from ref. 9.

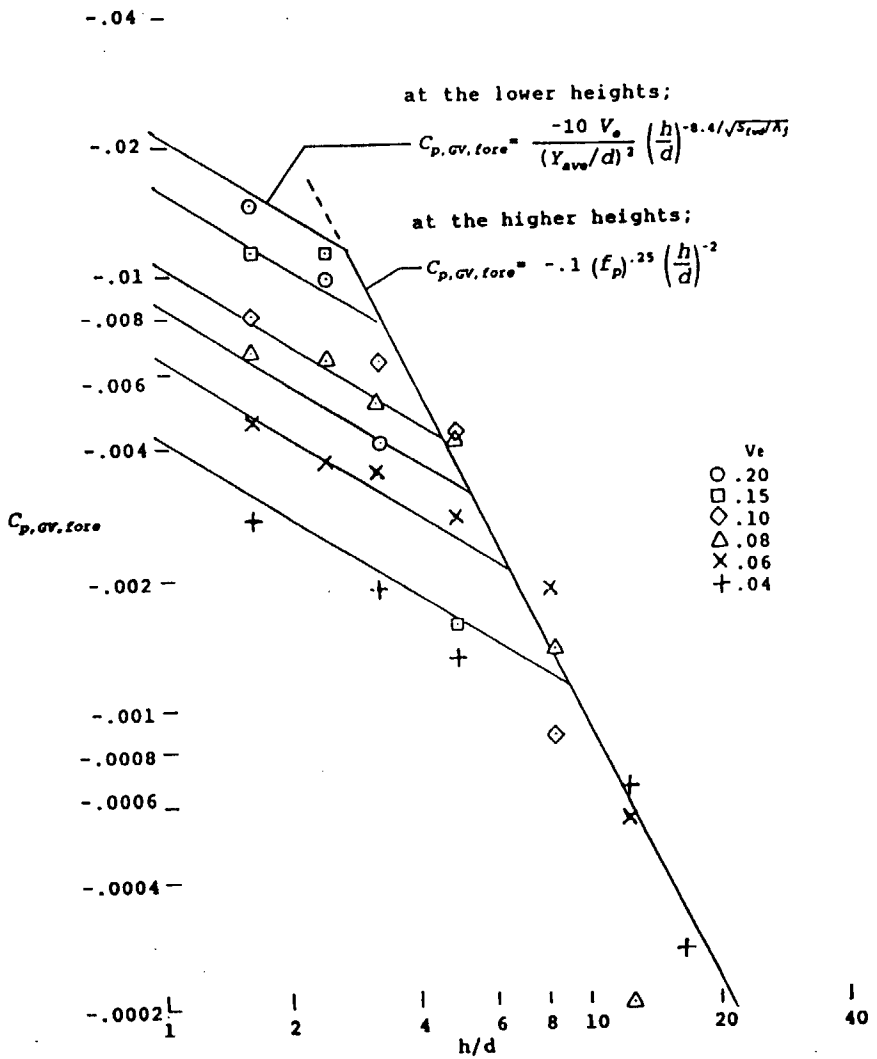

a) Jet at Station 20.

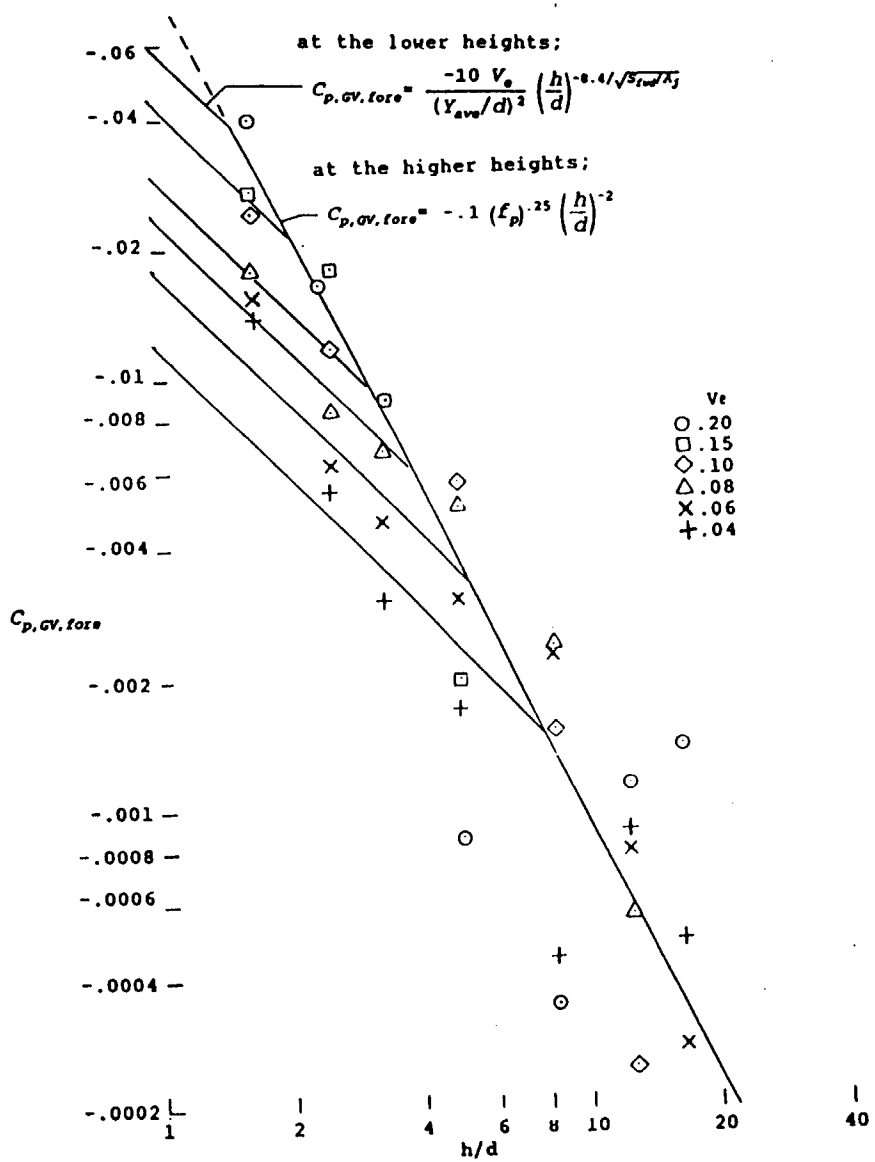

b) Jet at Station 12.

Figure 13.- Increments of pressure induced by the ground vortex between the zero pressure line and the jet.

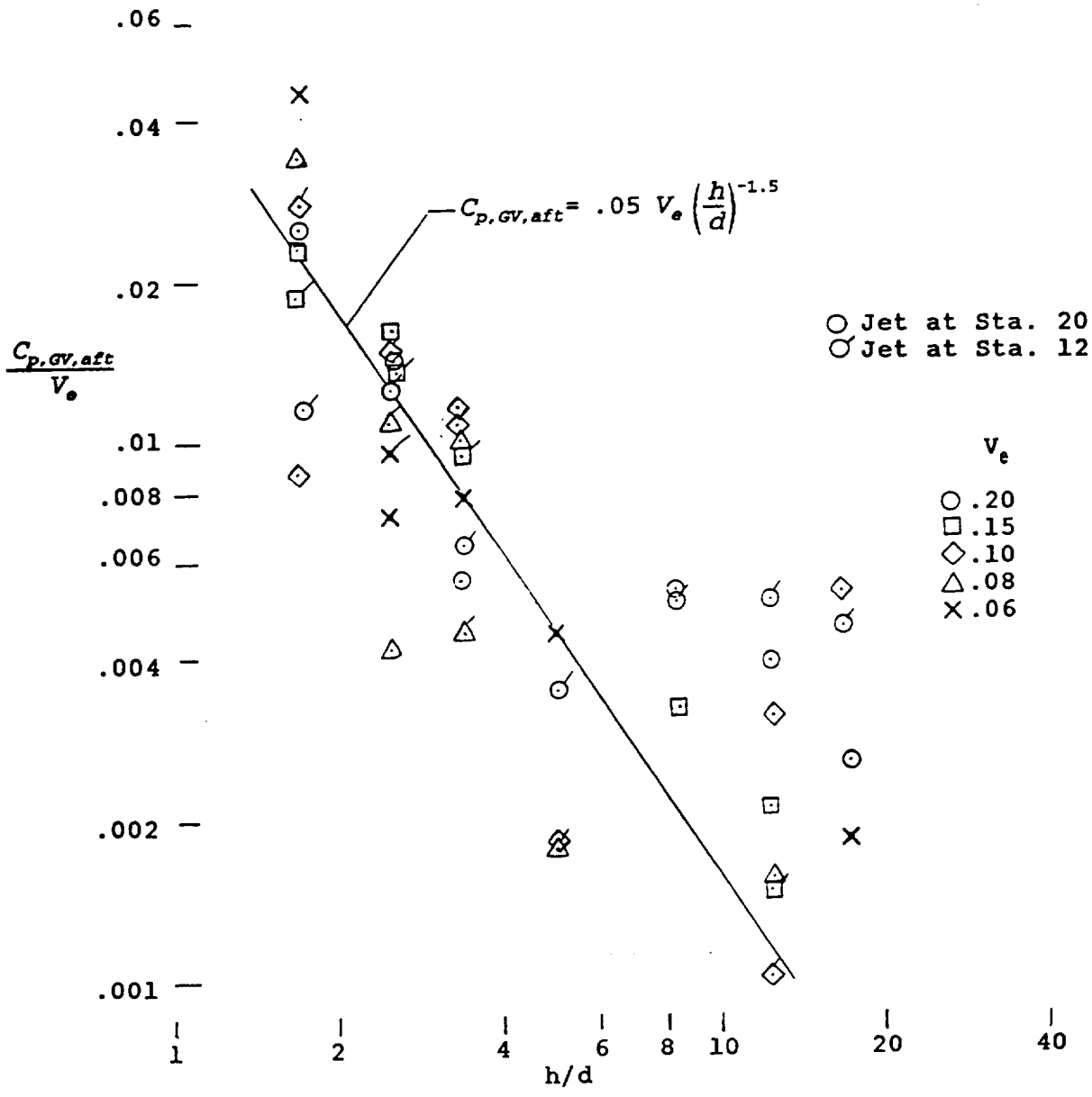

Figure 14.- Increments of pressure induced by the ground vortex aft of the jet.

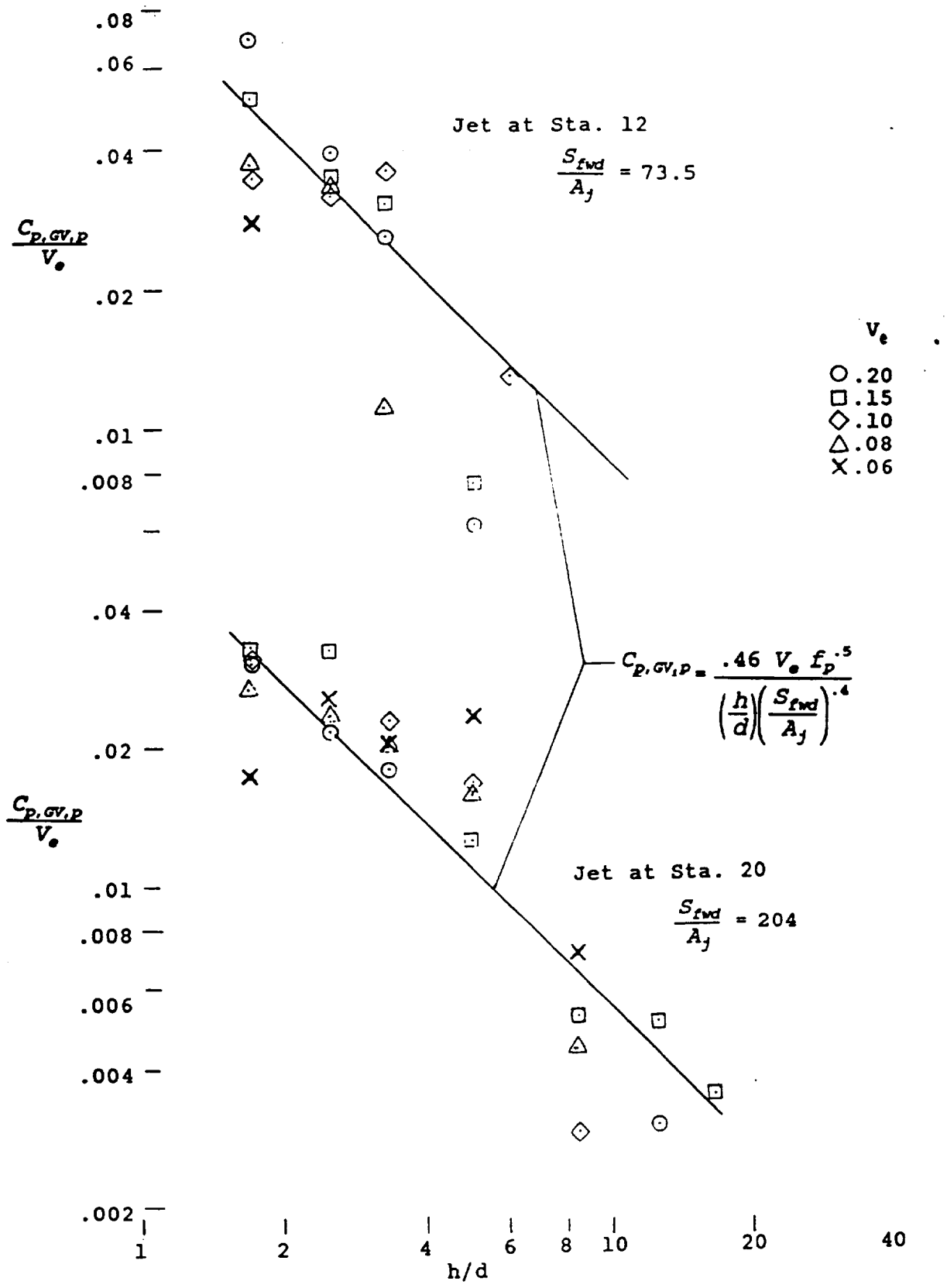

Figure 15.- Increment of pressure coefficient induced by the ground vortex in the positive pressure region forward of the zero pressure line.

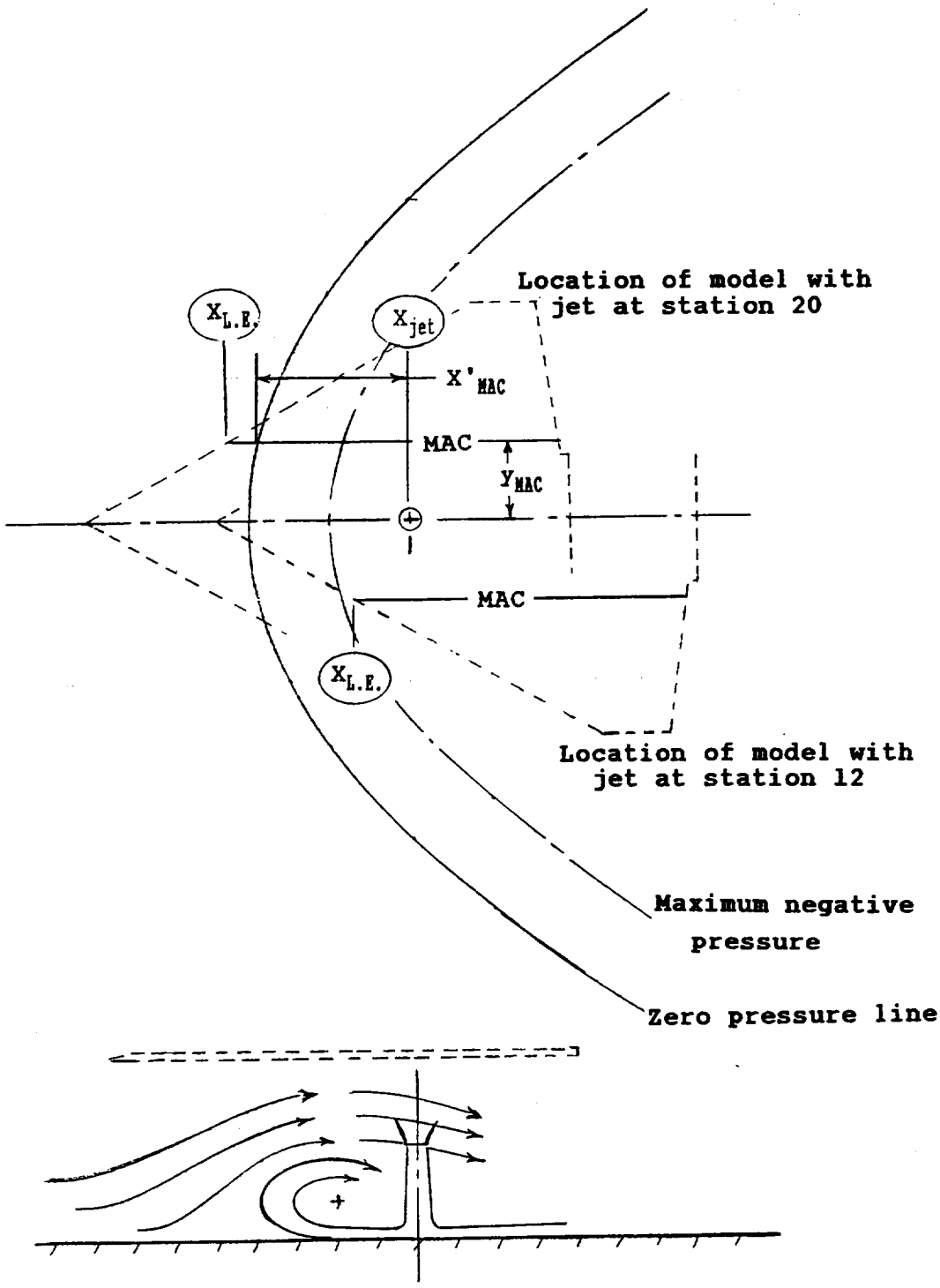

Figure 16.- Schematic of the effect of the ground vortex on the free stream flow. $V_o \approx .1$ $h/d \approx 5$

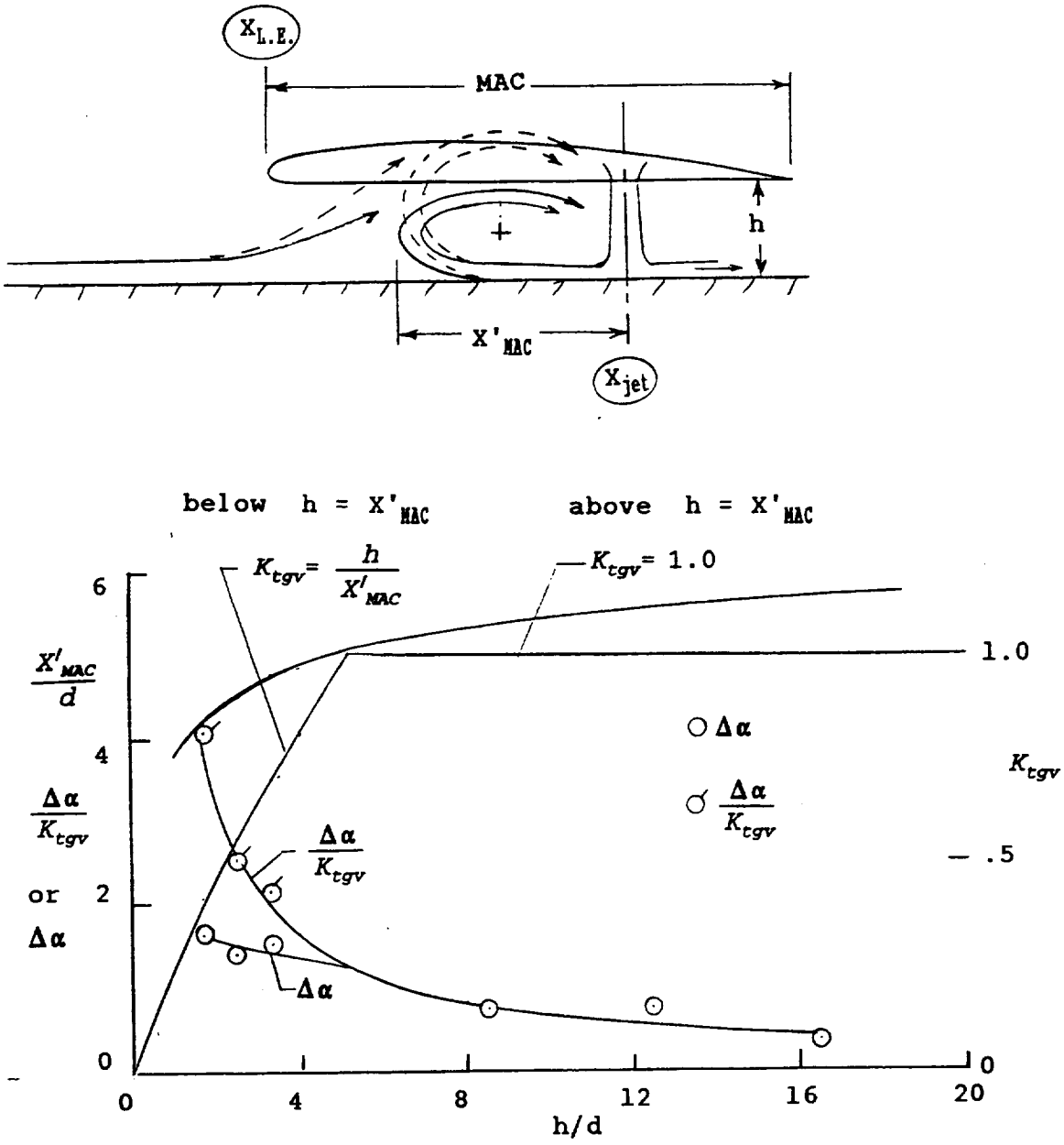

Figure 17.- Example of effect of 'trapping' the ground vortex at low heights; V_e = .2, jet at Sta. 20.

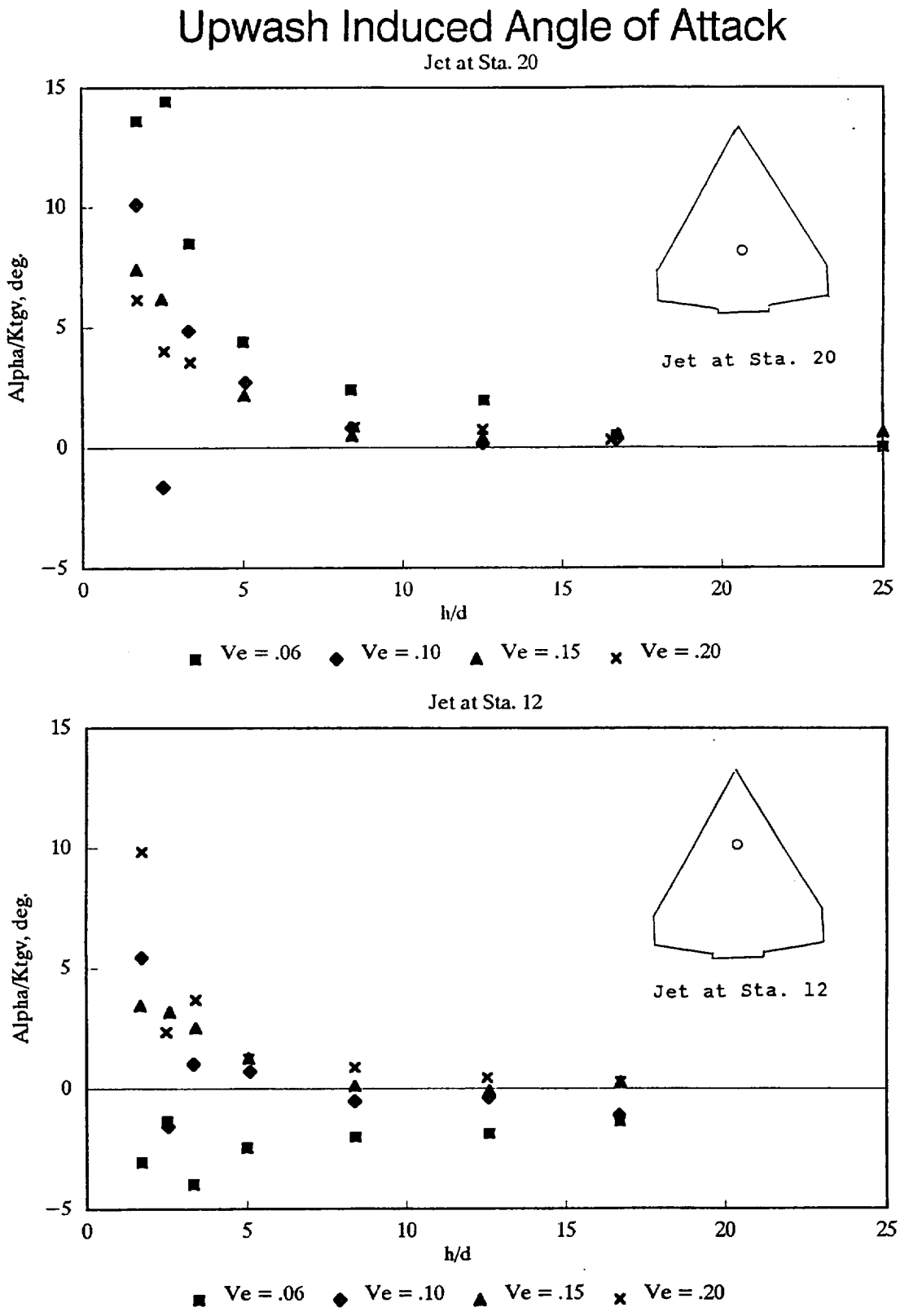

Figure 18.- Effect of height on the adjusted induced upwash angles experienced by the configuration of reference 14.

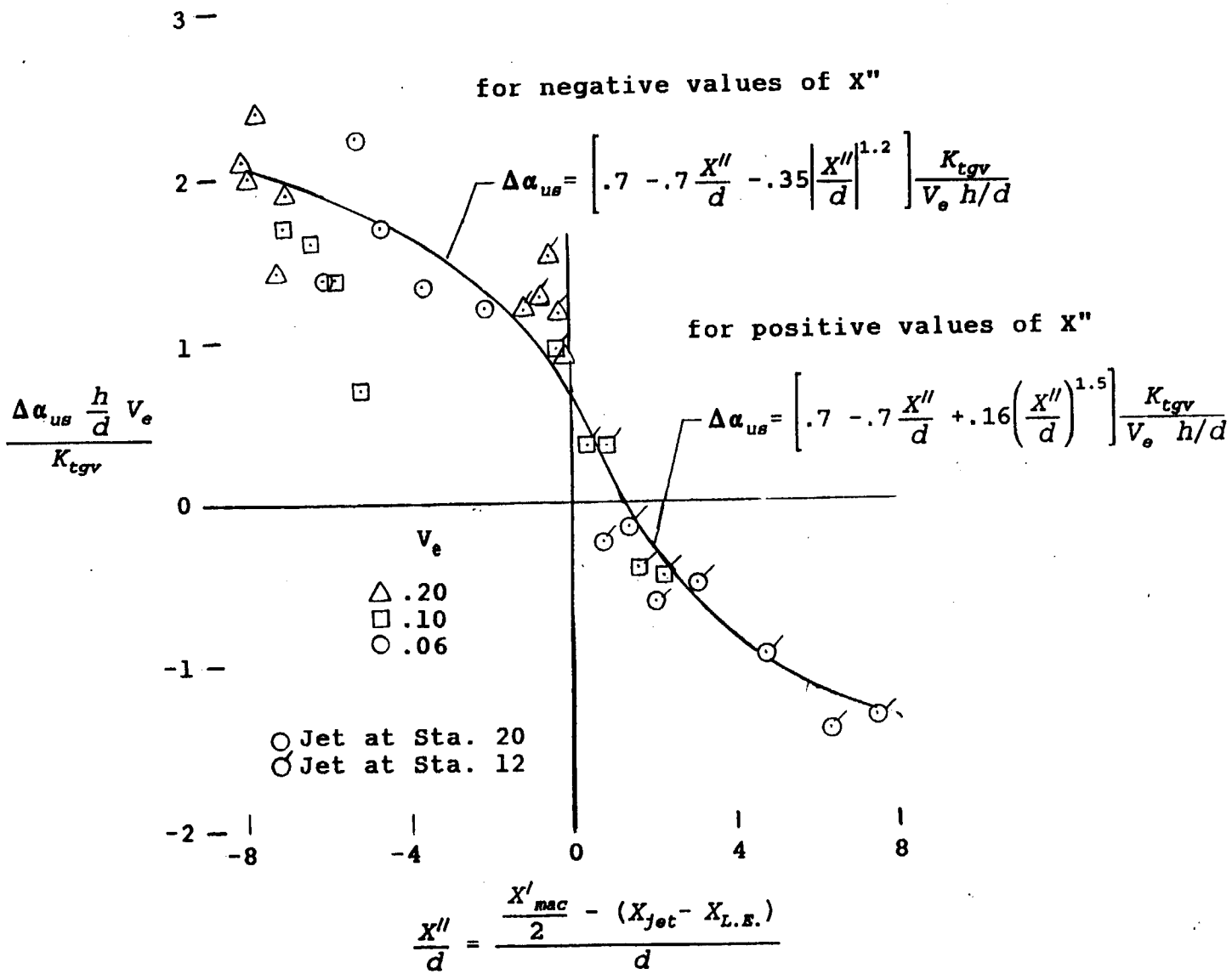

Figure 19.- Correlation of ground vortex induced upwash on the configuration of reference 14.

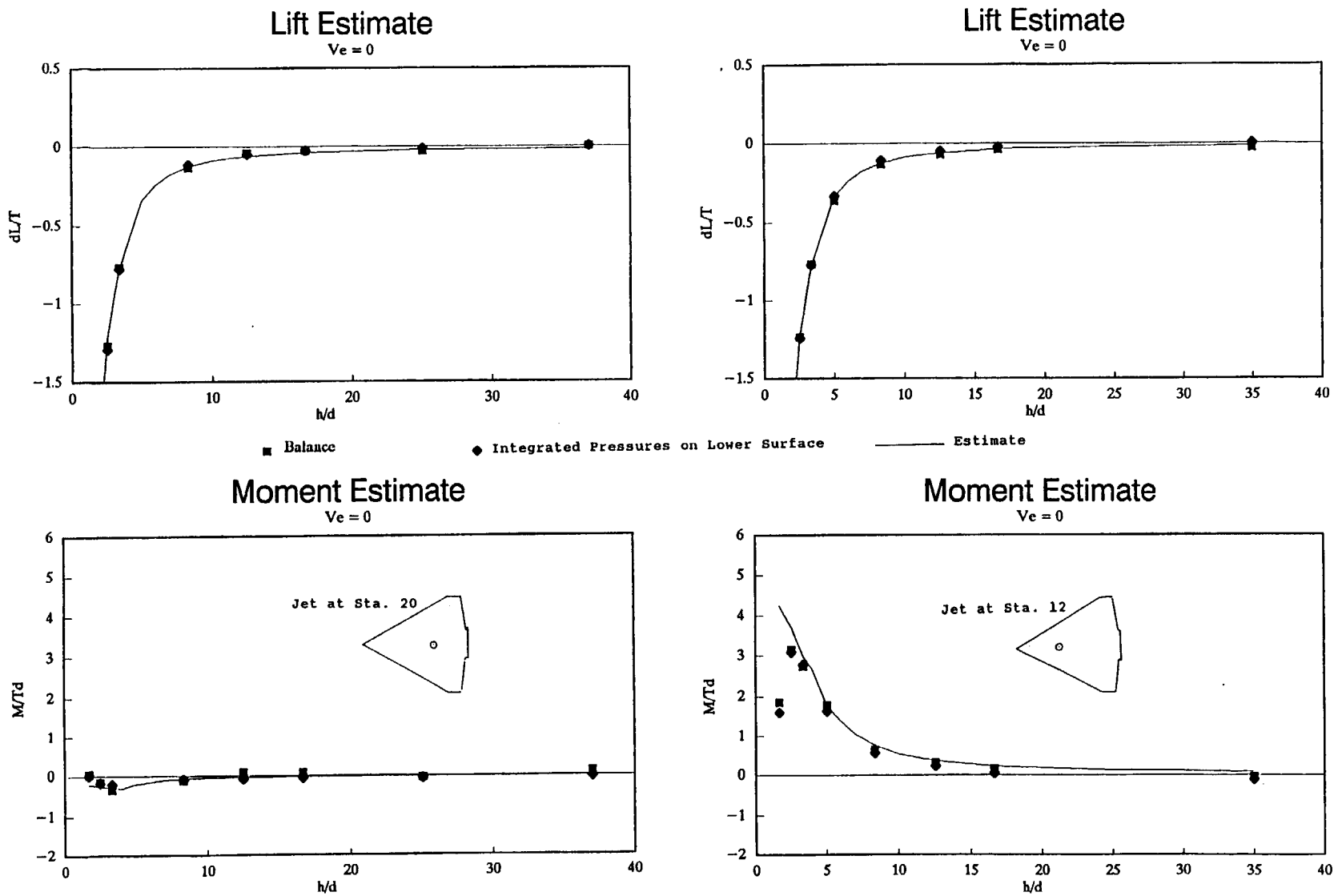

Figure 20.- Comparison of the estimated lift and moments induced in hover with the experimental data for two jet locations.

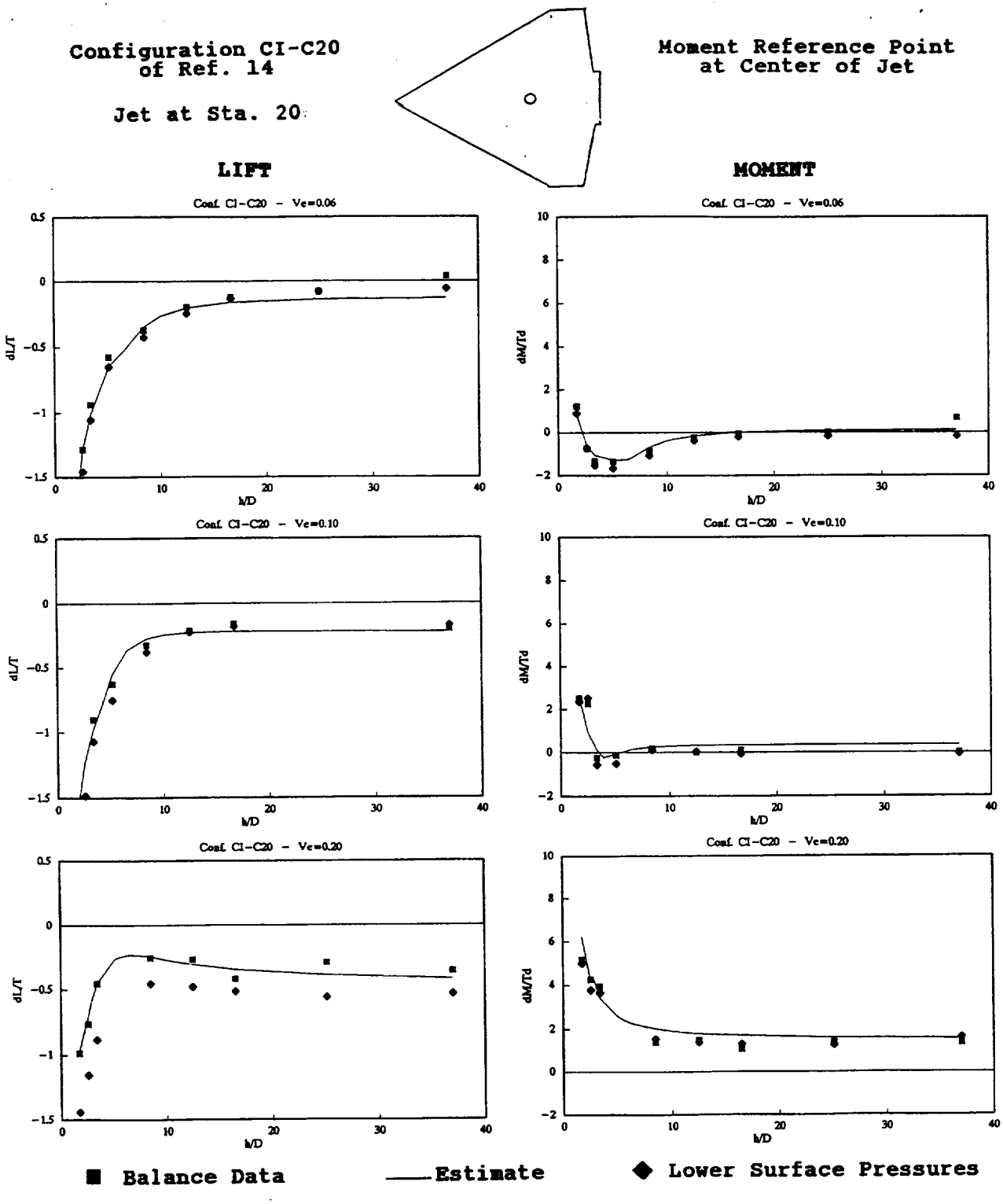

a) Total Lift and Moment

Figure 21.- Comparison of estimates with data, and breakdown of the estimates, for the model of reference 14 with the jet at station 20.

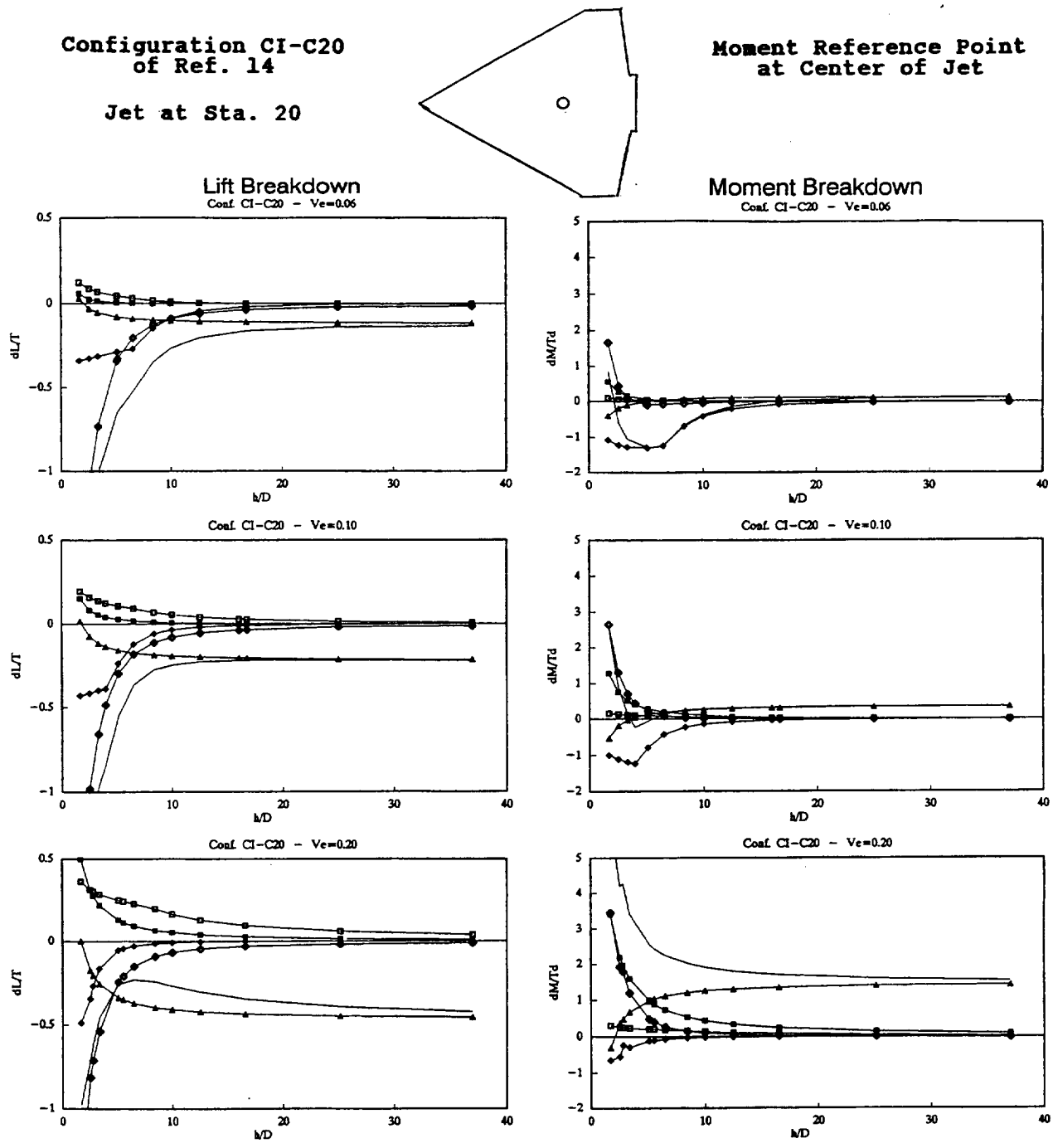

b) Breakdown of lift and moment estimates

Figure 21.- Concluded.

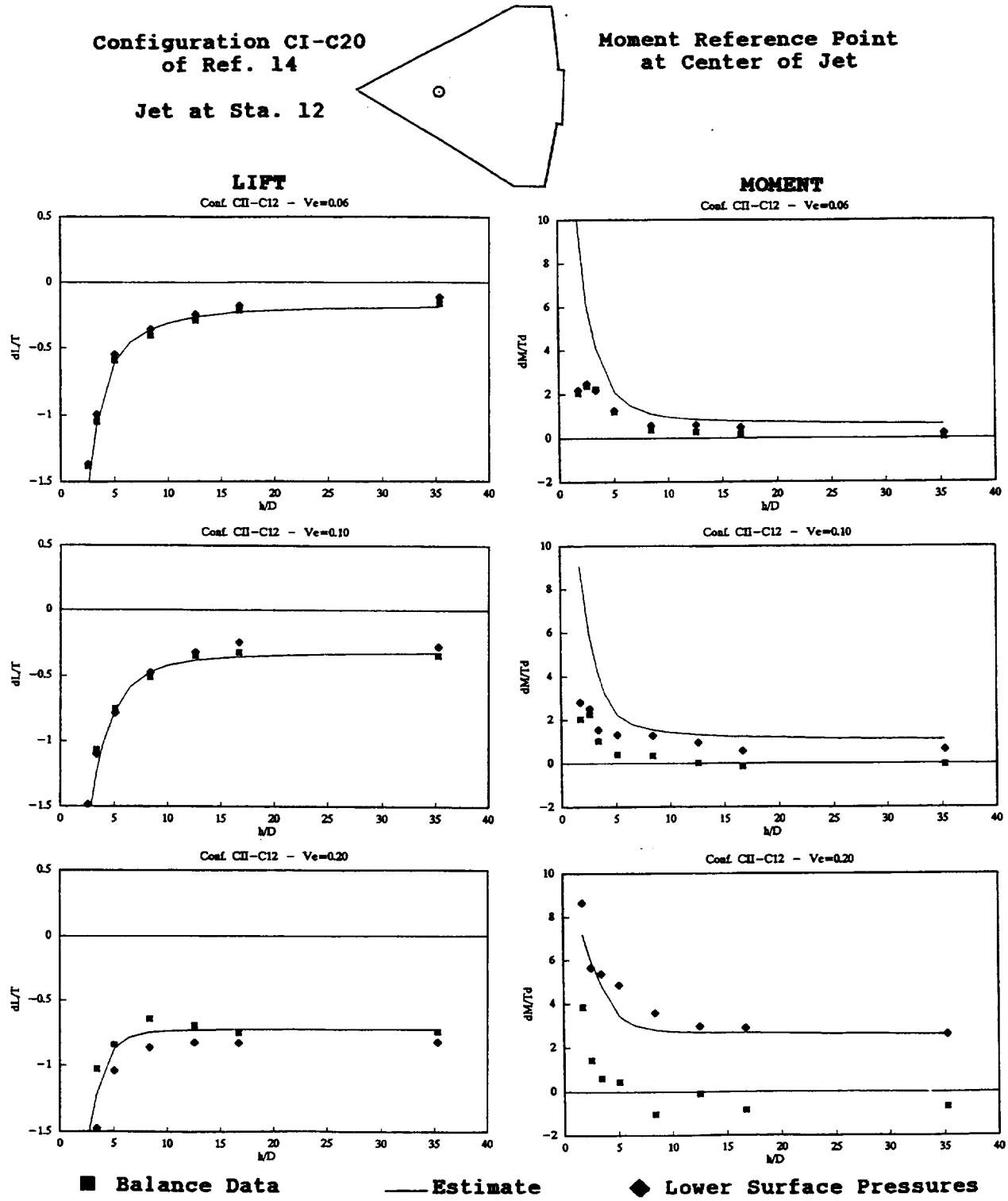

a) Total Lift and Moment

Figure 22.- Comparison of estimates with data, and breakdown of the estimates, for the model of reference 14 with the jet at station 12.

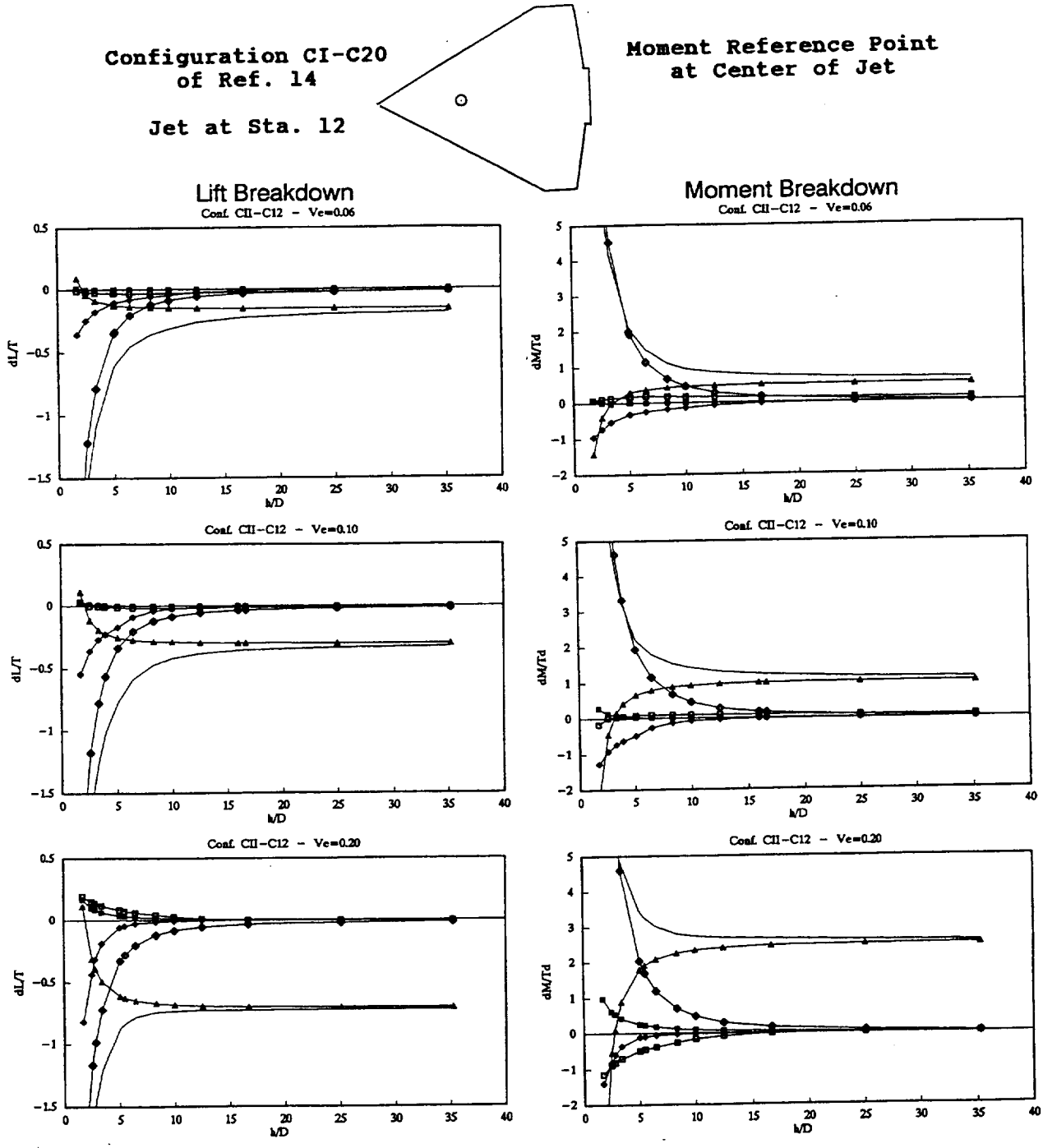

b) Breakdown of lift and moment estimates

Figure 22.- Concluded.

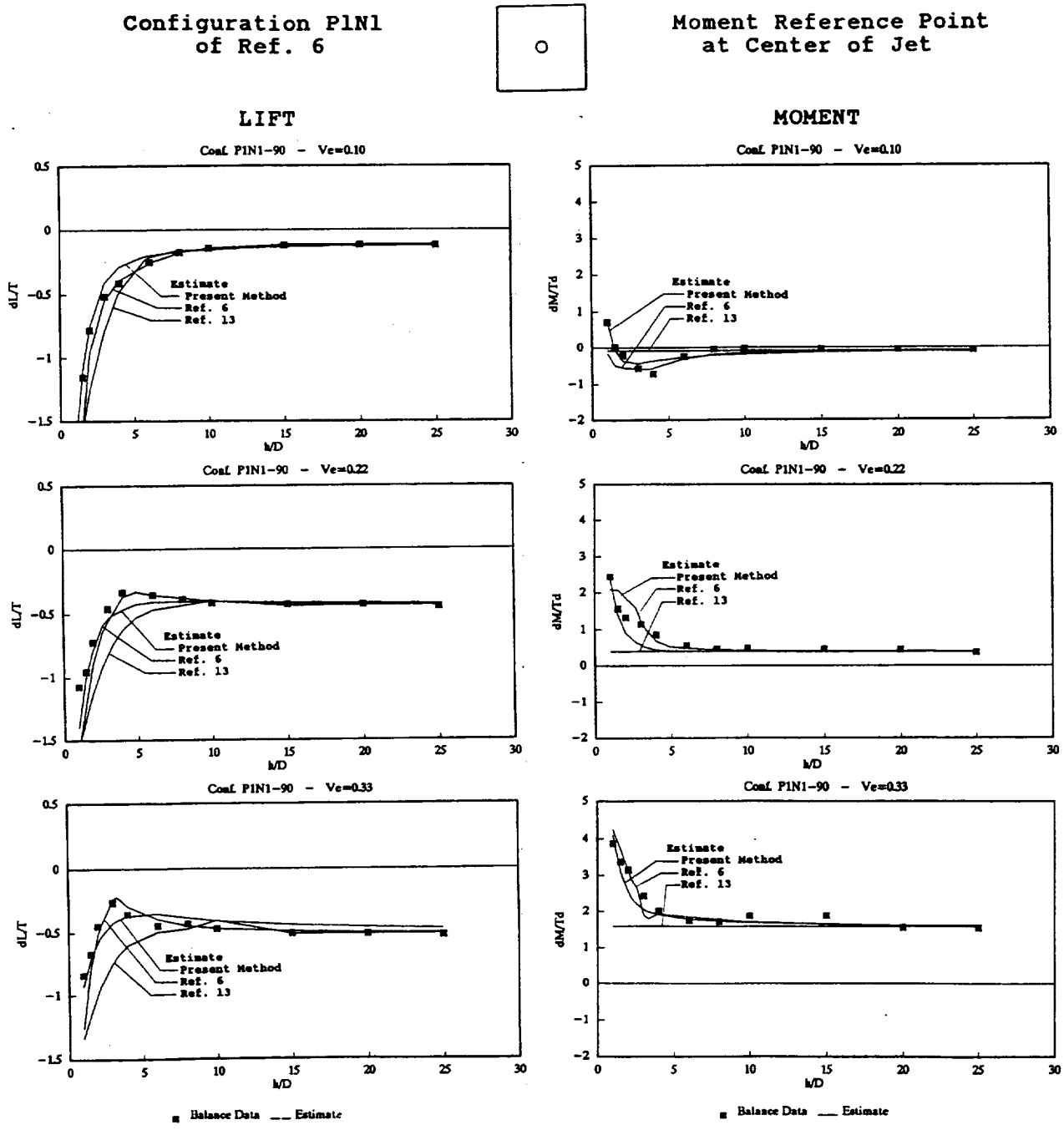

a) Larger plate - S/A_j = 127

Figure 23.- Comparison of estimates with data for two flat plate models of reference 6.

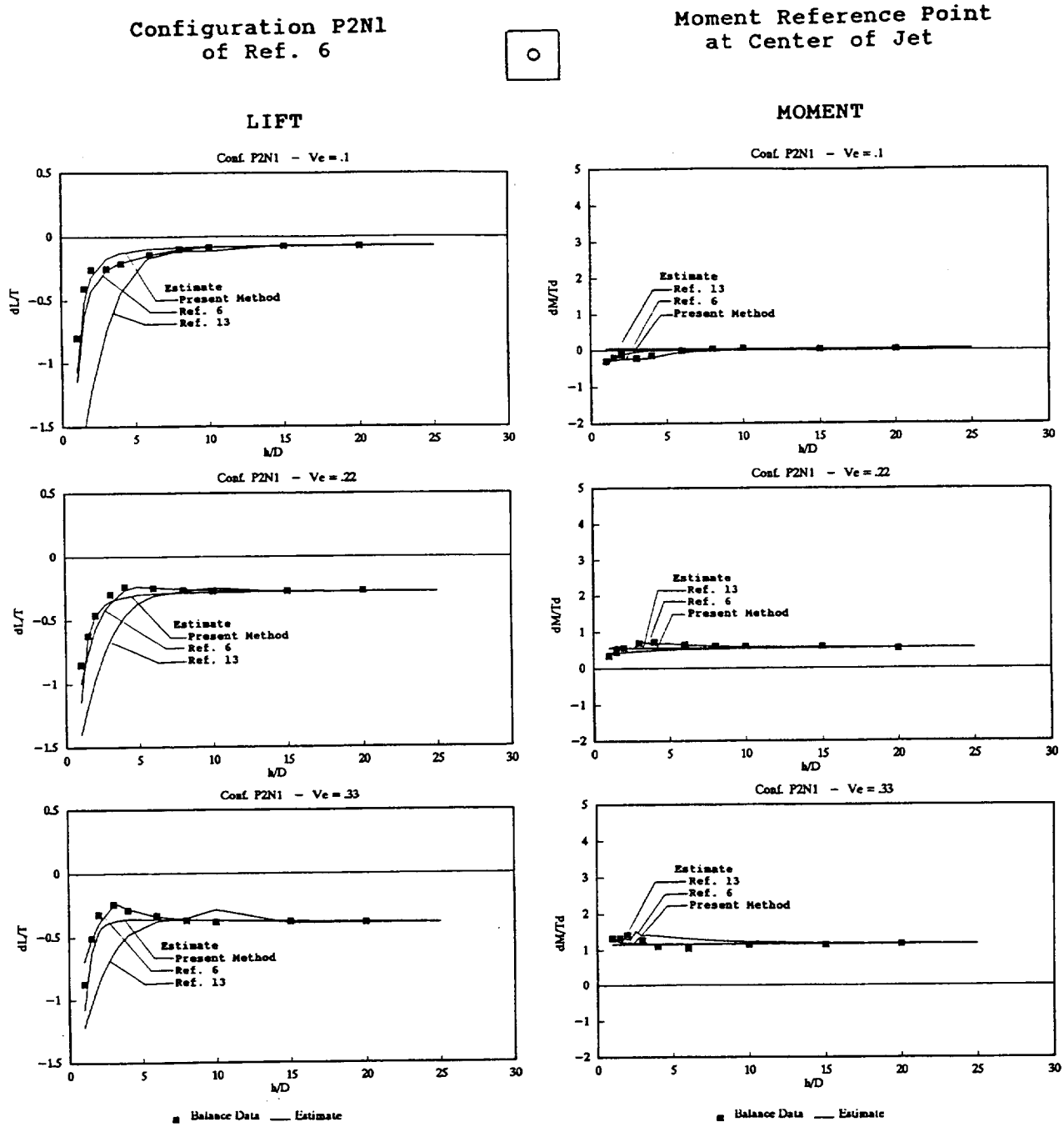

b) Smaller plate - $S/A_j = 46$

Figure 23.- Concluded.

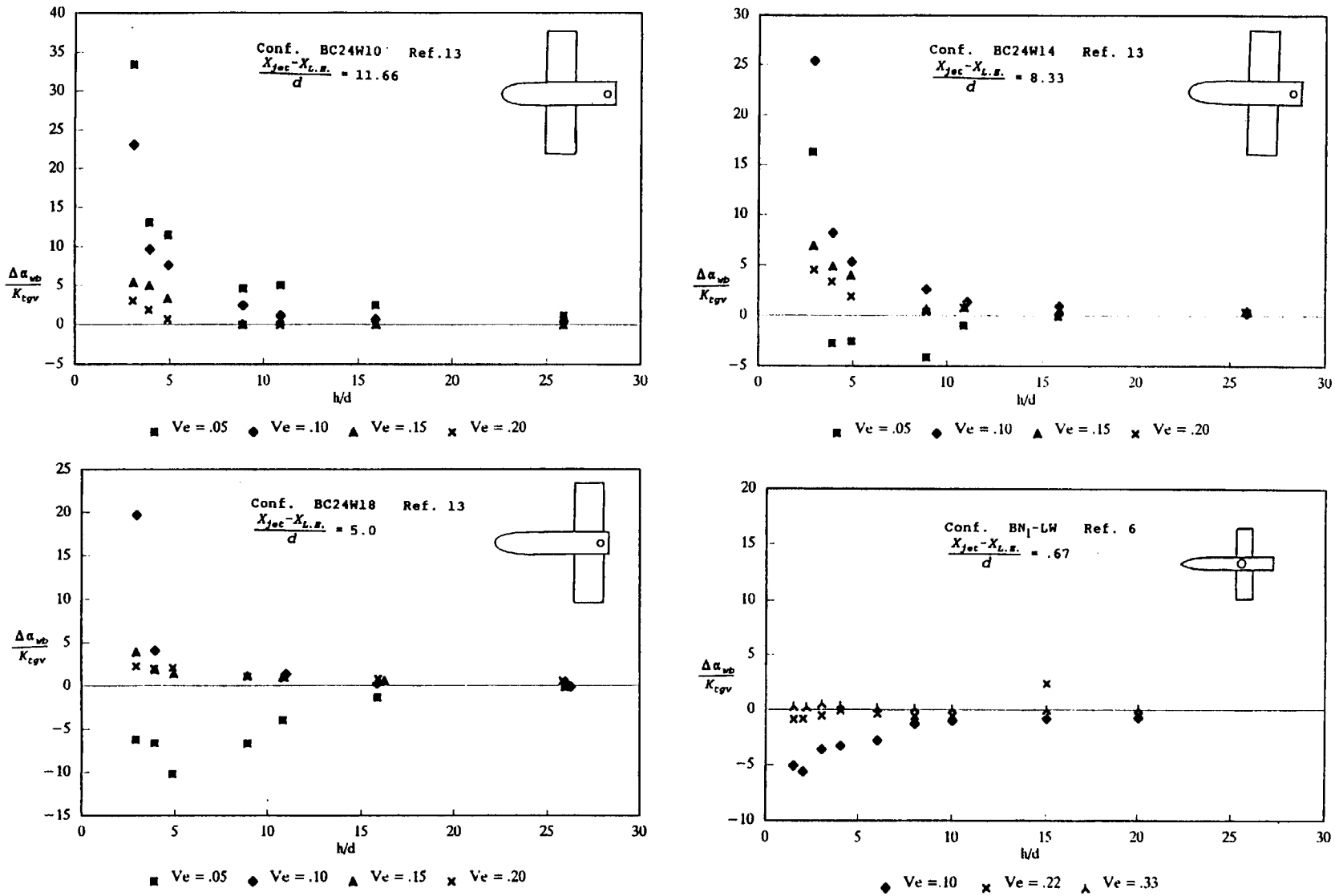

a) Cartesian Cordinants

Figure 24.- Effect of height on the apparent induced upwash angles experienced by three wing-body configurations of reference 13 and one of reference 6.

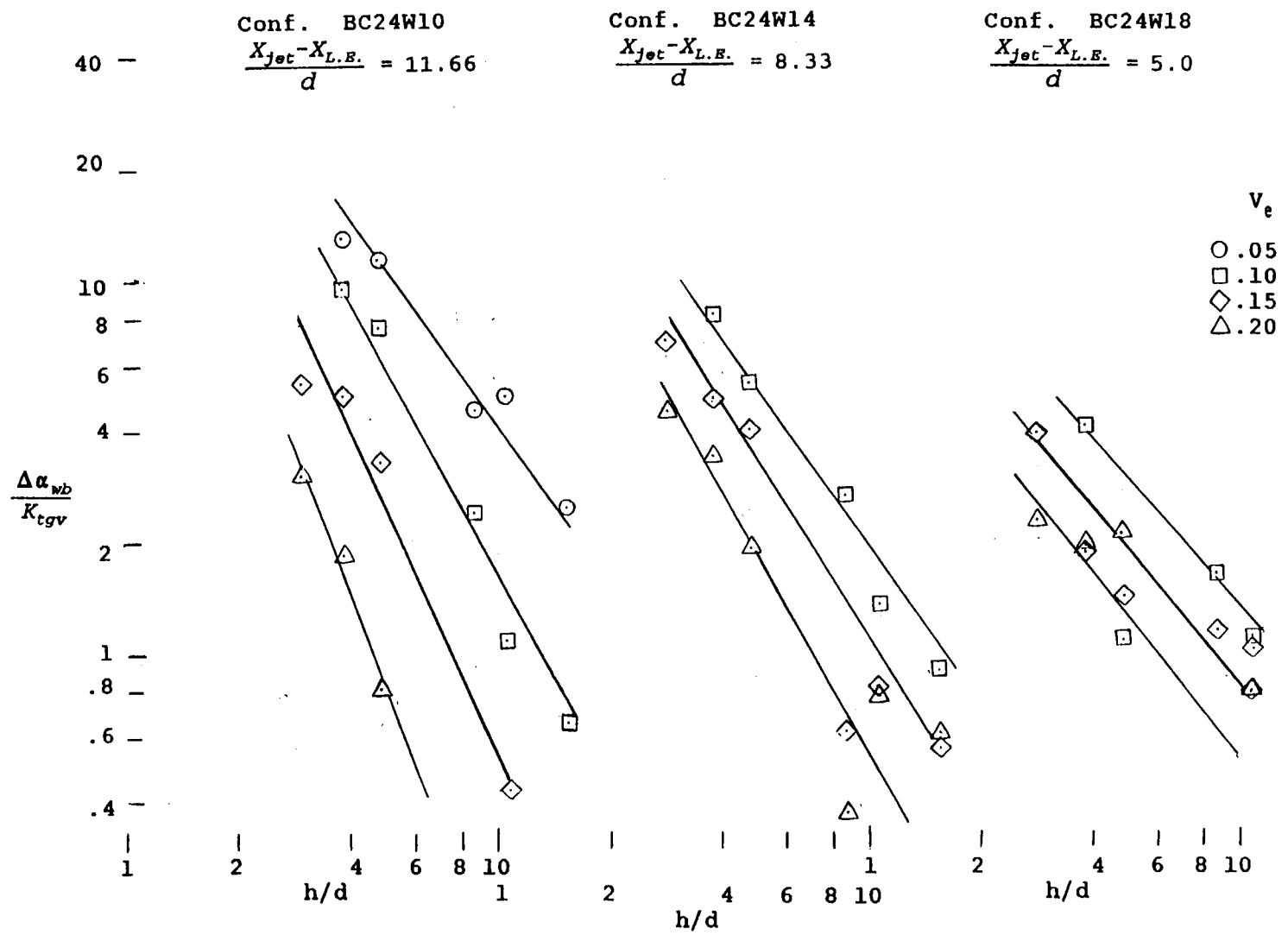

b) Log-Log plot

Figure 24.- Concluded.

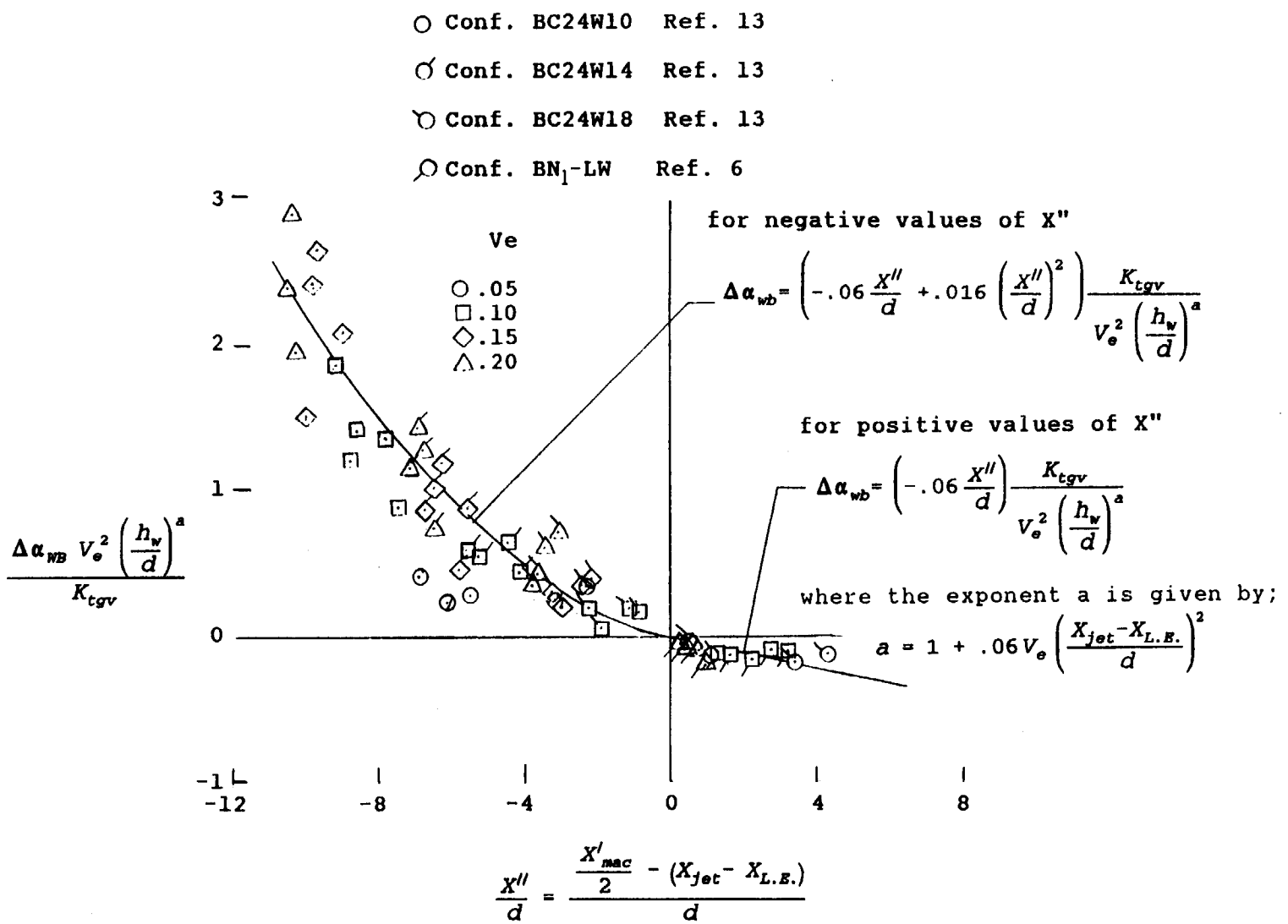

Figure 25.- Correlation of ground vortex induced upwash on three wing-body configurations of reference 13 and one of reference 6.

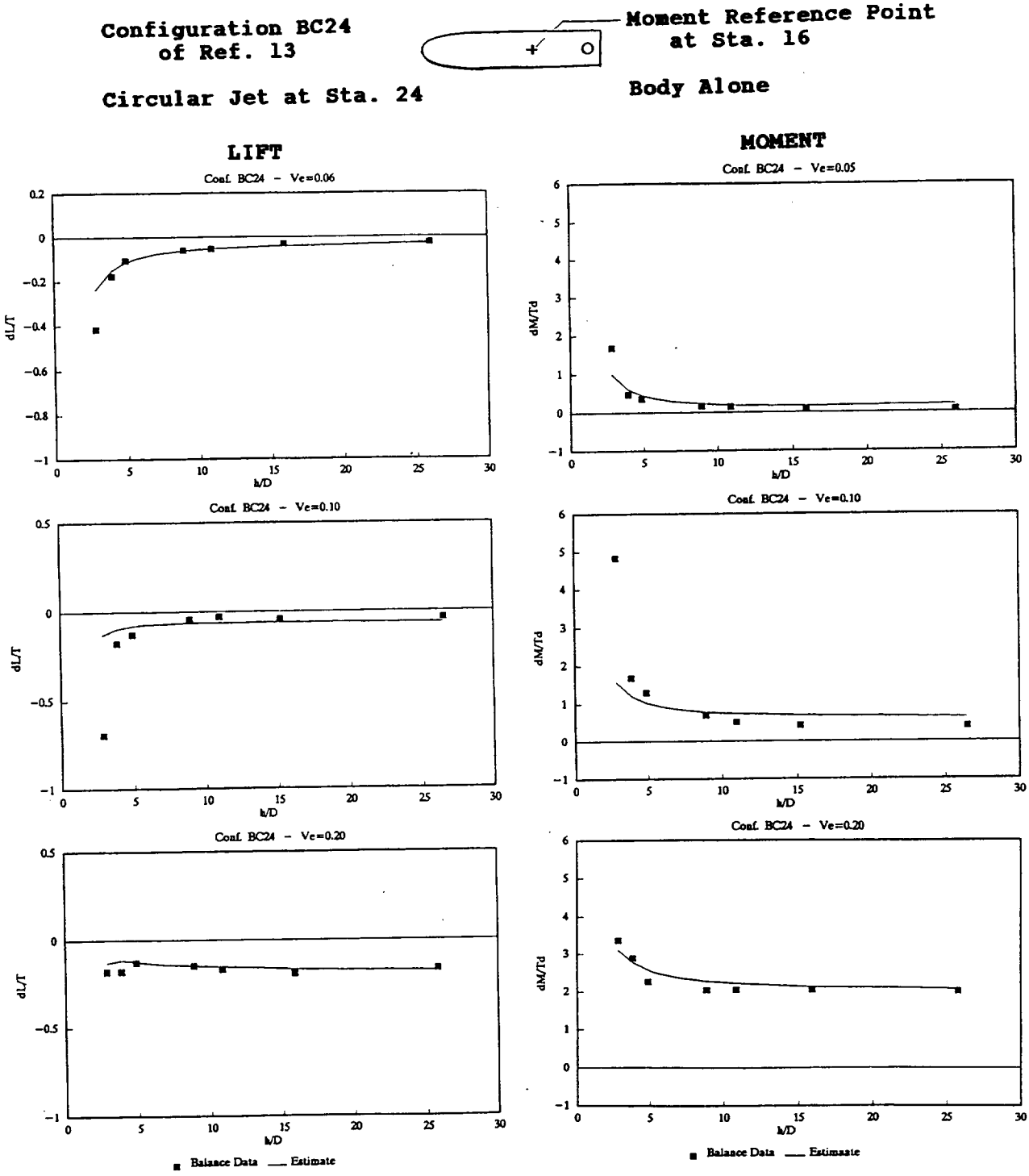

a) Body alone

Figure 26.- Comparison of estimates with data for several configurations of reference 13 tested over the fixed ground board.

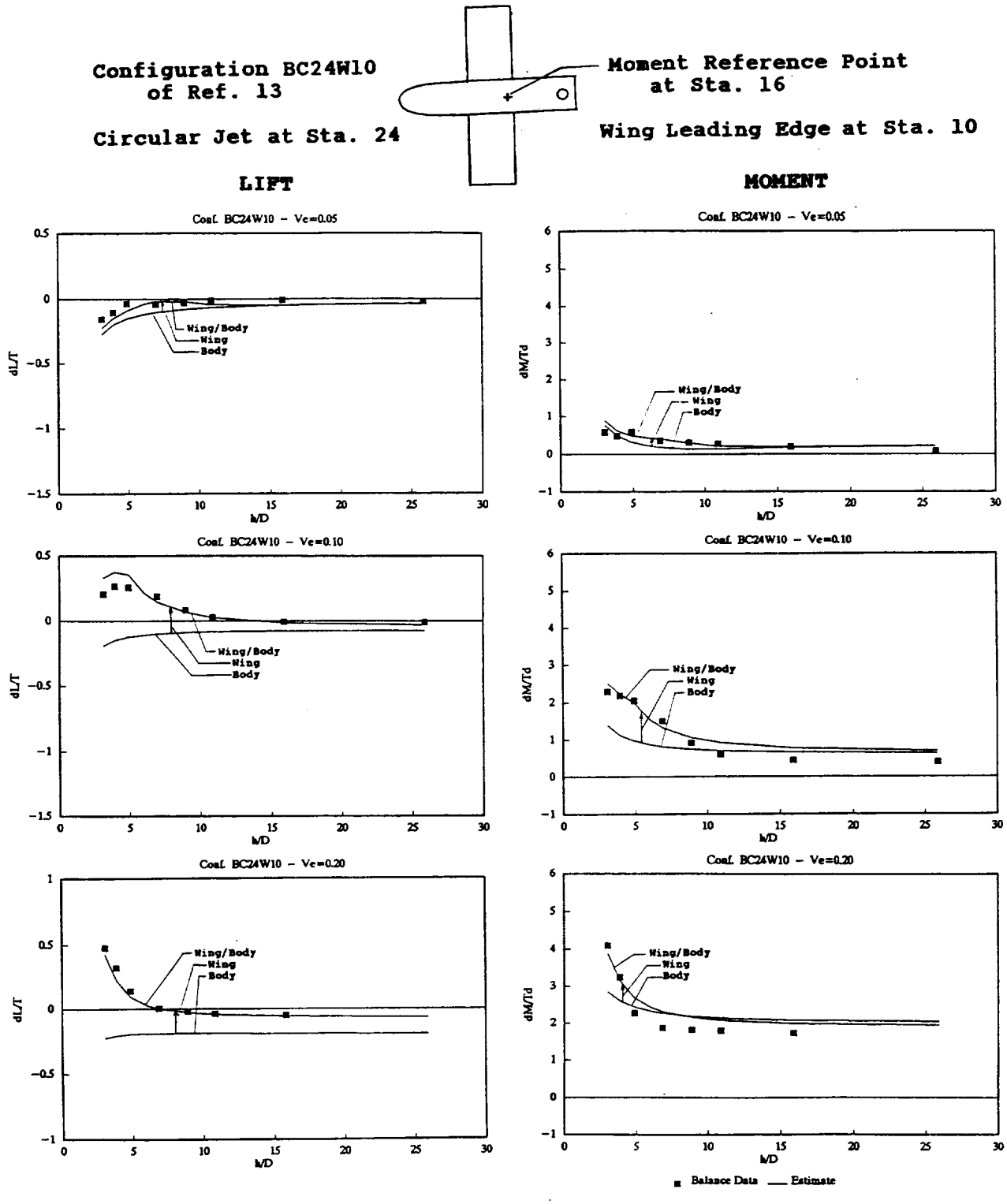

b) Wing-Body configuration with wing forward

Figure 26.- Continued.

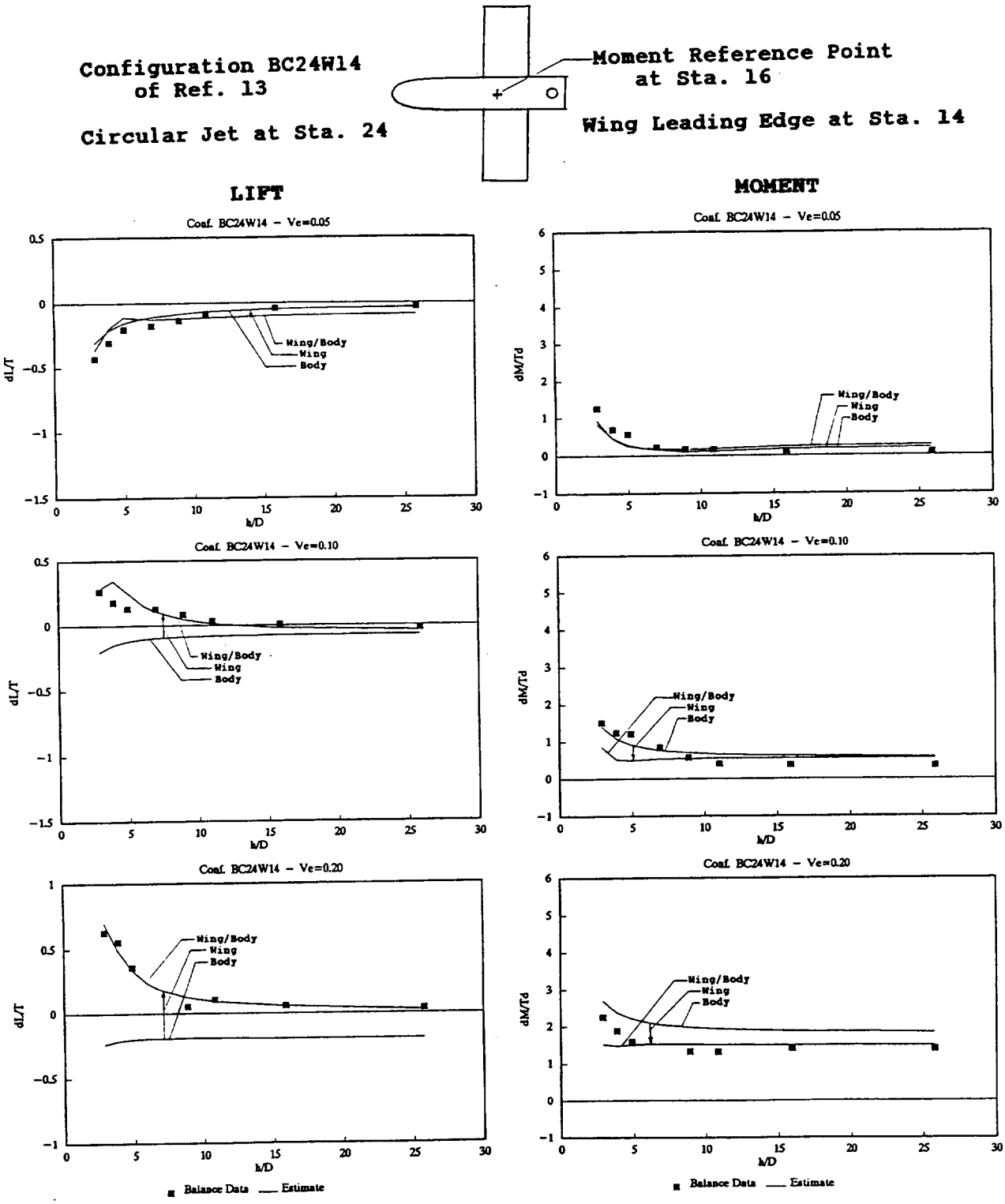

c) Wing-Body configuration with wing at mid position

Figure 26.- Continued.

This page intentionally blank

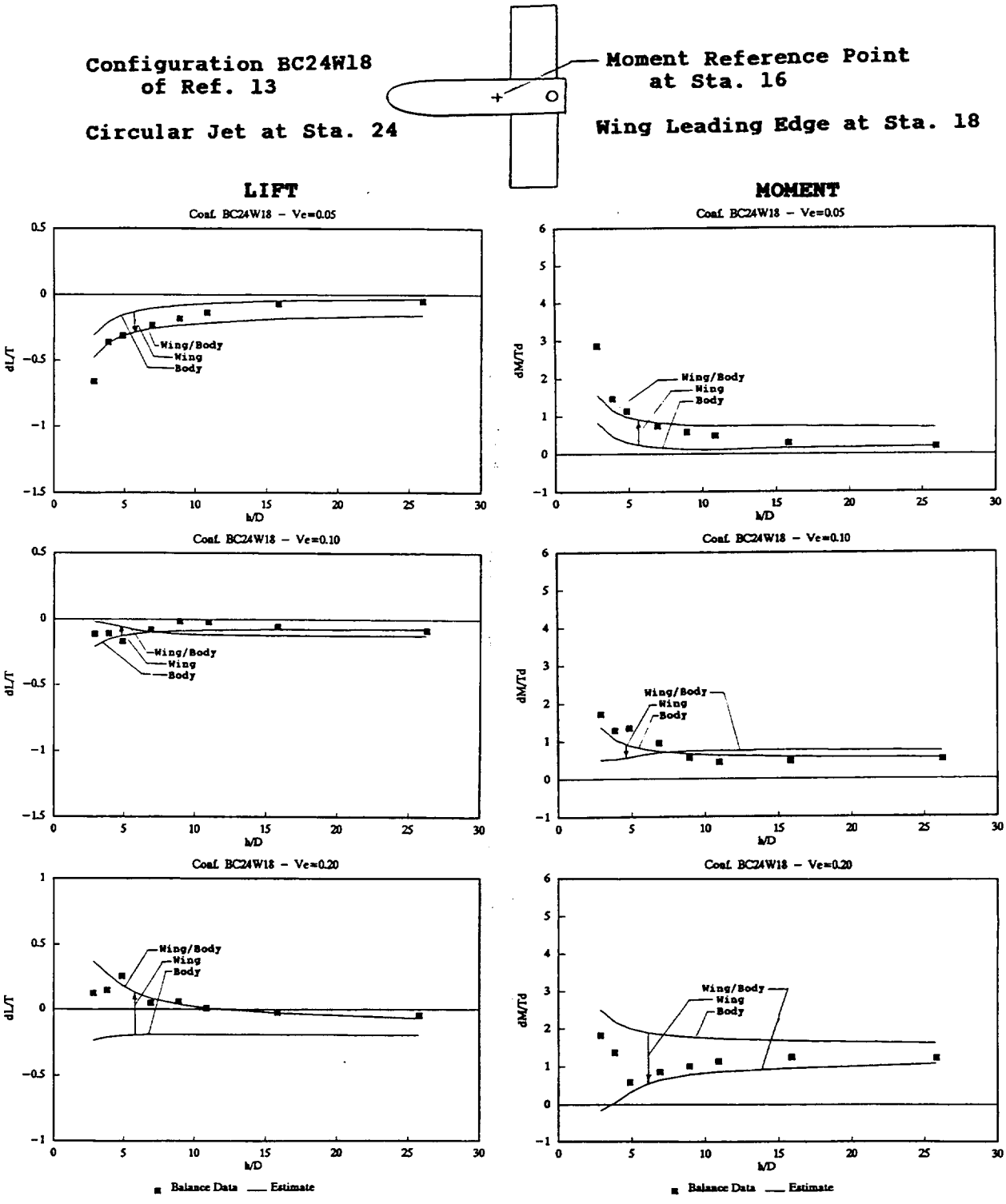

d) Wing-Body configuration with wing aft

Figure 26.- Concluded.

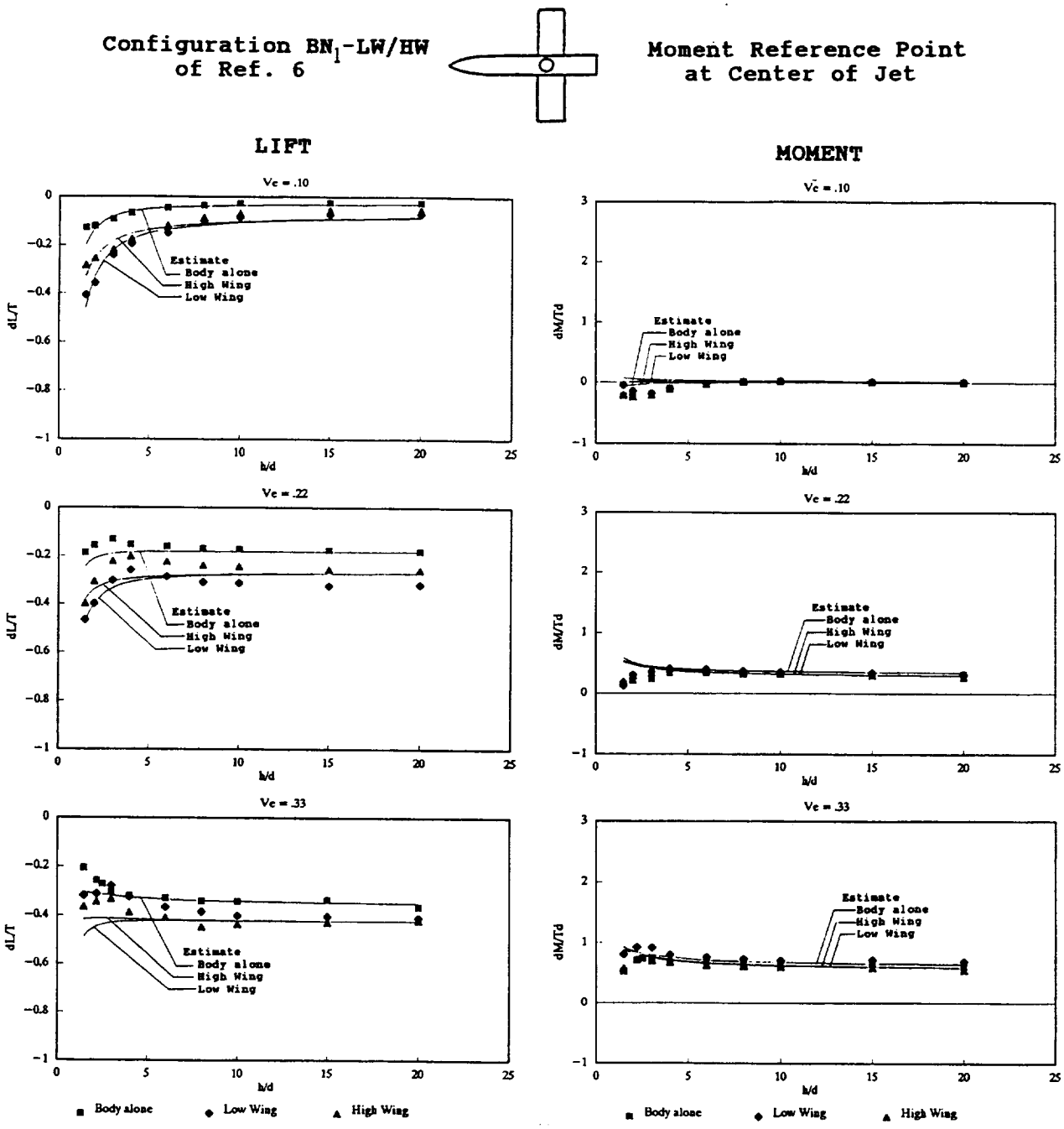

a) Total lift and moment

Figure 27.- Comparison of the estimated and experimental effect of wing height on wing/body model of reference 6.

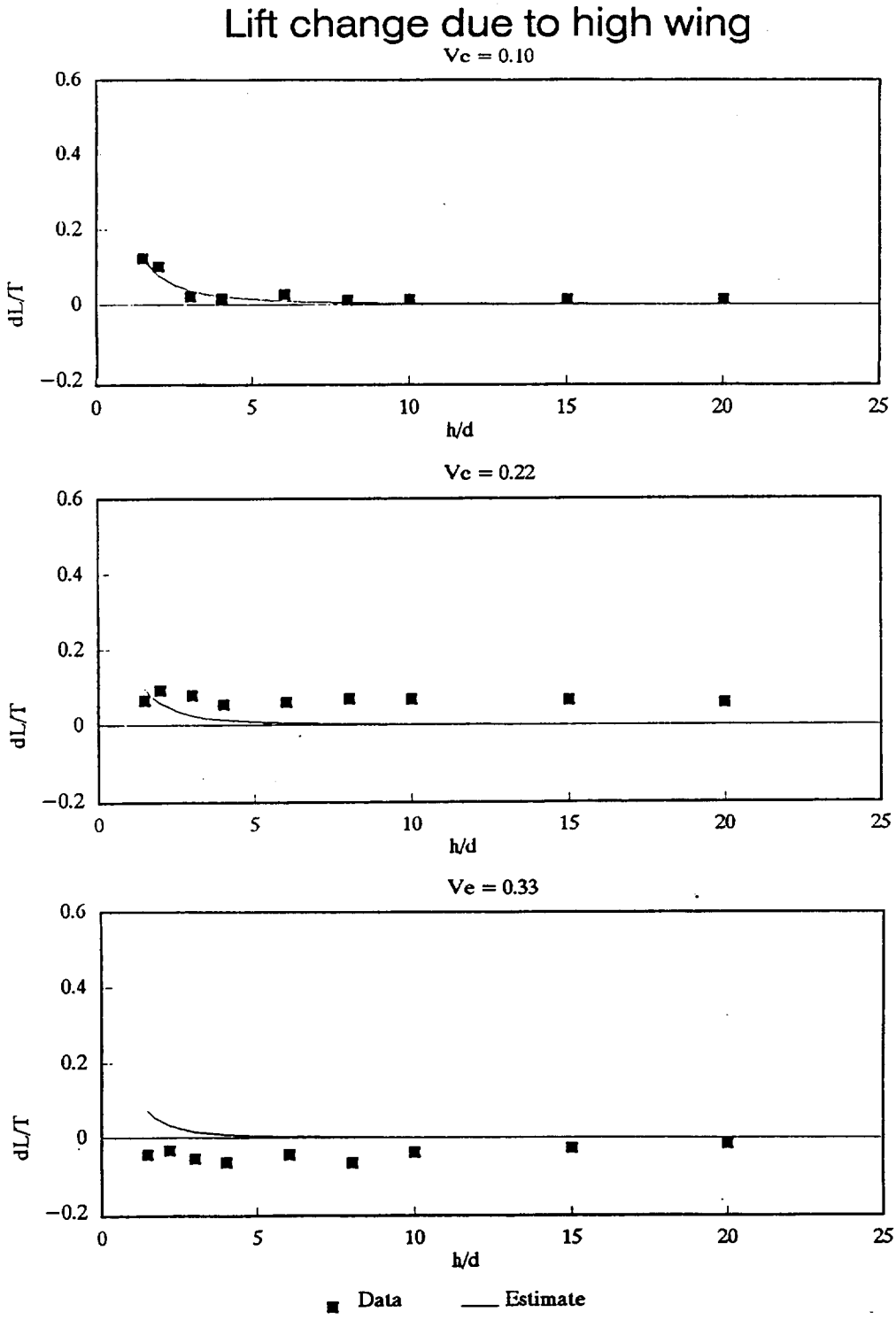

b) Lift increase due to raising wing to high position

Figure 27.- Concluded.

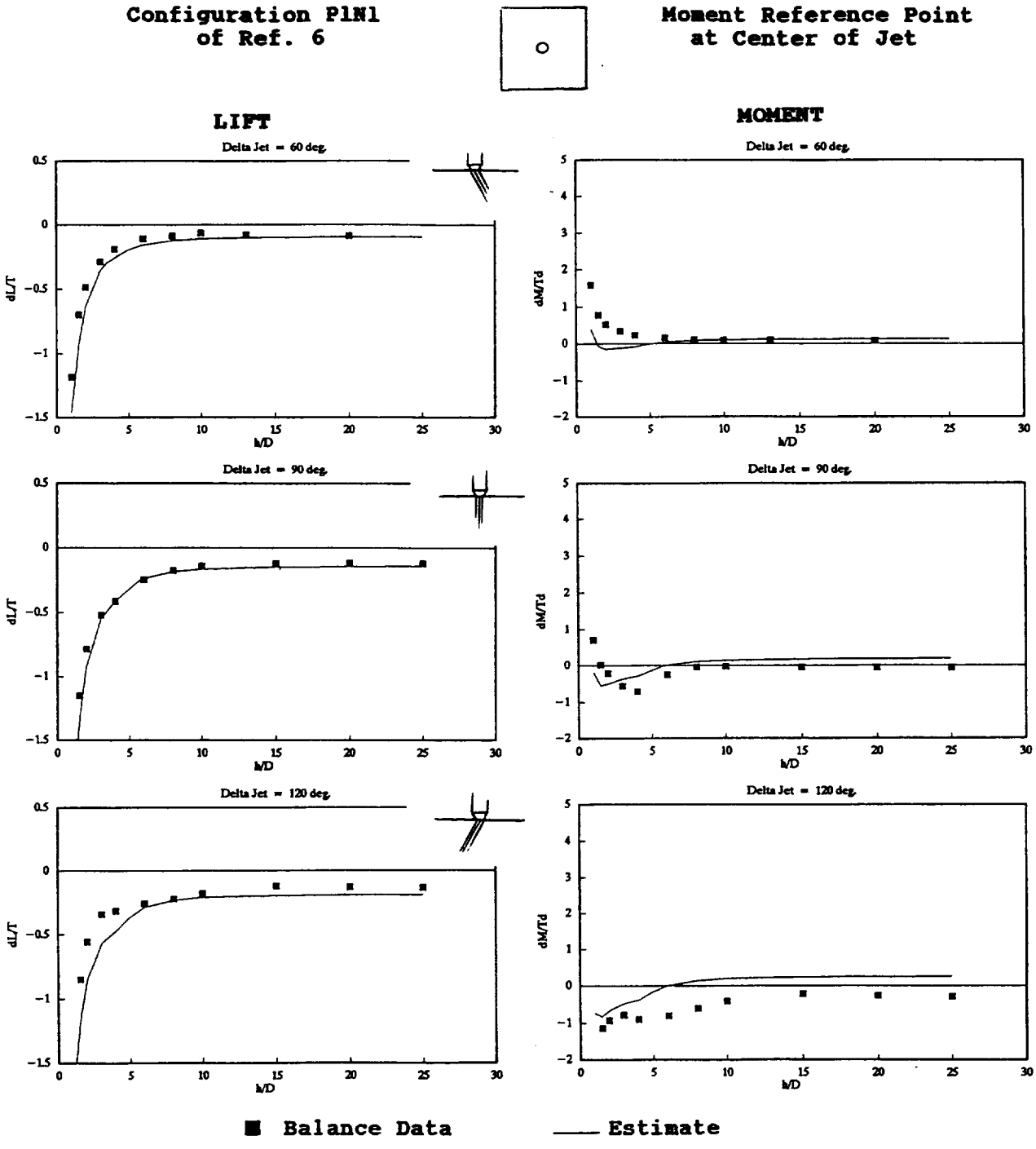

a) V_e = .10

Figure 28- Comparison of estimates with data on the effect of jet deflection.

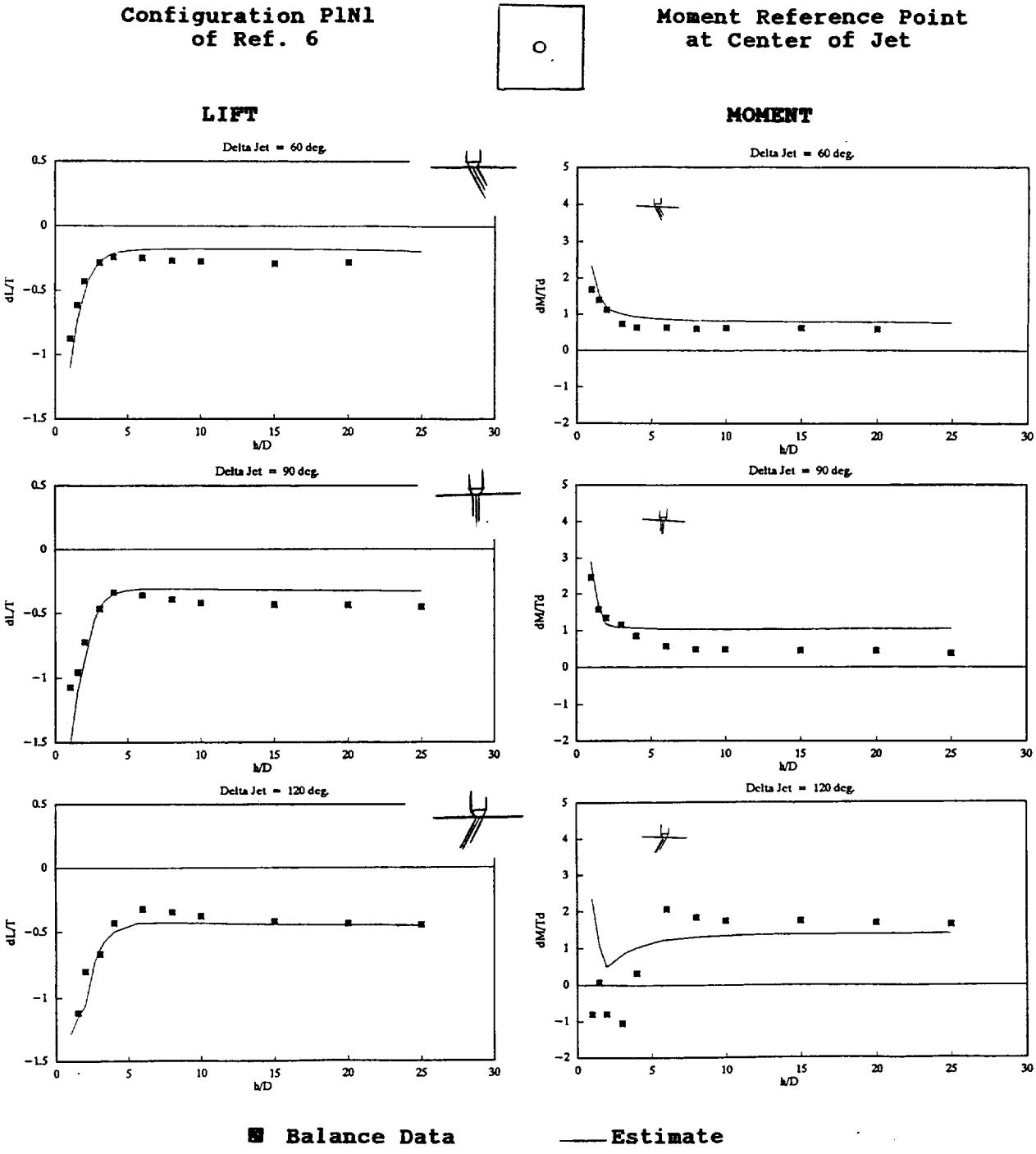

b) V_e = .22

Figure 28.- Concluded.

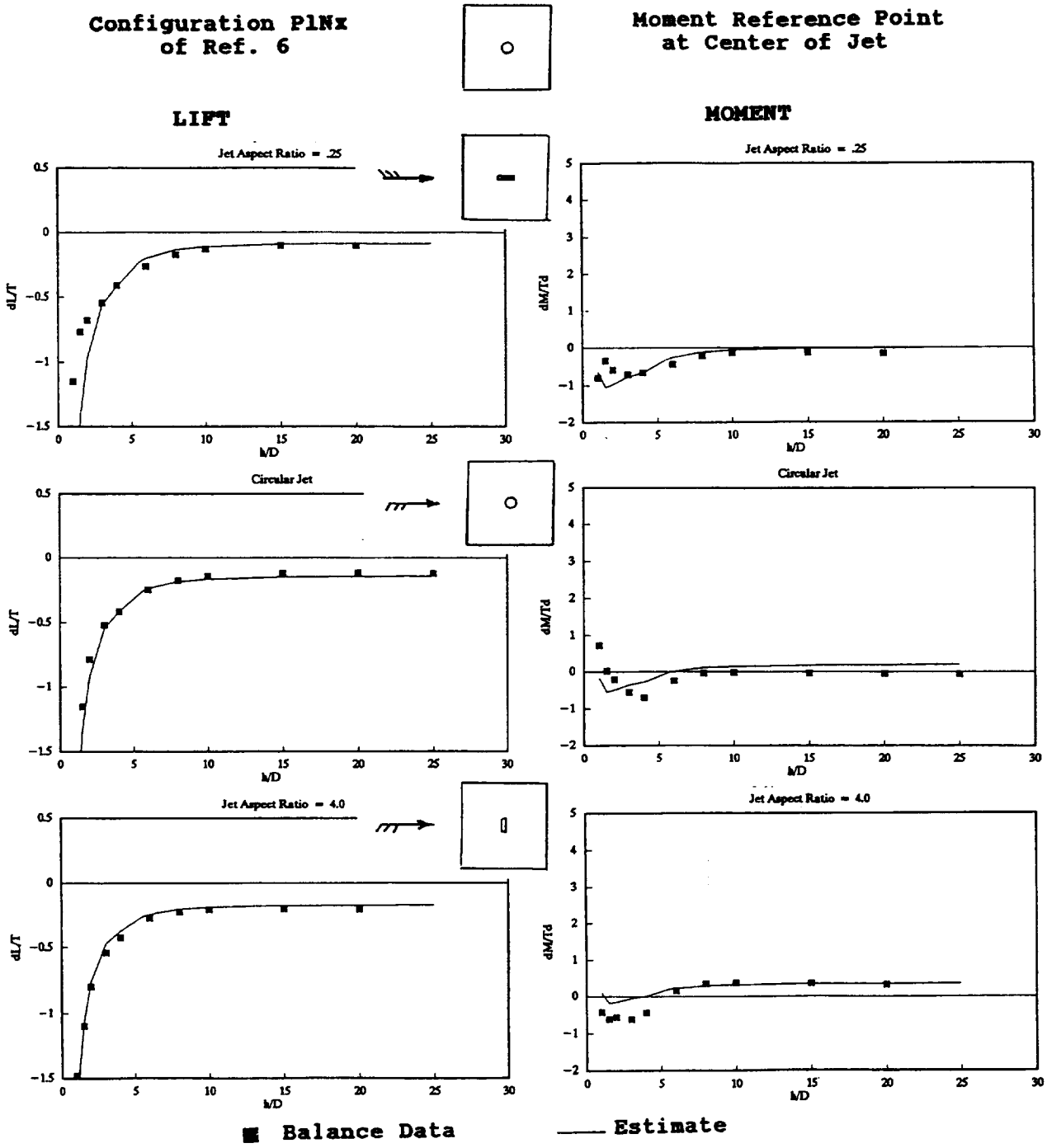

a) V_e = .10

Figure 29- Comparison of estimates with data on the effect of jet aspect ratio.

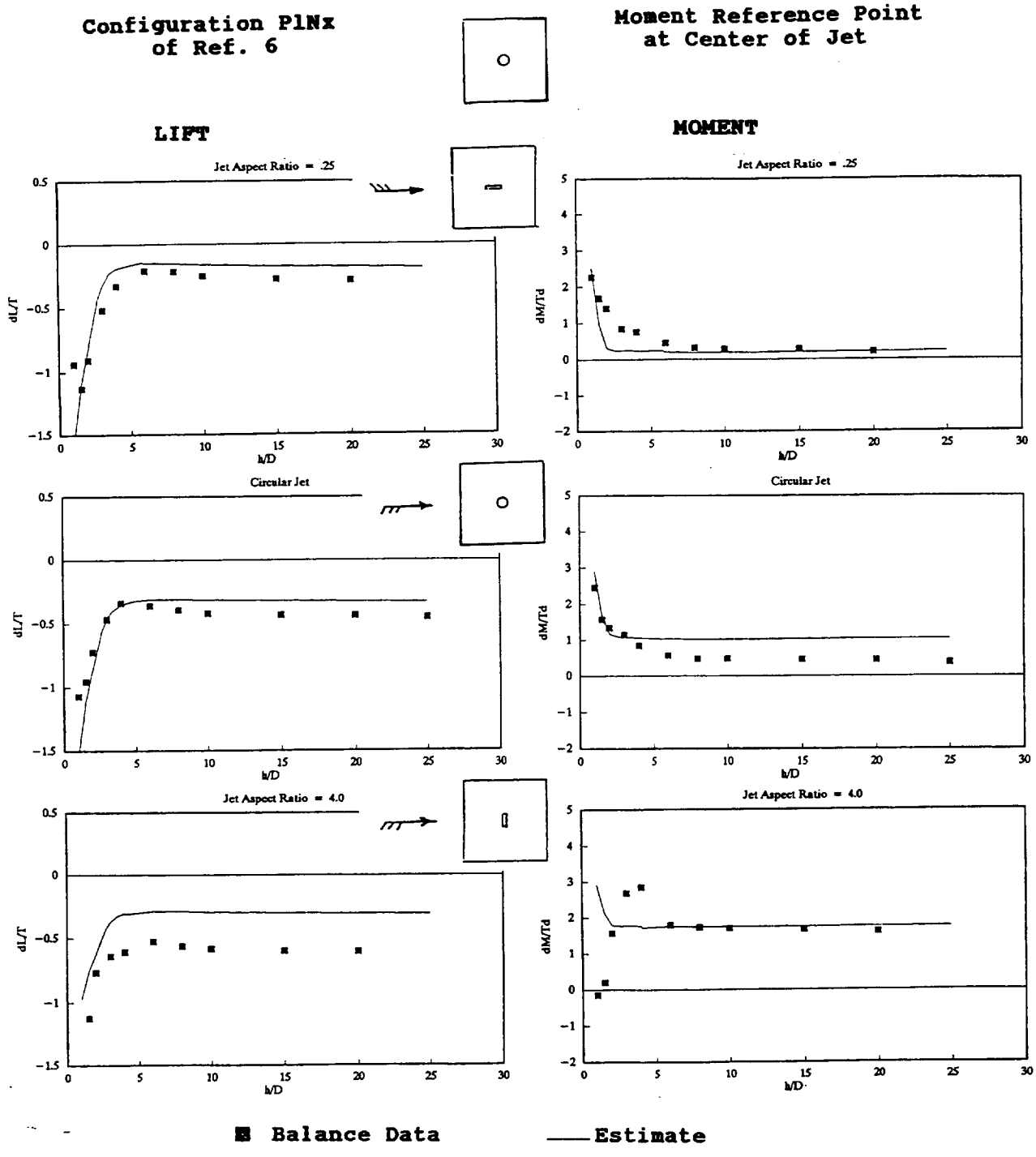

b) V_e = .22

Figure 29.- Concluded.

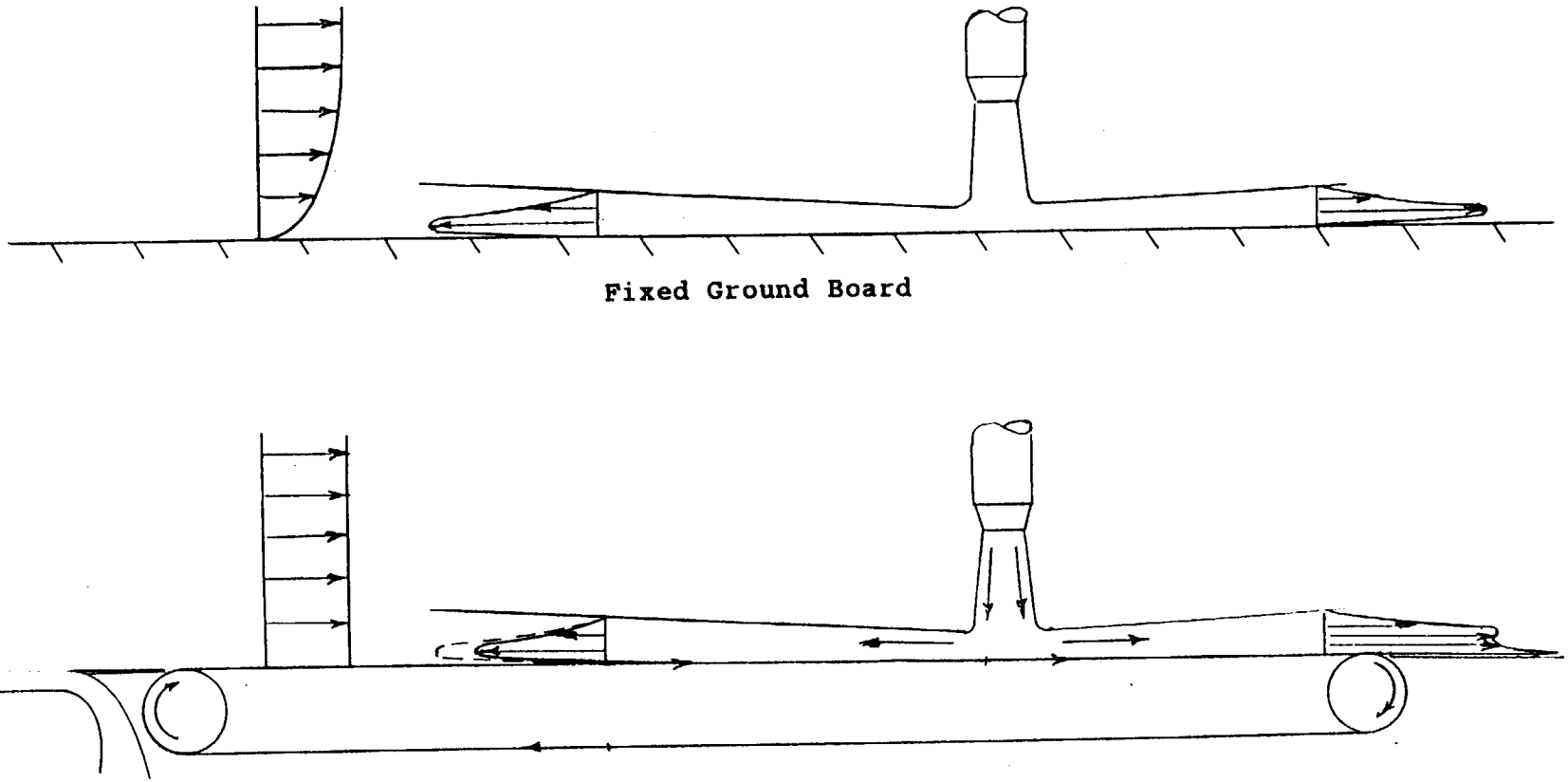

Figure 30.- Schematic of free stream flow and wall jet profiles experienced by jet impingement on a fixed ground board and on a moving ground surface.

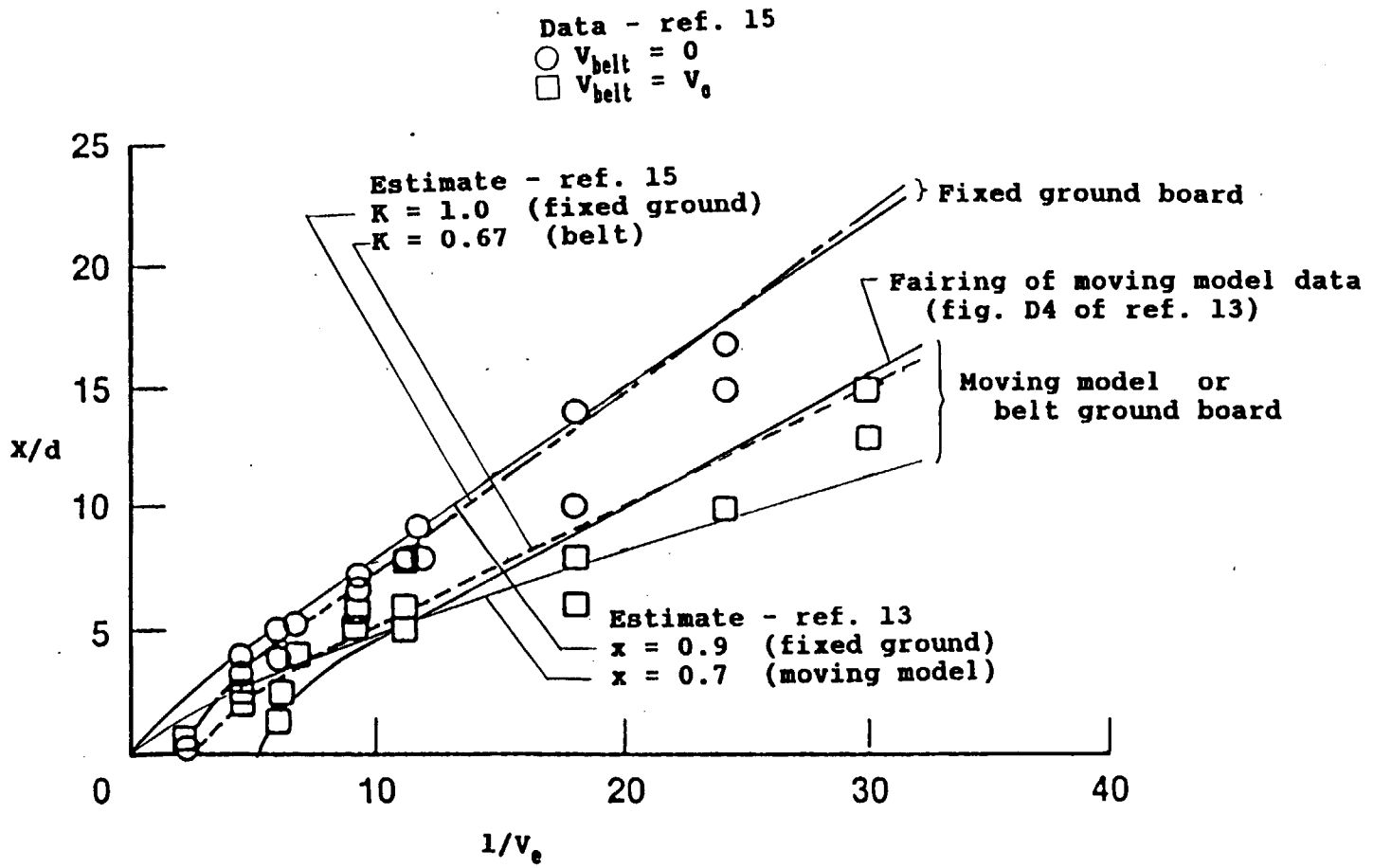

Figure 31.- Effect of belt or moving model on forward penetration of vortex as measured on the ground.

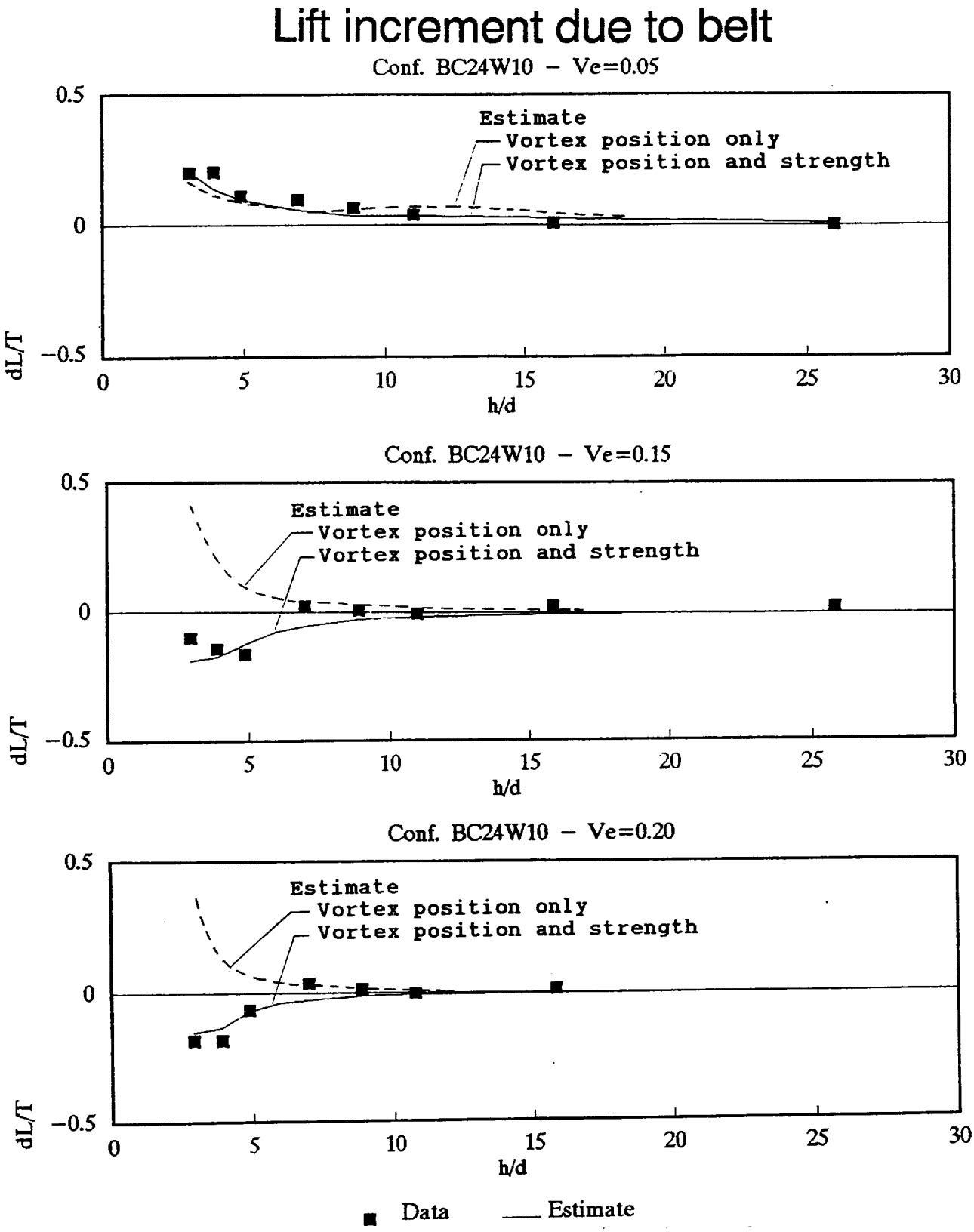

Figure 32.- Comparison of estimates with experimentally determined lift increment due to moving ground.

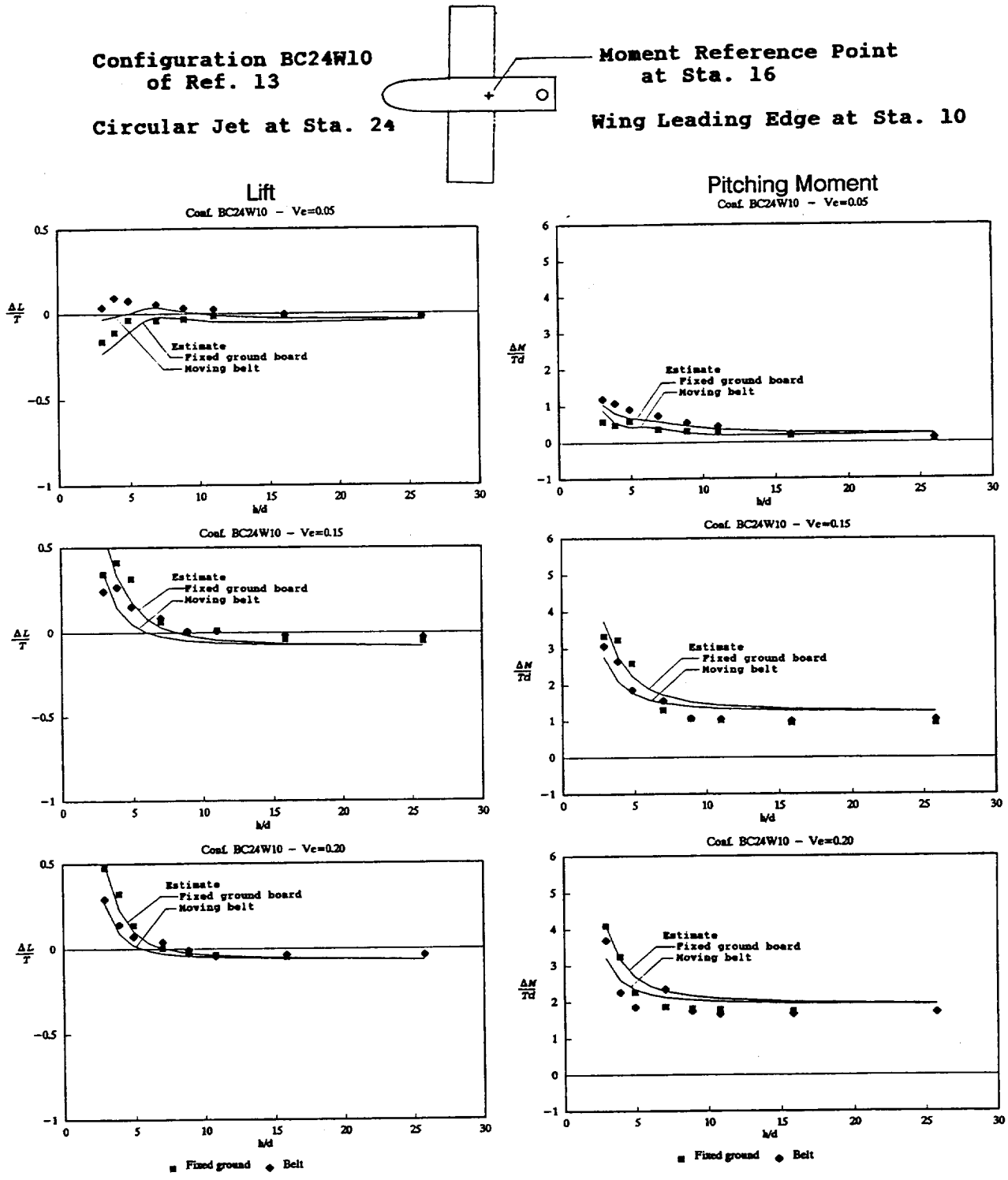

a) Circular jet - Wing forward

Figure 33.- Comparison of estimates with data for several wing-body configurations of reference 13 tested over fixed and moving belt ground boards.

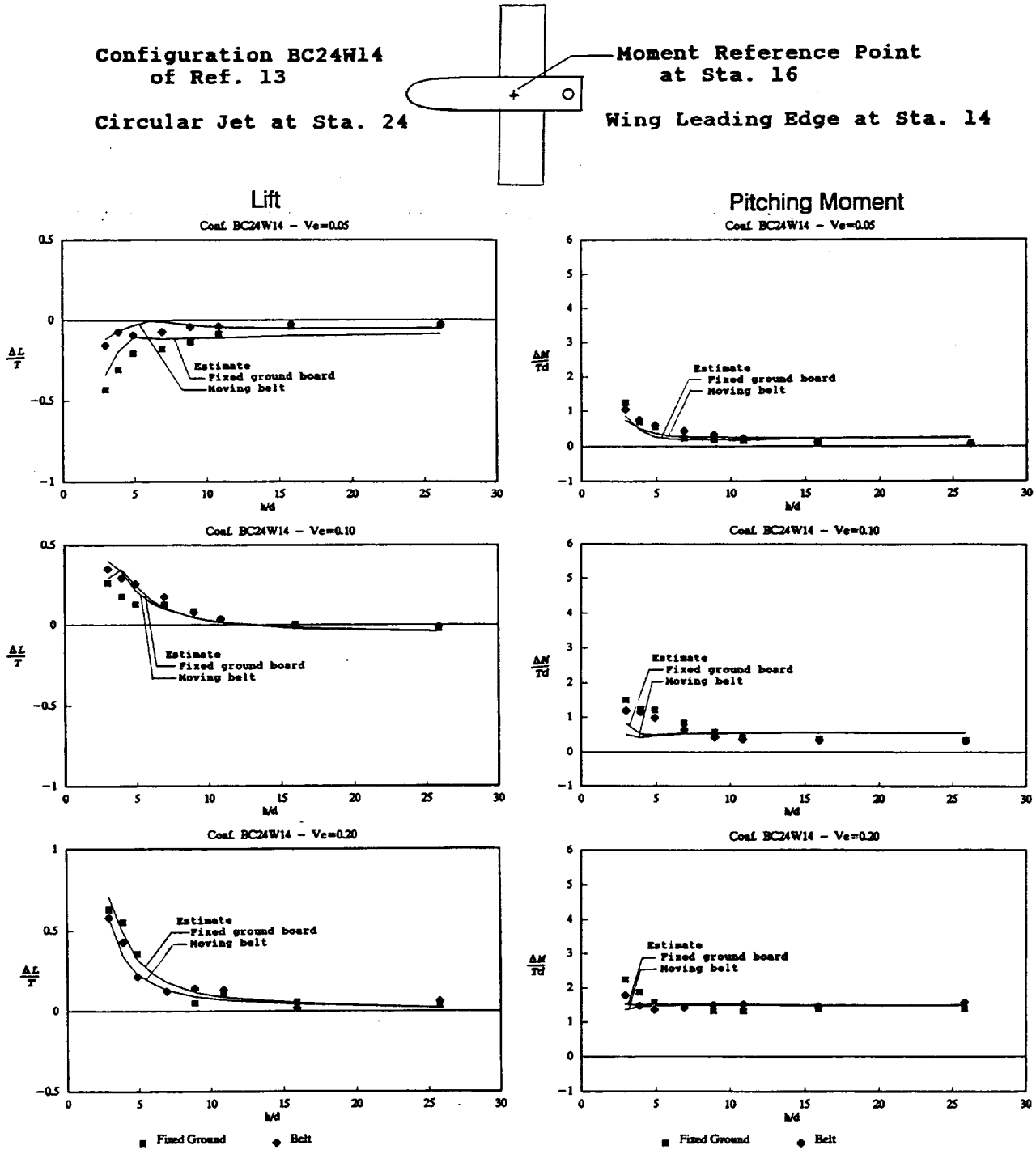

b) Circular jet - Wing at mid position

Figure 33.- Continued.

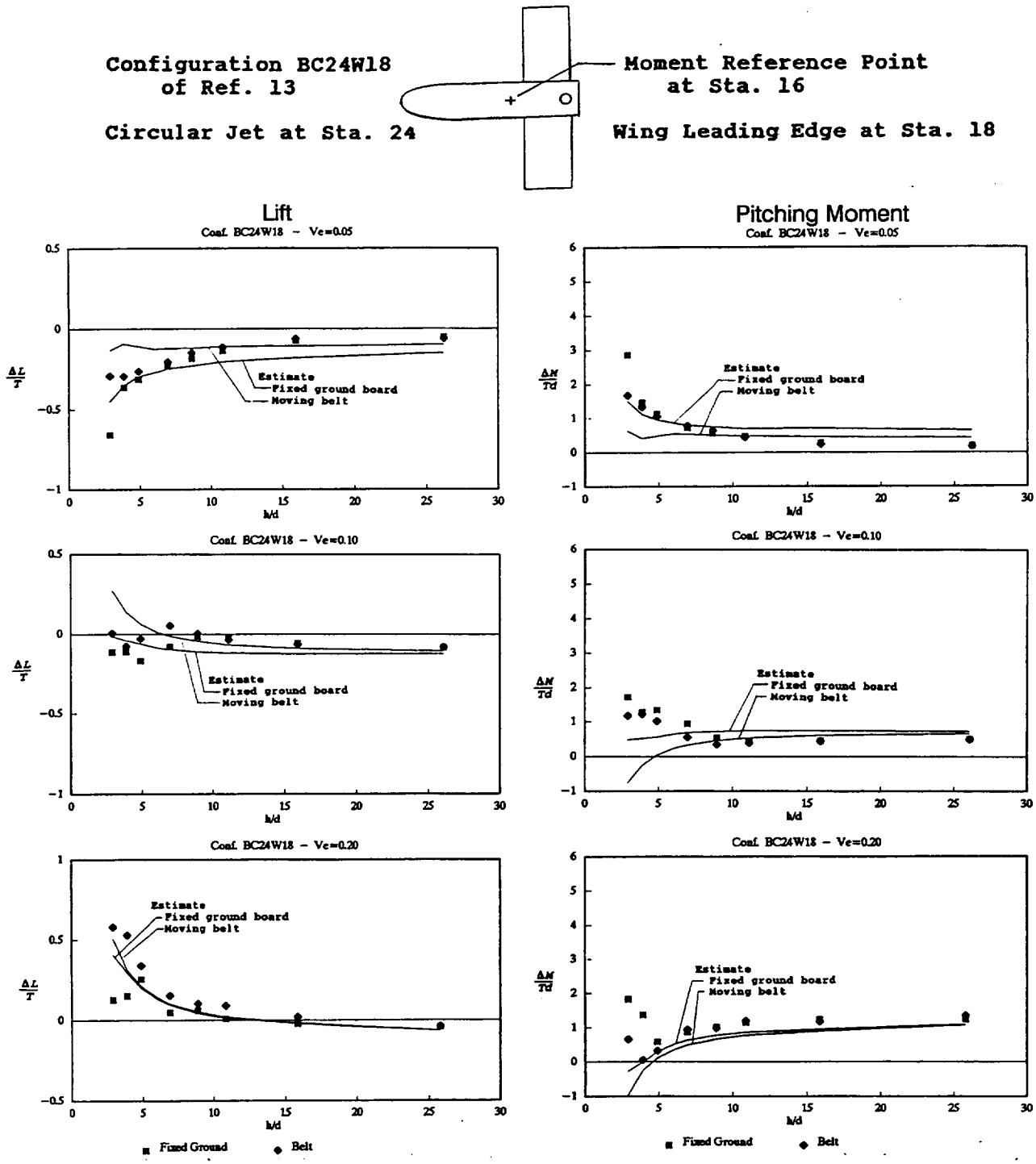

c) Circular jet - Wing aft

Figure 33.- Continued.

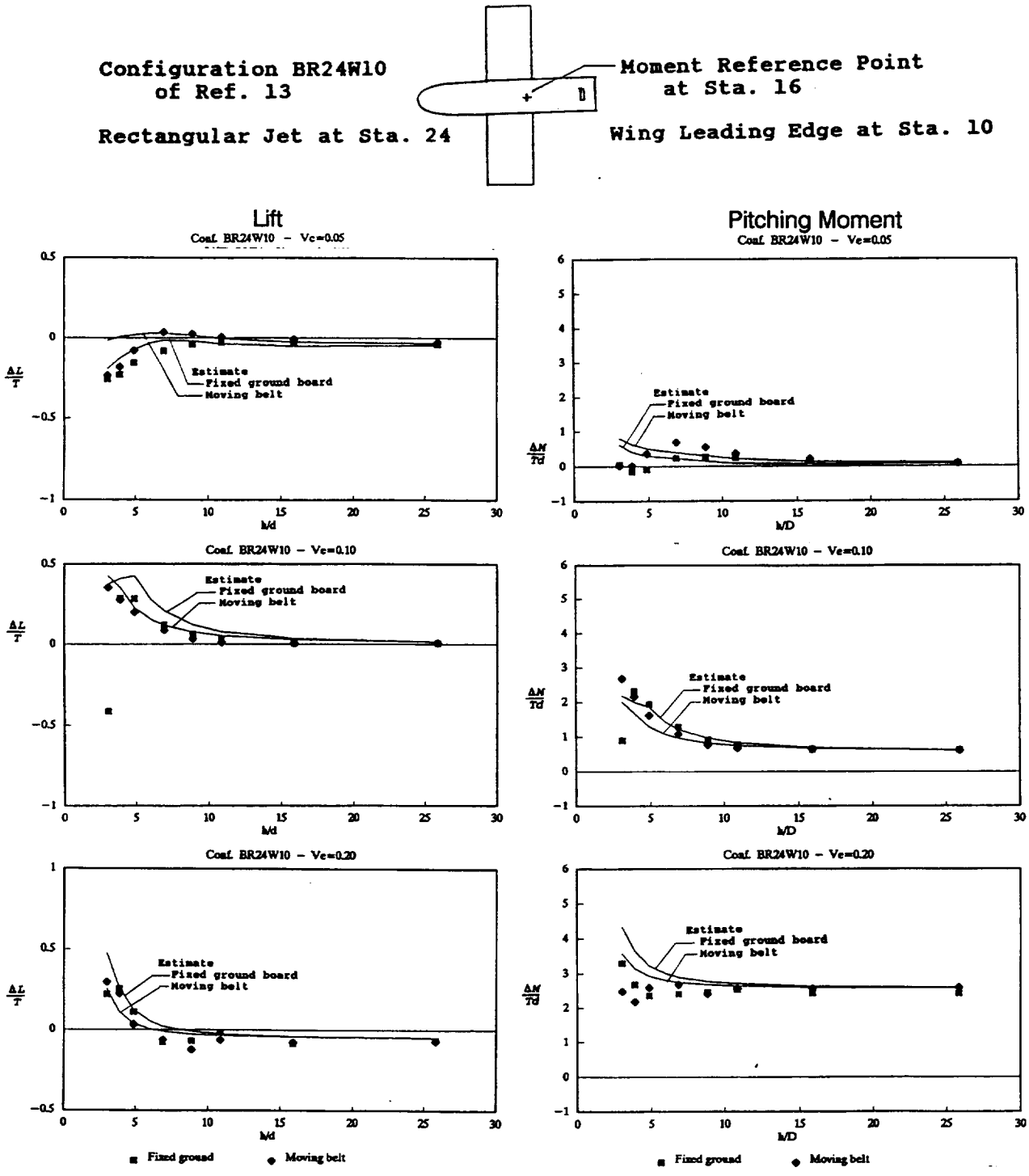

d) Rectangular jet - Wing forward

Figure 33.- Continued.

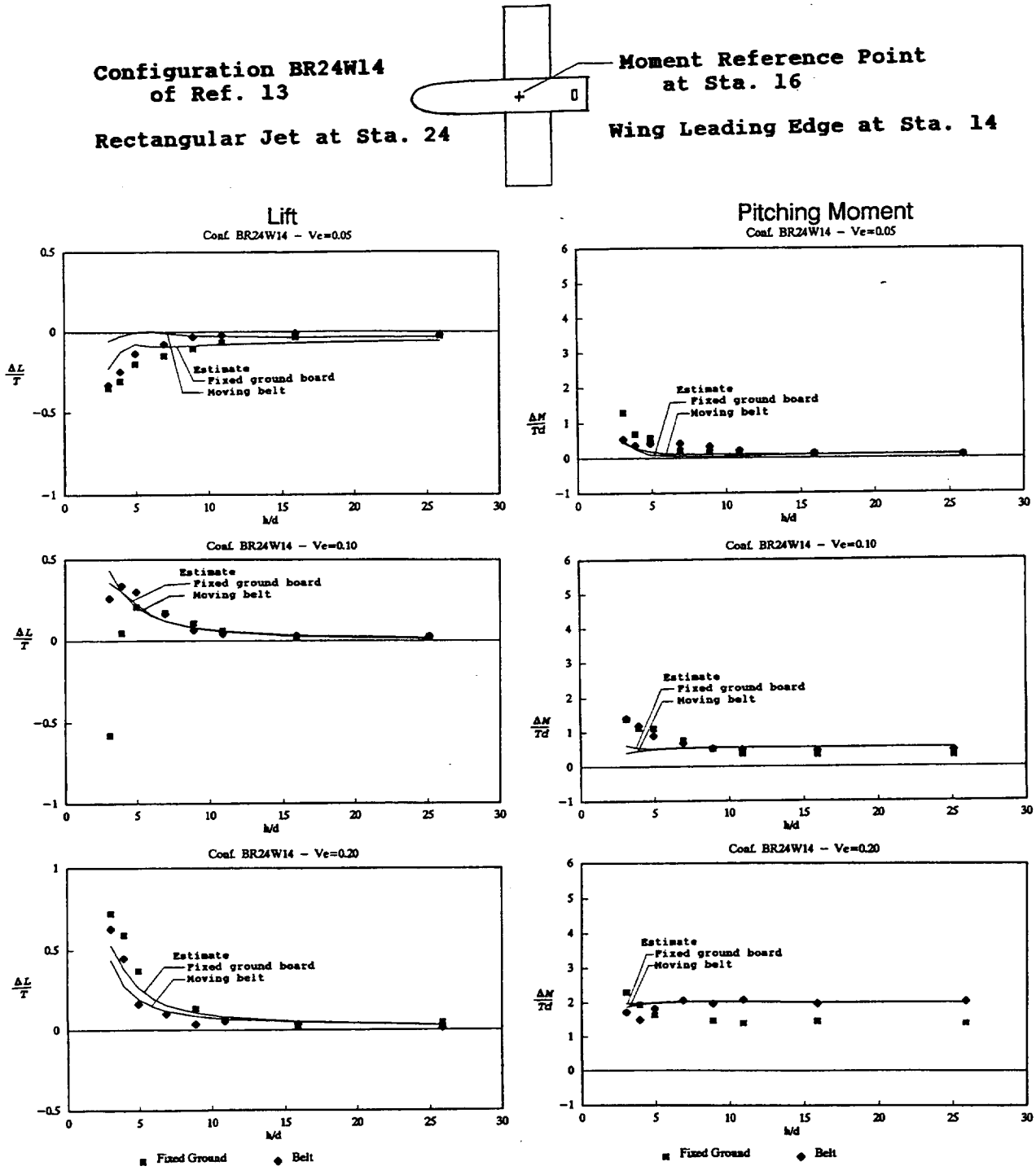

e) Rectangular jet - Wing at mid position

Figure 33.- Continued.

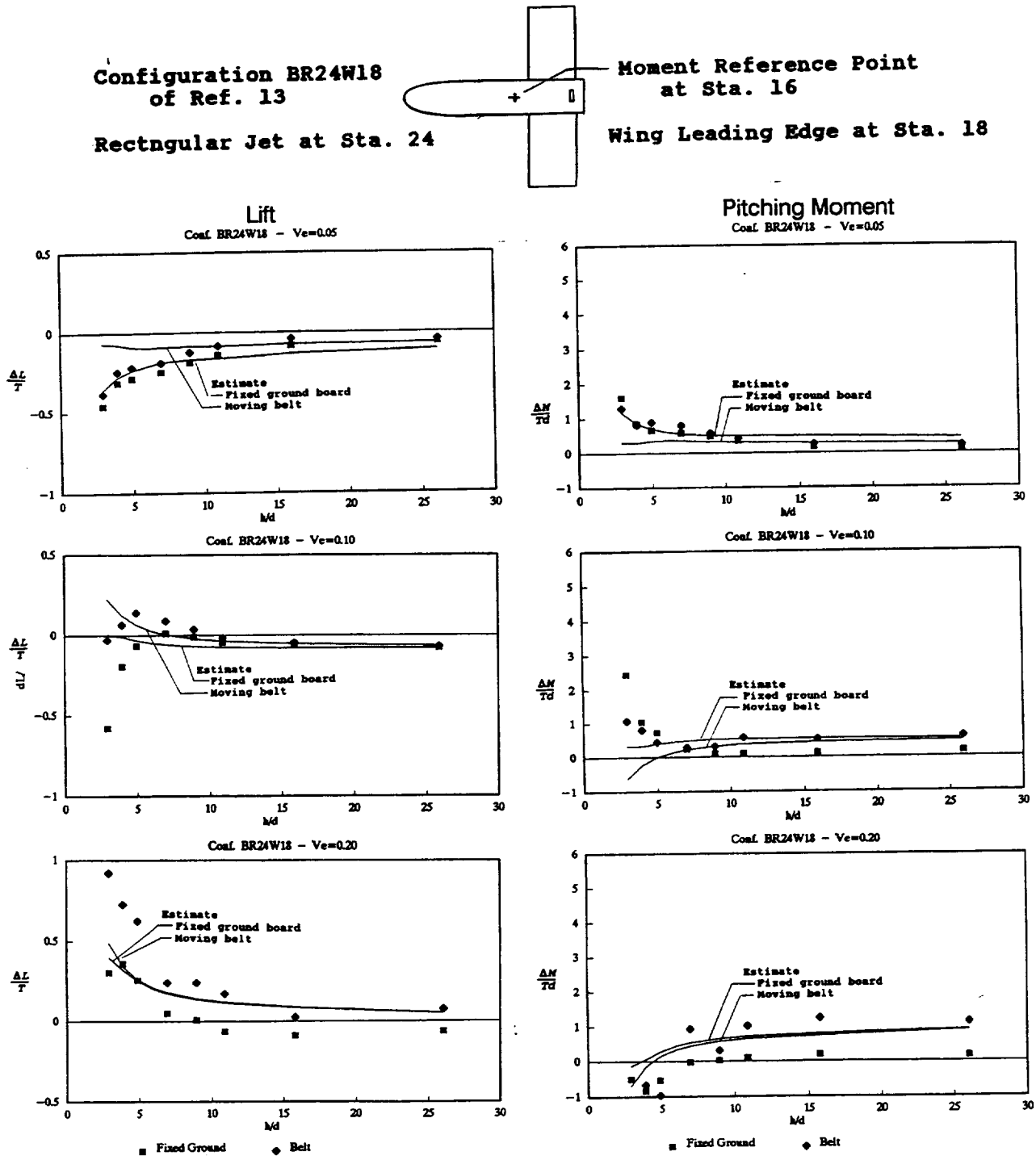

f) Rectangular jet - Wing aft

Figure 33.- Concluded.

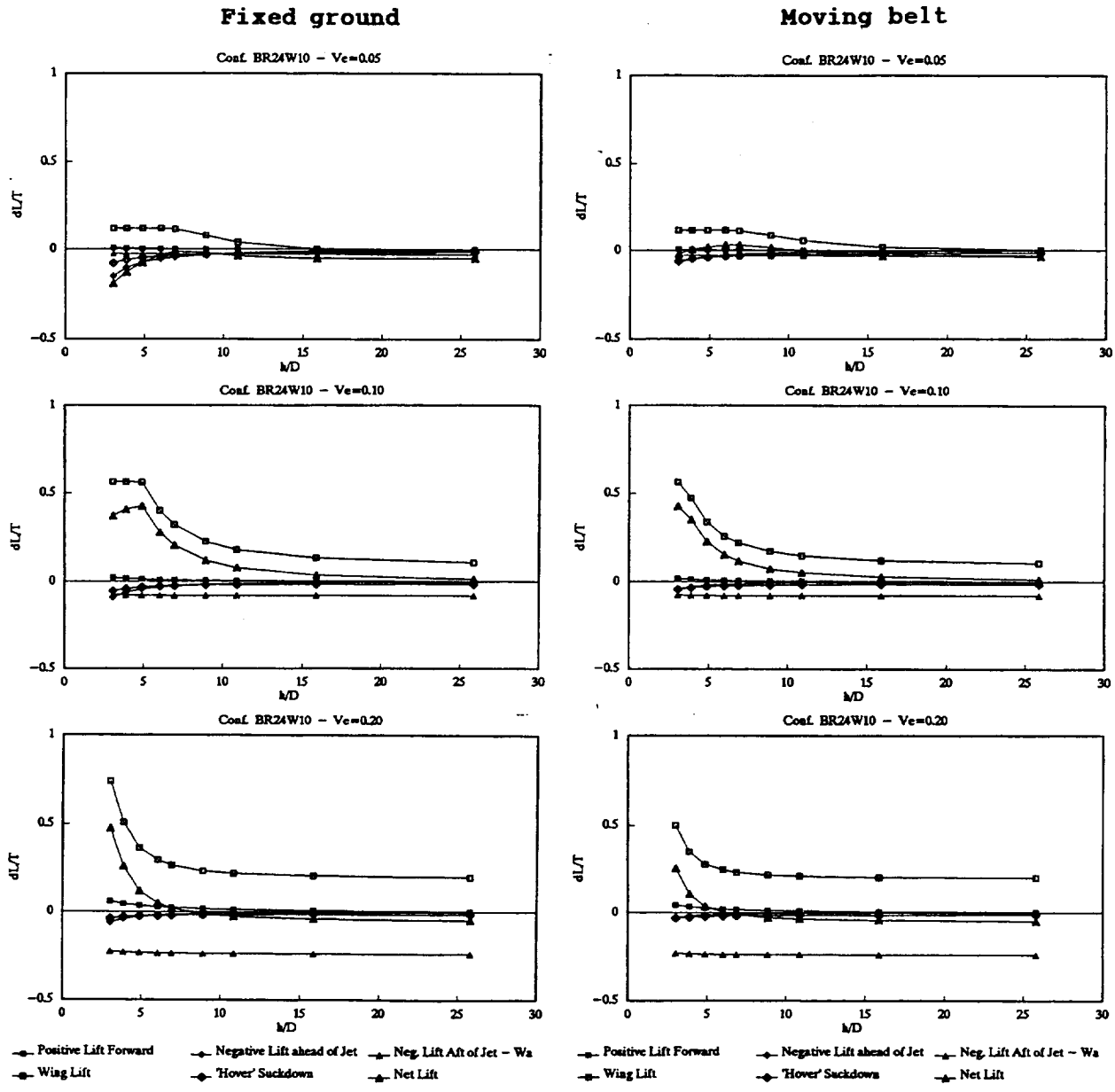

Figure 34.- Comparison of estimated lift breakdown for tests of wing/body model of reference 13 over fixed ground and over moving belt - wing forward - rectangular jet.

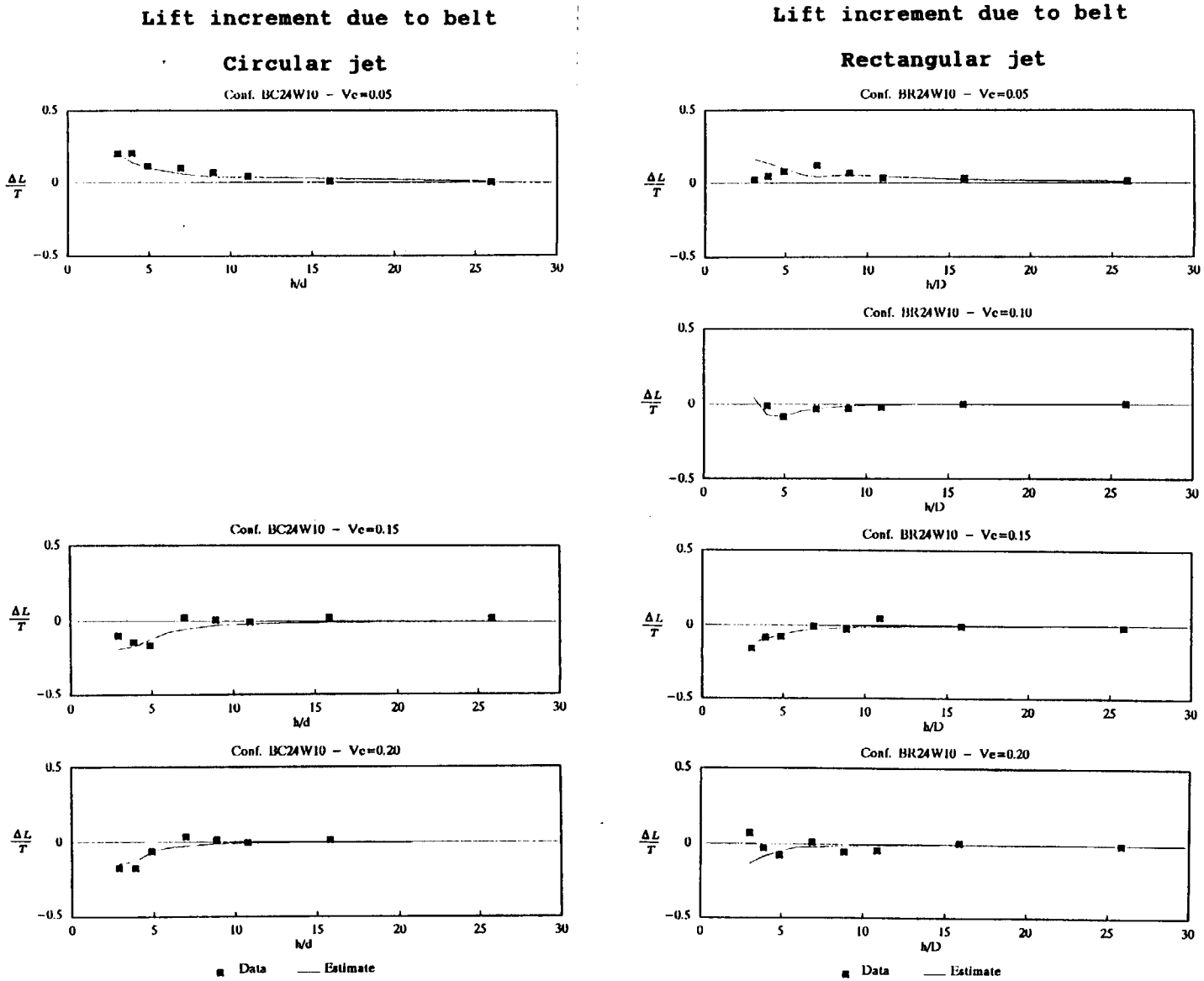

a) Wing in forward position

Figure 35.- Comparison of experimental and estimated increments of lift due to testing over moving ground relative to tests over the fixed ground board.

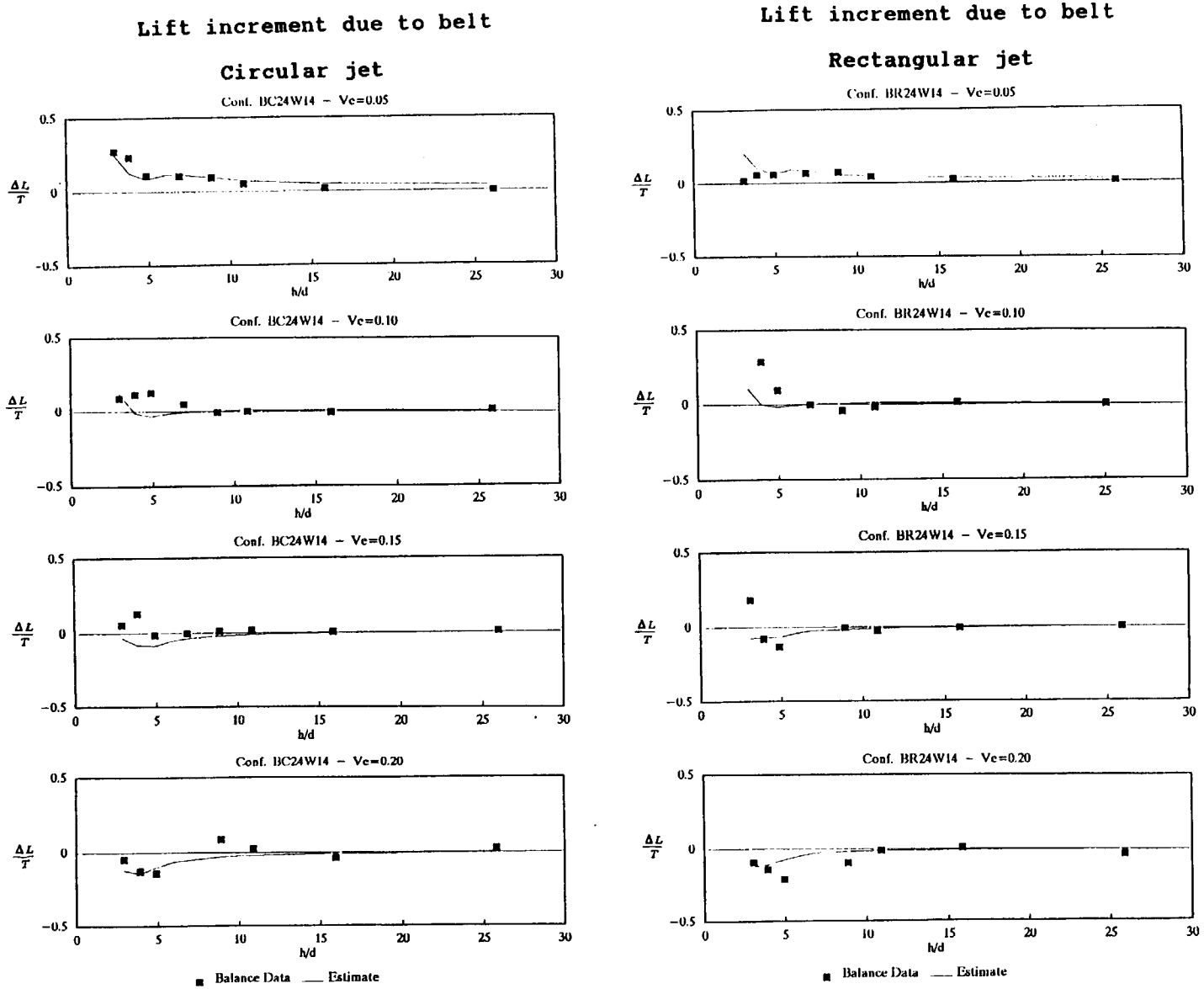

b) wing in mid position

Figure 35 Continued.

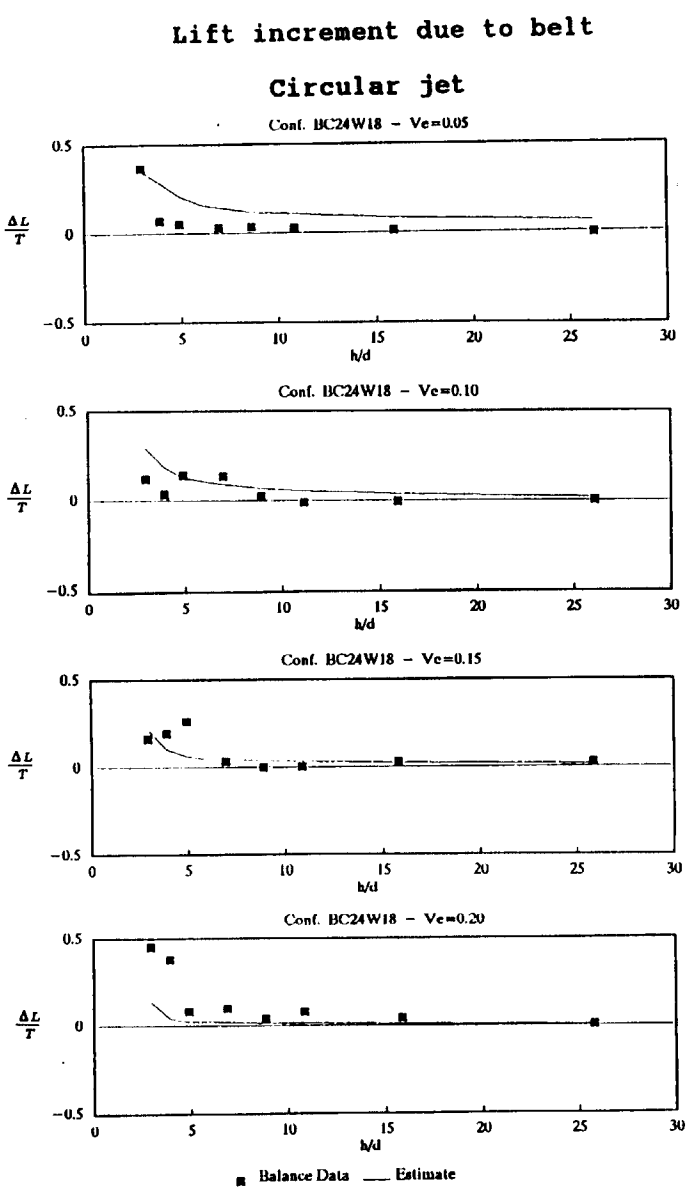

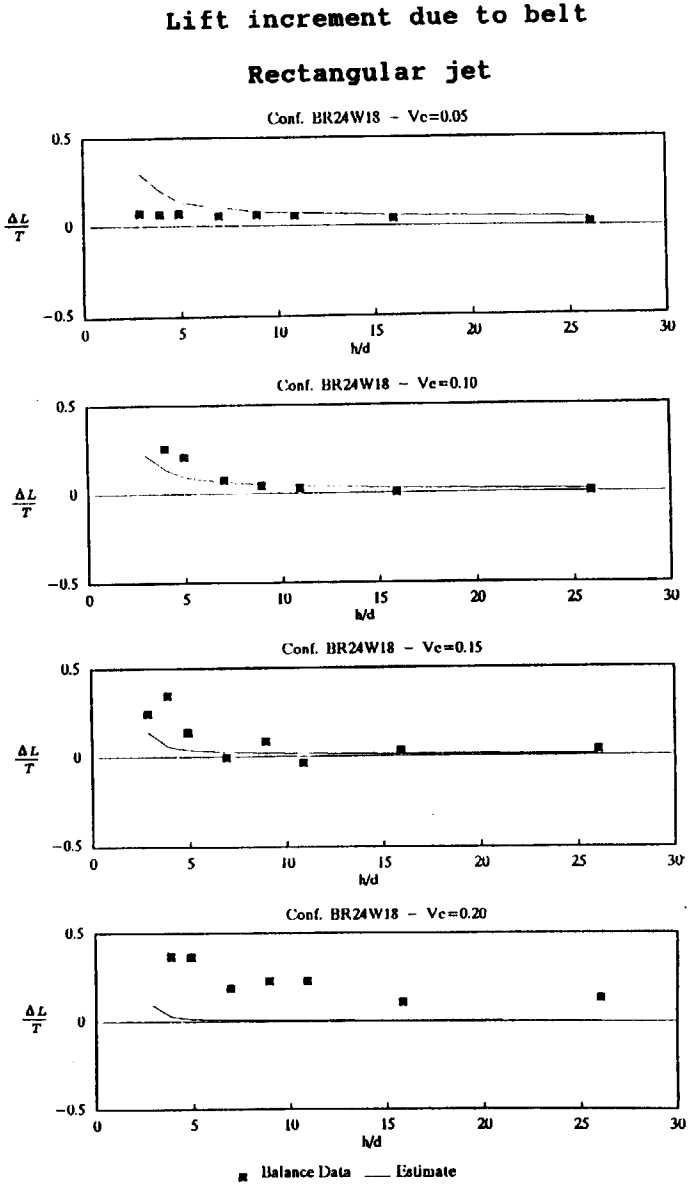

c) wing in aft position

Figure 35 Concluded.

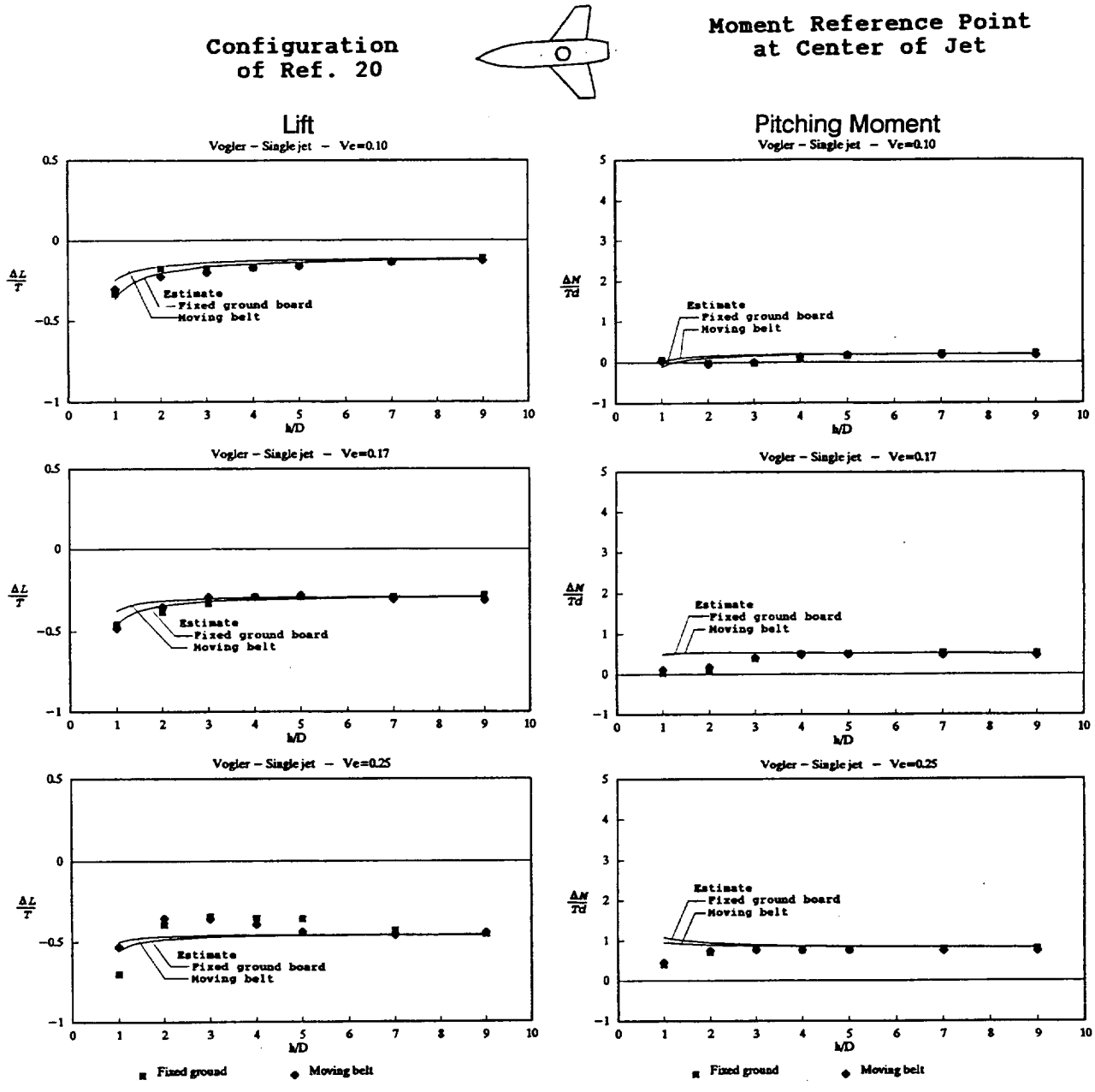

a) Lift and Pitching moment

Figure 36.- Comparison of estimates with data for wing-body configuration of reference 20 tested over fixed and moving belt ground boards.

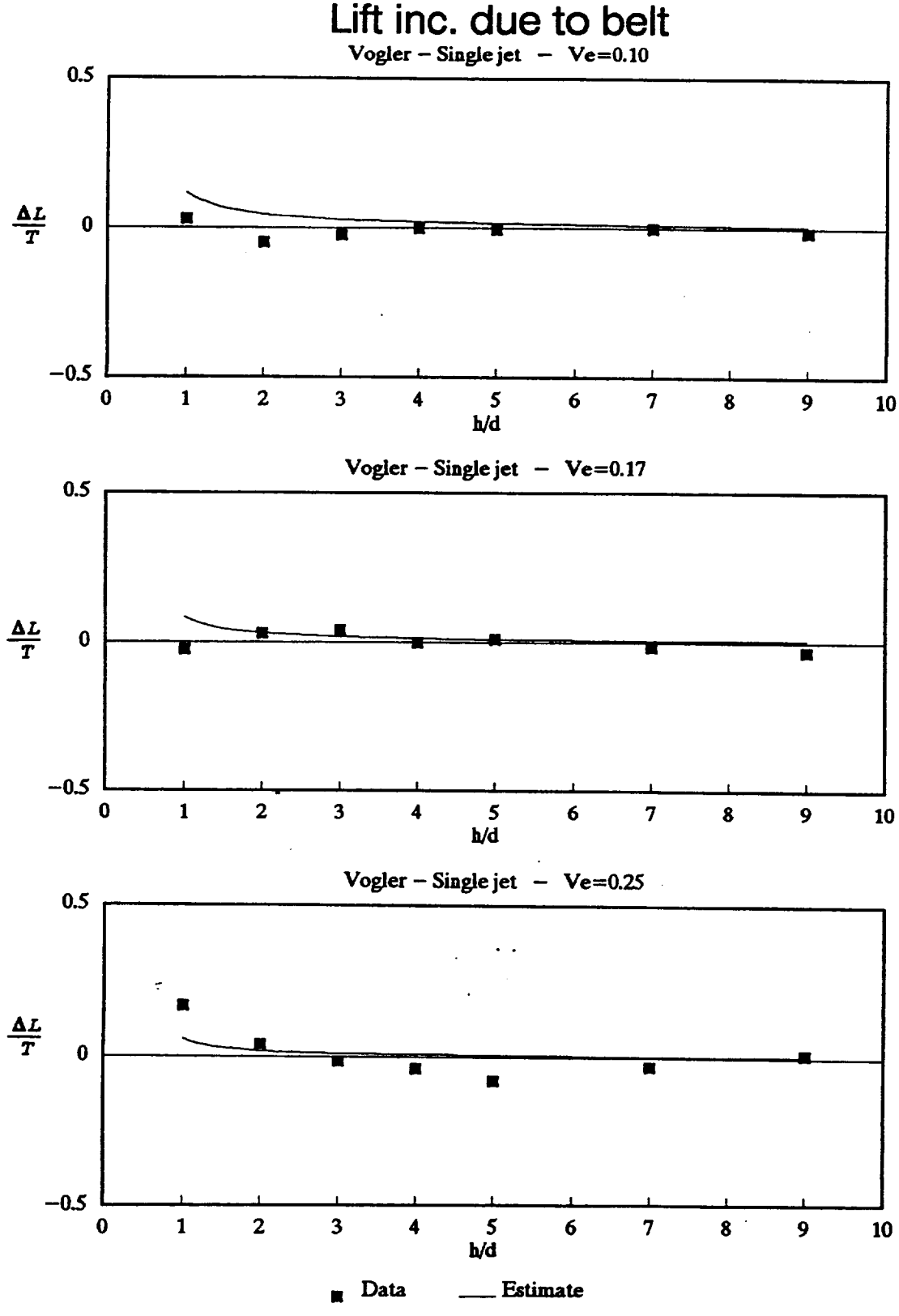

b) Lift increment due to moving ground

Figure 36.- Concluded.

REPORT DOCUMENTATION PAGE

Form Approved
OMB No. 0704-0188

1. AGENCY USE ONLY *(Leave blank)*	2. REPORT DATE	3. REPORT TYPE AND DATES COVERED
	February 1997	Contractor Report

4. TITLE AND SUBTITLE
An Analysis of the Pressures, Forces and Moments Induced by the Ground Vortex Generated by a Single Impinging Jet

5. FUNDING NUMBERS
505-68-32

6. AUTHOR(S)
Richard E. Kuhn

7. PERFORMING ORGANIZATION NAME(S) AND ADDRESS(ES)
Defense Group, Inc.
901 North Stuart St., Suite 801
Arlington, VA 22203

8. PERFORMING ORGANIZATION REPORT NUMBER
A-975988

9. SPONSORING/MONITORING AGENCY NAME(S) AND ADDRESS(ES)
National Aeronautics and Space Administration
Washington, DC 20546-0001

10. SPONSORING/MONITORING AGENCY REPORT NUMBER
NASA CR-4765

11. SUPPLEMENTARY NOTES
Point of Contact: Doug Wardwell, Ames Research Center, MS 237-2, Moffett Field, CA 94035-1000
(415) 604-6566

12a. DISTRIBUTION/AVAILABILITY STATEMENT
Unclassified–Unlimited
Subject Category – 02

12b. DISTRIBUTION CODE

13. ABSTRACT ***(Maximum 200 words)***

When a jet STOVL aircraft is in STOL operation the jets impinge on the ground and generate wall jets flowing radially outward from the points at which the jets impinge. When the forward flowing part of a wall jet meets the free stream flow it is rolled back on itself forming a parabolic shaped ground vortex. Positive pressures are induced on the lower surface of the configuration ahead of the ground vortex and suction pressures are induced over the ground vortex itself. In addition, the suction pressures induced aft of the jet out of ground effect are reduced and lifting pressures are induced on the upper surface.

This study analyzes available pressure and force data and develops a method for estimating the forces and moments induced in ground effect. The method includes the effects of configuration variables, height and operating conditions, as well as the effects of the location, deflection and shape of the jet. However, it is limited to single jets at subcritical nozzle pressure ratios.

An analysis of the effects of moving over the ground vs. tests over a fixed ground plane is included.

14. SUBJECT TERMS	15. NUMBER OF PAGES
Ground vortex, STOVL, Jet wake, Suckdown, Transition, Single jet, Pressure data	99
	16. PRICE CODE: APP

17. SECURITY CLASSIFICATION OF REPORT	18. SECURITY CLASSIFICATION OF THIS PAGE	19. SECURITY CLASSIFICATION OF ABSTRACT	20. LIMITATION OF ABSTRACT
Unclassified	Unclassified		